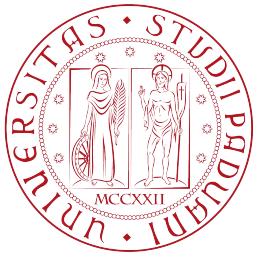

UNIVERSITÀ DEGLI STUDI DI PADOVA

Dipartimento di Fisica e Astronomia "Galileo Galilei"

Master Degree in Physics

Final Dissertation

Studies for the selection of the neutrino events collected in ICARUS T600 at FERMILAB

Thesis supervisor	Candidate
Dr. Christian Farnese	Daphne Diretto

Academic Year 2022/2023

Contents

Introduction

Neutrinos are the most abundant elementary particles in the universe interacting through weak force and gravity, making their detection challenging. One of the most intriguing characteristics of neutrinos is their ability to change flavour as they travel through space, a phenomenon known as "neutrino oscillation." Numerous experiments have confirmed this phenomenon by studying the neutrinos coming from the Sun, the atmospheric and reactor neutrinos and the neutrinos produced at accelerators.

Recent experiments such as LSND, MiniBooNE, and Neutrino-4 have observed new oscillation signals indicating the presence of an additional "sterile" state with a mass-squared difference ($\simeq$ 1 eV^2), beyond the active three-neutrino in the Standard Model. To include the sterile neutrinos, the standard model should be extended at least to a 3+1 model. The Short-Baseline Neutrino program at Fermilab (USA) is devoted to investigate the anomalies indicating the possible existence of sterile neutrinos at 1 eV mass scale with three large Liquid Argon Time Projection Chamber (LAr-TPC) detectors installed on-axis on the Booster neutrino beamline. ICARUS T600 is presently operated as a far detector, located at a 600 m distance from the target.

The ICARUS T600 LAr-TPC detector restarted to record new interesting neutrino events in 2020 at Fermilab. Its primary goal is to definitively address the unanswered questions related to the potential existence of sterile neutrinos and to verify the results observed by the Neutrino-4 experiment. Additionally, it records neutrino interactions from the NuMI off-axis beam, which will be used for precise measurements of neutrino-argon cross-sections.

The focus of this thesis will be on the development of a selection procedure designed to identify and select neutrino interactions recorded in the ICARUS detector by simple requirements. The selected events can be then visually studied in detail and most of all they will be used as a benchmark for the validation of the high-level reconstruction/selection that will be used for the oscillation analysis in the experiment.

The event filter under preparation should take into account that the T600 is presently operating at a shallow depth, protected only by about 3 m concrete overburden, where numerous cosmic muons are continuously crossing the detector. Therefore, it is necessary to employ automated selection criteria to recognize the particle generating the trigger in the detector and to distinguish neutrino interactions from cosmic events. These tools should utilize all available information from the TPC, from the internal PMTs, located behind the TPC wire planes, and from an external Cosmic Ray Tagging system surrounding the detector.

The prepared selection procedure will be applied to both recorded data and Monte Carlo (MC) events to assess its performance. The selected candidates in the real collected events will also undergo visual study in order to recognize the genuine selected neutrino events and to have a

better understanding of the selection efficiency in real data. The emphasis will be on the selection of fully-contained muon neutrino interactions and in particular on quasi-elastic events.
In Chapter 1 a brief introduction to neutrino physics and on the neutrino oscillation measurements is reported. In particular, the sterile neutrino anomalies will be described in detail.
In Chapter 2 the SBN program will be presented in detail, with particular emphasis on the ICARUS T600 detector, which is the main subject of this thesis.
In Chapter 3 I will briefly describe how the events are simulated and/or reconstructed in ICARUS. In addition, the data sample used in the analysis of this thesis will be presented.
In Chapter 4, the first element for the event selection will be developed with the study of the light signal generating the trigger to identify the region of the detector where this particle is located. This PMT-TPC signal association will be studied in detail on simulated events and in real data in order to estimate the association efficiency.
Finally, in Chapter 5 I will discuss the different criteria considered for the selection of the events. The performance of the selection procedure will be also evaluated, including a preliminary data-MC comparison.

Chapter 1

Neutrino physics

1.1 Neutrino oscillation

Neutrino are neutral fermions that were first postulated by W. Pauli in 1930 while studying the beta decay processes. Neutrinos exist in three different flavours, associated with their charged lepton: electronic ν_e, muonic ν_μ and tauonic ν_τ, and each particle has an associated antiparticle (antineutrino, $\bar{\nu}$).
These particles interact only via weak interaction (cross-section $\sigma \sim 10^{-38} cm^2/\text{GeV}$) and gravity. In addition, since neutrinos are neutral particles, they can be detected only in an indirect way, studying the products of their interactions. For all these reasons neutrinos have been observed for the first time only in 1956 by Reines and Cowan.
Thanks to their properties, neutrinos became soon after their discovery the best candidate particle to be studied in order to understand the processes in the interior of the Sun. These reactions produce in fact a large flux of electron neutrinos that can cross very large amount of matter without interacting so they pass unscathed through the Sun and can be detected directly on the Earth surface. In 1968 Ray Davis (Nobel prize in 2002) reported[1] the first measurement of the neutrino flux from the Sun. In this deep underground experiment in South Dakota, the neutrinos were detected using a Chlorine-based detector studying the reaction:

$$\nu_e + {}^{37}\text{Cl} \rightarrow {}^{37}\text{Ar} + e^-$$

The result from this experiment was unexpected: the measured total flux was one-third of the one predicted by the Solar Standard Model. This deficit was defined as *Solar neutrino problem*. Soon, many other experiments detected the same discrepancy from the theory.
Bruno Pontecorvo in 1968 proposed a possible explanation[2]: electron neutrinos produced by the Sun are transformed in flight into different species of neutrinos that can not be detected in Davis's experiment. More in general, a neutrino produced in a *flavour eigenstate* $\nu_\alpha = \left(\nu_e \nu_\mu \nu_\tau\right)$ can be detected at a distance L from its source as a neutrino with a flavour β and in principle β can be different from the initial flavor α: this mechanism is called *neutrino oscillation*.
The hypothesis of the neutrino oscillation is strictly related to the fact that neutrino should have a mass, even if initially in the Standard Model these particles were considered without mass. If at least one neutrino has mass, the neutrino *flavor eigenstate* ν_α can be written as a mixing of

three *mass eigenstates* ν_i:

$$\nu_\alpha = U_{\alpha i}\nu_i \tag{1.1}$$

where $U_{\alpha i}$ is an unitary matrix called PMNS matrix (Pontecorvo-Maki-Nakagawa-Sakata) and the mass eigenstate ν_i has eigenvalue m_i. The probability to observe the oscillation from a flavor α to a flavor β is defined as the probability to detect at the time t a neutrino of flavour β on initial α neutrino flavour.

$$P_{\alpha\beta}(t) = |<\nu_\beta|\nu_\alpha(t)>|^2 \tag{1.2}$$

To fully compute the oscillation probability, for simplicity we can reduce to a two-state system, considering the flavor α and β, the mass eigenstates ν_i with *i: 1, 2* and the mixing matrix

$$U = \begin{pmatrix} U_{\alpha 1} & U_{\alpha 2} \\ U_{\beta 1} & U_{\beta 2} \end{pmatrix} = \begin{pmatrix} cos\theta & sin\theta \\ -sin\theta & cos\theta \end{pmatrix} \tag{1.3}$$

If a neutrino ν_α is generated at t=0, its temporal evolution is:

$$|\nu_\alpha(t)>= U_{\alpha 1}e^{-iE_1 t}|\nu_1> + U_{\alpha 2}e^{-iE_2 t}|\nu_2> \tag{1.4}$$

and assuming a monochromatic neutrino beam, the energy associated to the mass eigenstates are:

$$E_{i=1,2} = \sqrt{p^2 + {m_i}^2} = p\sqrt{1 + \frac{{m_i}^2}{p^2}} \simeq p + \frac{{m_i}^2}{p} \simeq E + \frac{{m_i}^2}{2E} \tag{1.5}$$

Using this expression, the probability to observe at a distance L the same neutrino flavor generated at t=0 (survival probability) is defined as:

$$\begin{aligned} P_{\alpha\alpha}(L) &= \left|e^{\frac{-i{m_1}^2 L}{2E}}\left(|U_{\alpha 1}|^2 + |U_{\alpha 2}|^2 e^{\frac{({m_2}^2 - {m_1}^2)L}{2E}}\right)\right|^2 \\ &= 1 - 4|U_{\alpha 1}|^2|U_{\alpha 2}|^2 \sin^2\left(\frac{({m_2}^2 - {m_1}^2)L}{2E}\right) \end{aligned} \tag{1.6}$$

$$P_{\alpha\alpha}(L) = 1 - \sin^2 2\theta \sin^2 \frac{\Delta m^2 L}{4E} \tag{1.7}$$

in which $\Delta m^2 = m_2^2 - m_1^2$. The probability $P_{\alpha\beta}$ to observe at a distance L a neutrino ν_β (oscillation probability) can be then obtained using the probability conservation $P_{\alpha\alpha} + P_{\alpha\beta} = 1$ obtaining

$$P_{\alpha\beta}(L) = \sin^2 2\theta \sin^2 \frac{\Delta m^2 L}{4E} \tag{1.8}$$

Looking at the oscillation probability, it becomes clear that the study of the oscillations is sensitive to the **mass splitting** Δm^2 and to the **mixing angle** θ. In addition since the oscillation probability depends on $\Delta m^2 \times \frac{L}{E}$, it results fundamental to properly define the distance L between the source and the detector and the energy of the neutrino E in order to be sensitive to specific interval of Δm^2. Moreover, the oscillation measurements are sensitive only to the mass splitting $|\Delta m^2_{ij}|$, so no direct information on the overall mass scale can be obtained from the neutrino oscillation studies.

In general, for a three-type neutrino model:

$$\begin{pmatrix} \nu_e \\ \nu_\mu \\ \nu_\tau \end{pmatrix} = \begin{pmatrix} U_{e1} & U_{e2} & U_{e3} \\ U_{\mu 1} & U_{\mu 2} & U_{\mu 3} \\ U_{\tau 1} & U_{\tau 2} & U_{\tau 3} \end{pmatrix} \cdot \begin{pmatrix} \nu_1 \\ \nu_2 \\ \nu_3 \end{pmatrix}$$

the PMNS matrix can be parametrized as follow:

$$\begin{pmatrix} c_{13}c_{12} & c_{13}s_{12} & s_{13}e^{-i\delta_{CP}} \\ -c_{23}s_{12} - s_{13}s_{23}c_{12}e^{i\delta_{CP}} & c_{23}c_{12} - s_{13}s_{23}s_{12}e^{i\delta_{CP}} & c_{13}s_{23} \\ s_{23}s_{12} - s_{13}c_{23}c_{12}e^{i\delta_{CP}} & -s_{23}c_{12} - s_{13}c_{23}s_{12}e^{i\delta_{CP}} & c_{13}c_{23} \end{pmatrix}$$

where $c_{ij} = cos\theta_{ij}$, $s_{ij} = sin\theta_{ij}$ and δ is the CP phase.
In total, there are six independent parameters that can be studied in oscillation experiments: two squared mass splitting $\Delta {m_{21}}^2$ and $\Delta {m_{31}}^2$; three mixing angles θ_{12}, θ_{13}, θ_{23}; one phase δ_{CP}. Presently the experiments indicates that $|\Delta m^2_{12}| = |\Delta m^2_{sun}| = 0.76 \cdot 10^{-4} eV^2$ and $|\Delta m^2_{13}| \simeq |\Delta m^2_{32}| = |\Delta m^2_{atm}| = 3 \cdot 10^{-3} eV^2$. Solar neutrino measurements fix the ordering $m_2 > m_1$. Since the sign of Δm^2_{32} is still unknown, two possibilities are still under investigation: $m_3 > m_1$ or $m_3 < m_1$. These two cases are usually defined as *normal* hierarchy and *invertend* hierarchy (Figure 1.1).

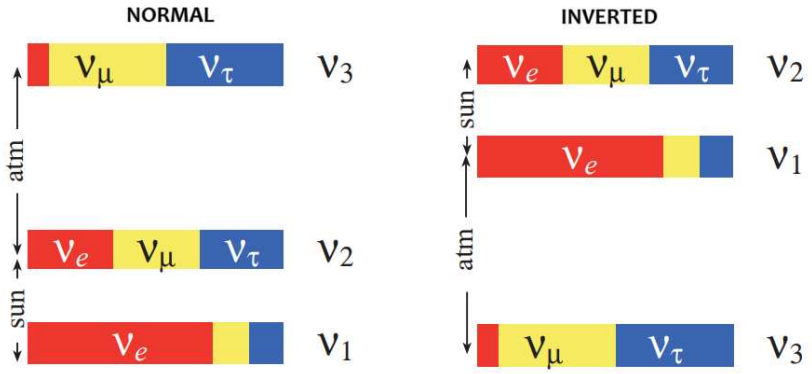

Figure 1.1: Pattern of neutrino masses for the normal and inverted hierarchies. Δm^2_{atm} and Δm^2_{sol} stands for the atmospheric and the solar mass-squared splitting, respectively[3]

1.2 Experimental observation of the neutrino oscillations

The neutrino oscillations can be observed considering two different studies: in the *disappearance* experiments, the neutrinos of a given flavor are studied at a defined distance from its source and the oscillation is identified by a reduction in the observed flux with respcet to the expectations; neutrino *appearance* experiments look instead for an excess in the number of events associated to a given neutrino flavour that is not present or is only weakly produced at the neutrino source. Since its first theorization, several experimental results have confirmed the neutrino oscillation hypothesis: in this section, only few of them are shortly mentioned, together with their estimated value of the mass splitting and of the mixing angle.

Solar neutrino: the SNO experiment

The Sudbury Neutrino Observatory (SNO) is a Canadian experiment devoted to solve the solar neutrino problem. It collected data between 1996 and 2006 using a detector located 2 km

underground and filled with 1000 t of heavy water. The neutrino oscillation has been demonstrated by studying simultaneously the charge current interactions, which can be observed only for the electron neutrinos, and the neutral current interactions, which can be observed for all three different neutrino flavours[1]. The measurement of the charge current events highlighted a clear reduction of the electron neutrino flux while the analysis of the NC events showed that the flux measurement was in agreement with the predictions (figure 1.2).

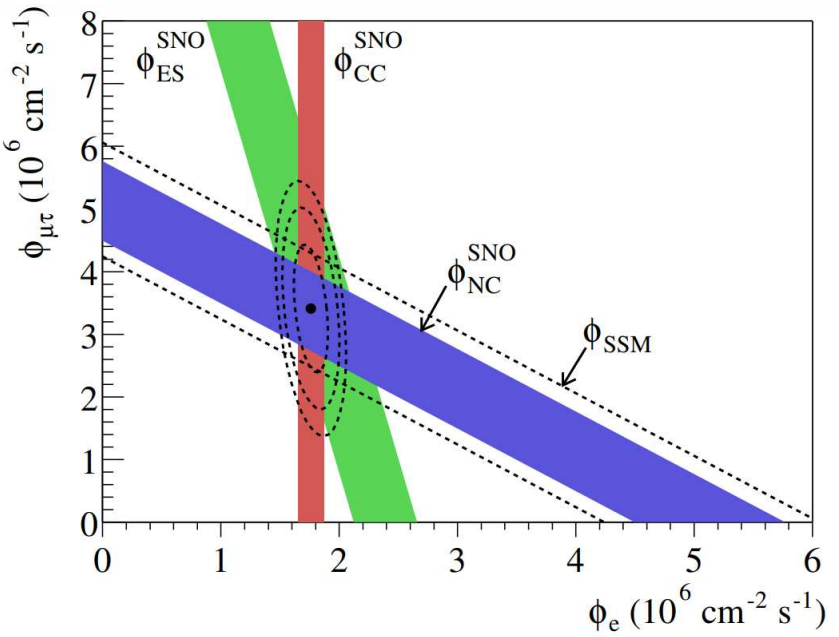

Figure 1.2: The flux of ν_e with the combined ν_μ and ν_τ fluxes. Together the three rates are consistent with a mix of about 1/3 ν_e and 2/3 ν_μ and/or ν_τ. The intersection of the 3 bands in the figure represents the $\pm 1\sigma$ error. The results are compatible with the neutrino flavour oscillation from the source, with no distortion in the spectrum of the ^8B. See as reference[4]

These results demonstrated that the solar electron neutrino produced by the ^8B decay in the Sun significantly changes their flavour in their journey to the Earth. The best-fit value are $\tan^2\theta_{12} = 0.427^{+0.033}_{-0.029} eV^2$ and $\Delta m^2_{12} = 5.62^{+1.92}_{-1.36}$ eV^2.

Atmospheric neutrino: the Super Kamiokande experiment

Super Kamiokande is the largest water Cherenkov detector ever built and it is an updated version of the original Kamiokande detector constructed in 1970. The detector is located 1 km underground in the Mozumi Mine in Hida's Kamioka area in Japan. It consists of a cylindrical stainless steel tank of 50000 tons of ultra-pure water surrounded by 13000 PMTs that collect the Cherenkov light inside the detector generated from the passage of a charged particle inside the detector itself.

Super Kamiokande has collected data since 1996 and it is devoted to the study of the solar neutrinos, of the neutrino produced via the interaction of cosmic rays with the Earth's atmosphere

[1] In Charge-Current interaction (CC) there is an exchange of a $W^\pm$ boson with the nucleons N, while in Neutral-Current interaction (NC) there is an exchange of the Z boson. In the CC interactions, a lepton l associated with the neutrino ν_l is produced so, for example, characteristic muon tracks are produced when ν_μ interact via CC, while electromagnetic showers associated to the electron can be present in an electron neutrino interaction. This property can be used to recognize the neutrino flavour starting from the product of its interaction.

(atmospheric neutrinos) and of the T2K neutrino beam [5]. The experiment observed a deficit of upward-going muon neutrinos that can be interpreted as evidence of $\nu_\mu \rightarrow \nu_\tau$ oscillation. The measured oscillation parameters result 5 x 10^{-4} < Δm^2 < 6 x 10^{-3} eV^2 and $\sin^2 2\theta$= 0.82 at 90% confidence level. As shown in figure 1.3 Super-K lowered the values of Δm^2 with respect to the previous results from Kamiokande. Starting from 2010 a successor of Super-K is under construction: Hyper-K. This new detector is 20 times bigger than Super-K and aims to investigate the difference in the neutrino oscillation probabilities between neutrinos and anti-neutrino. It will take data starting from 2027 [6].

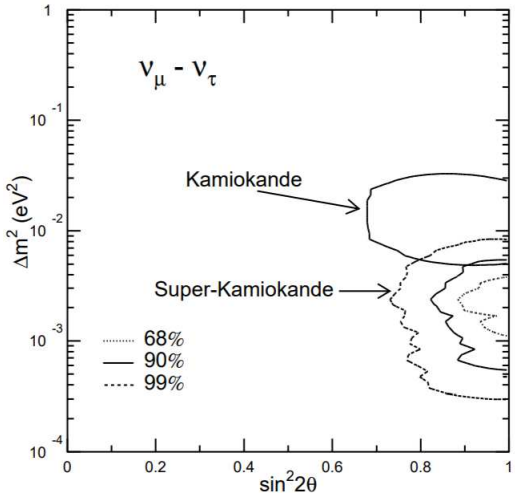

Figure 1.3: In the figure are reported the 68%, 90% and 99% confidence level region of Super-K. It is possible to see an overlap with the 90% contours for Kamiokande [5].

Neutrinos at accelerators and long-baseline experiments

A fundamental tool for the development of neutrino physics is certainly represented by the neutrino beams produced at accelerators. This technique, widely used and continuously under development, is based on the production of muon neutrinos by means of a beam of protons against a suitable target. Since the oscillation probability is strongly related to the ratio L/E, the usage of neutrino beams, combined with the proper location of the detector, allows to obtain the desired L/E range, that corresponds to investigate particular Δm^2 range.
Experiments are generally classified as short or long baseline on the basis of the corresponding L/E: in a long-baseline neutrino experiment the ratio L/E is greater than 100 m/MeV and the detector can be positioned at a long distance from the neutrino beam source. These experiments had the primary objective of confirming the results obtained through the study of atmospheric neutrinos. For example, the MINOS experiment (Main Injector Neutrino Oscillation Search) at FERMILAB, was a 100 m underground experiment that provided evidence of muon neutrino oscillations. Exposed to the NuMI beam, it collected data from 2005 to 2012 and then, after an upgrade, MINOS+ took data from 2013 until 2016. It is composed of a Near detector, 1 km distance from the source, and a Far detector located at 734 km from the first one, in Soudan. The usage of these two near and far detectors is fundamental for the neutrino studies: in fact the near detector can provide a direct measurement of the neutrino flux and the comparison of this measurement with the spectrum observed in the far detector can provide the evidence for

the neutrino oscillations. MINOS results are in complete agreement with the oscillation picture shown by Super-K and the results obtained in the measurement between 2006 and 2007 show the most precise value: $\Delta m^2_{23} = (2.43 \pm 0.13)$ x 10^{-3} eV^2 at 68% confidence level and $\sin^2 2\theta_{23} > 0.90$ at 90% confidence level. Important evidence of neutrino oscillations, in particular in the $\nu_\mu \rightarrow \nu_e$ channel, has been also provided by the T2K and NOνA experiments[7].

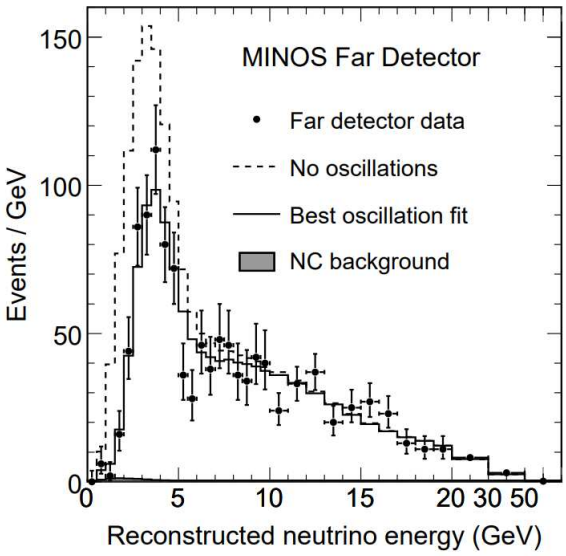

Figure 1.4: Distribution of the reconstructed ν_μ energy for the events recorded in the MINOS detector. The best oscillation fit and the expected spectrum assuming no oscillations are also shown[8].

In the future long-baseline neutrino experiments will play a fundamental role to solve the still open questions related to the neutrino oscillation. An important contribution will be provided in particular by DUNE [9]. This experiment will be composed by a small detector, located at FNAL, near the source of the neutrino beam, and a giant 40-kiloton detector, based on the liquid Argon TPC technology developed first by the ICARUS collaboration and composed by 4 separate modules. This far detector will be located 1 km underground and at 1300 km from the near detector, at the Sanford Underground Research Facility (SURF) in South Dakota, USA. The muon and electron neutrino observed in this experiment will allow to study in particular the neutrino mass ordering and the δ_{CP} phase, which are presently not determined.

Reactor neutrino

Nuclear reactors produce electron antineutrino at the MeV scale that can be studied by dedicated experiments in order to identify an electron antineutrino disappearance signal. Recently the study of these neutrinos by the Daya Bay, RENO and Double Chooz experiments is providing interesting measurements of the θ_{13} mixing angle. In particular, the Daya Bay experiment, in China, consists of eight liquid scintillator antineutrino detectors, clustered in three locations within 1.9 km of six nuclear reactors. The most recent result of this experiment, on April 2023, shows the most precise result of θ_{13}, that is $\sin^2\theta_{13} = 0.0851 \pm 0.0024$; in addition it provides also a measurement of $\Delta m^2_{32} = (2.466 \pm 0.060)$ x 10^{-3} eV^2 for the normal mass ordering or $\Delta m^2_{32} = (-2.571 \pm 0.060)$ x 10^{-3} eV^2 for the inverted mass ordering with 68% confidence level [10].

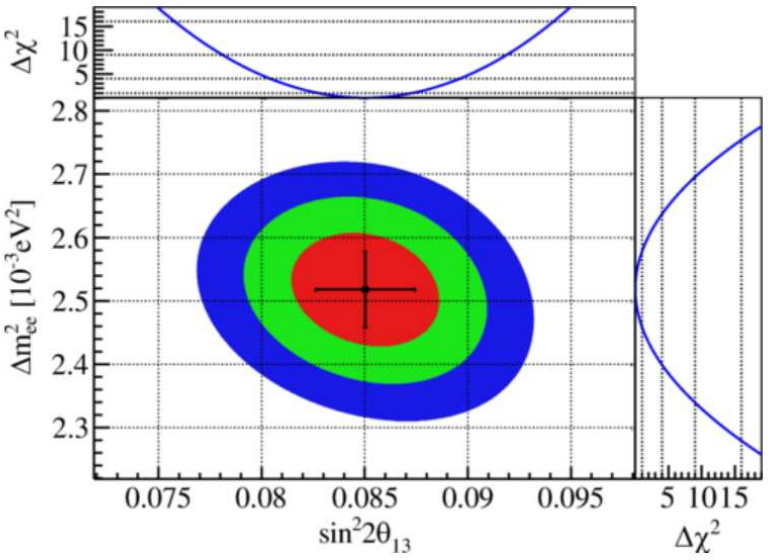

Figure 1.5: Best fit obtained studying the neutrino signals recorded in Daya Bay with the corresponding error ellipses in the $\sin^2\theta_{13}$ and Δm^2_{ee} space. Colors represent 1, 2, and 3 standard deviations, with error bars corresponding to the one-dimensional 1 standard deviation confidence interval.

Fundamental contributions on the understanding of the neutrino oscillations will be also provided in the near future by JUNO. This experiment is situated within the Jiangmen Underground Laboratory in China, built upon liquid scintillator technology with a total active mass of 20 kt, and operates underground to minimize interference from cosmic ray background noise. Its primary goal is the determination of the neutrino mass hierarchy and the measurement of the oscillation parameters detecting and recording electron antineutrinos emitted by nuclear reactors located at about 53 km from the detector.[11].

1.3 Sterile neutrino

In the attempt to identify new evidences of neutrino oscillations and give better bounds on the oscillation parameters, some experiments found anomalous results that are not consistent within the available three-flavour neutrino Standard Model framework. This section will give an overview of some of these anomalies.

1.3.1 Evidences for sterile neutrino

LSND anomaly

The Liquid Scintillator Neutrino Detector (LSND) was a short baseline experiment that took data from 1993 to 1998 at the Los Alamos National Laboratory. The studied neutrinos were produced by a 800 MeV proton beam interacting on a beam stopper formed by water, copper and iron. A hadronic cascade made by neutrons, protons and $\pi^{\pm}$ is generated and the decay products of the $\pi^{\pm}$ give rise to an electronic and muonic anti-neutrino flux. The produced neutrino had an energy between 20-53 MeV and were studied in the detector containing 167 tons of mineral oil and located at about 30 m from the neutrino source. This experiment provided evidence of an electron anti-neutrino appearance related to the $\bar{\nu_\mu} \rightarrow \bar{\nu_e}$ oscillation [12]. Globally

89.7± 22.4±6.0 electron anti-neutrino candidate events in addition to the expected backgrounds have been observed, corresponding to a 3.8 σ evidence for the oscillations as shown in figure 1.6. The measured oscillation probability was 0.264±0.067±0.045% and taking into account that the L/E parameter for this experiment was about 1 m/MeV the corresponding allowed Δm^2 results in the 1 eV^2 region. The result from the LSND experiment was in conflict with other similar experiments (like KARMEN experiment[13]) that were looking for the same appearance channel but didn't find any oscillation evidence. An hypothesis to solve this anomaly is the introduction of a fourth-type neutrino with a mass in the eV scale, that doesn't interact as the other neutrinos but that can be involved in the oscillation phenomena: the *sterile neutrino*.

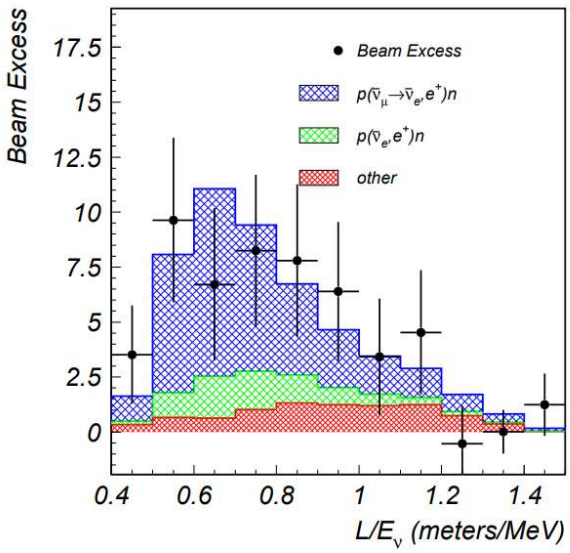

Figure 1.6: The $\bar{\nu_e}$ excess found in LSND (black dots) was 87.9 ± 22.4 ± 6.0 events, where the first error is the statistic and the second arises from background uncertainty. More details in [12]

MiniBooNE experiment

MiniBooNE (Mini Booster Neutrino Experiment) was an experiment located at Fermilab (US) that searched for a confirmation of the LSND anomaly. It measured the neutrino interactions produced by a neutrino beam composed mainly by (anti)ν_μ (Booster Neutrino Beam - BNB) and it was designed in particular to study the (anti)ν_e events. The neutrino beam was produced by an 8 GeV proton beam interacting on a Beryllium target and the detector was located at about 500 m from the target: the $L/E_\nu \simeq 1 m/MeV$ resulted similar to the LSND experiment. This experiment took data from 2002 to 2012 and globally collected about $12 \cdot 10^{20}$ POT (proton on target) in the BNB neutrino mode and a similar statistics in the anti-neutrino mode.

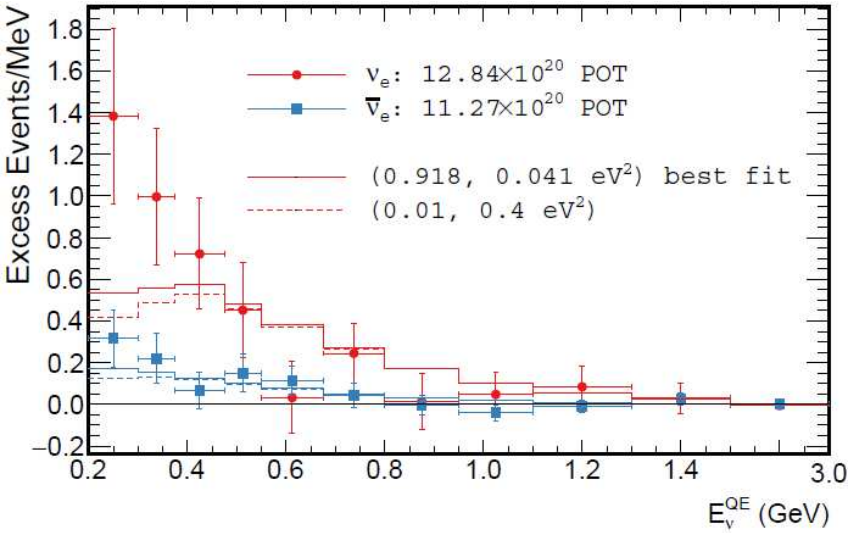

Figure 1.7: Total event excesses in both neutrino mode and antineutrino mode in MiniBooNe experiment [14].

In this experiment, a global excess of 460.5 ± 99.0 events related to (anti) electron neutrino interactions has been observed (4.7σ) as shown in figure 1.7. This signal can be interpreted as an oscillation signal related to an additional mass-squared difference in the eV^2 scale, similar to LSND [15].

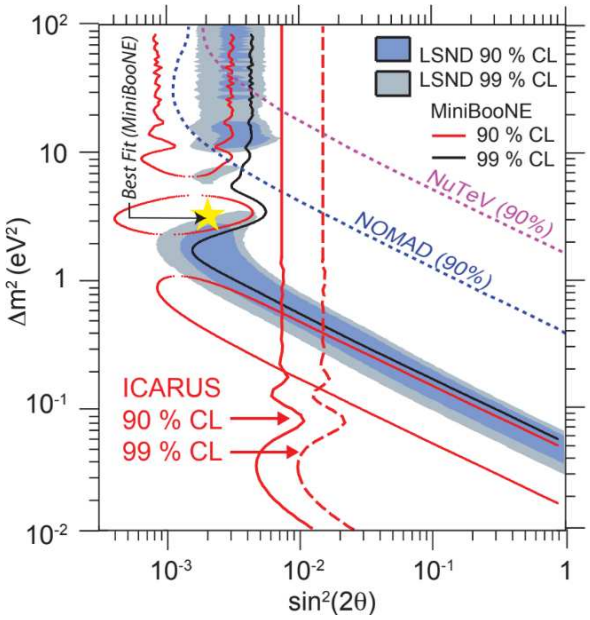

Figure 1.8: Δm^2 as a function of $sin^2(2\theta)$ for the LSND, MiniBooNE and ICARUS experiment [16]

Different experiments have recently tried to confirm the results obtained by the LSND and MiniBoone experiments. In particular, the MicroBooNE experiment has taken data starting from 2015 and was designed to investigate the excess of events at low energy observed by the MiniBooNE experiment. Also the ICARUS Collaboration, using the events recorded during the data taking in Gran Sasso between 2010 and 2012, has performed a sensitive dedicated search to identify a possible electron neutrino excess in the CNGS muon neutrino beam. The obtained exclusion area is shown in figure 1.8: the ICARUS result allowed to define a narrow allowed

parameter region centered around $\Delta m^2 \sim 0.5eV^2$ where there was a 90 C.L. agreement between all the available results (see Chapter 2 for more details related to the BNB beam, the MicroBoone and the ICARUS experiment).

Reactor anomalies

The reactor antineutrino anomalies arise from the observation of a discrepancy between the expected and the observed electron antineutrino flux in experiments that study the neutrinos produced in nearby nuclear reactors. This anomaly was initially explained in the context of the 3+1 neutrino model and the estimated oscillation parameters in a 3 active neutrino + 1 new flavour were: $\Delta m^2_{new} > 1.4eV^2$ and $\sin^2 2\theta_{new} = 0.14 \pm 0.08$ [17]. However, more recent studies (2023) show that there is another possible explanation for the anomaly: it seems that the anomaly arises from biases in the reference spectra of fission electrons [18]. In this context, reactor anomalies are under study and more research is needed to have a more precise answer.

GALLEX, SAGE and BEST experiments

A complementary measurement related to the electron neutrino disappearance has been provided also by radiochemical experiments such as GALLEX and SAGE that used intense radioactive sources. These experiments have shown an anomalous deficit of electron neutrinos, commonly referred to as the "gallium anomaly": the measured ratio between the actual measurements of the neutrino interactions and the predicted rates results in these experiments 0.86 ± 0.05. This anomaly has been recently confirmed by the Baksan Experiment on Sterile Transitions (BEST). Including also the BEST measurements the gallium anomaly results even more evident: in fact the weighted average value of the ratio between the observed and the expected neutrino rate results 0.80 ± 0.05. The possible explanation is based on oscillations into a sterile neutrino with a mass of the order of the eV. Figure 1.9 shows the best-fit oscillation parameters for BEST experiment $\Delta m^2 = 3.3^{+\infty}_{-2.3} eV^2$ and $\sin^2 2\theta = 0.42^{+0.15}_{-0.17}$ [19]

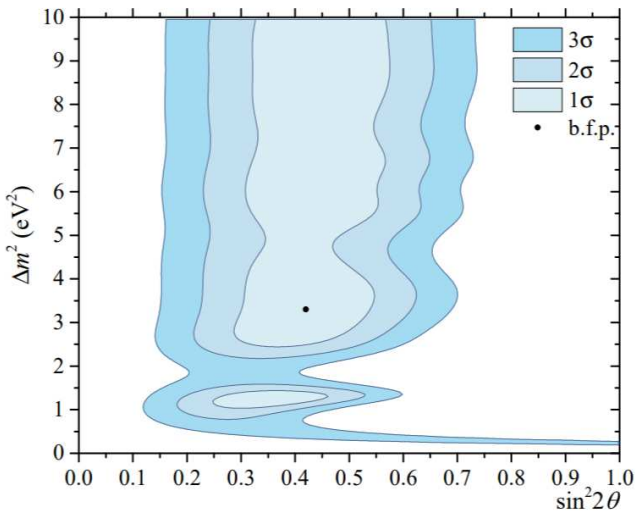

Figure 1.9: Allowed regions for BEST results. Different colours represent different confidence levels. The black point represents the best-fit point [19].

Neutrino-4 experiment

Recently another experiment devoted to the reactor electron anti-neutrinos brought important evidence for the possible existence of sterile neutrinos: the Neutrino-4 experiment. In this experiment the detector can be located in different positions at a distance between 6 and 12 m from the neutrino source: in this way it is possible to study the neutrino rate as a function of L/E. In addition, the detector has taken data both when the reactor was active and when it was off, providing a direct measurement of the backgrounds. Using the events recorded, after subtracting the measured expected background, a sterile neutrino search has been performed and the results are shown in figure 1.10. The best-fit parameters $\sin^2 2\theta_{14} = 0.36$ and $\Delta {m_{14}}^2 = 7.3eV^2$ indicates a possible contribution from a fourth sterile neutrino [20].

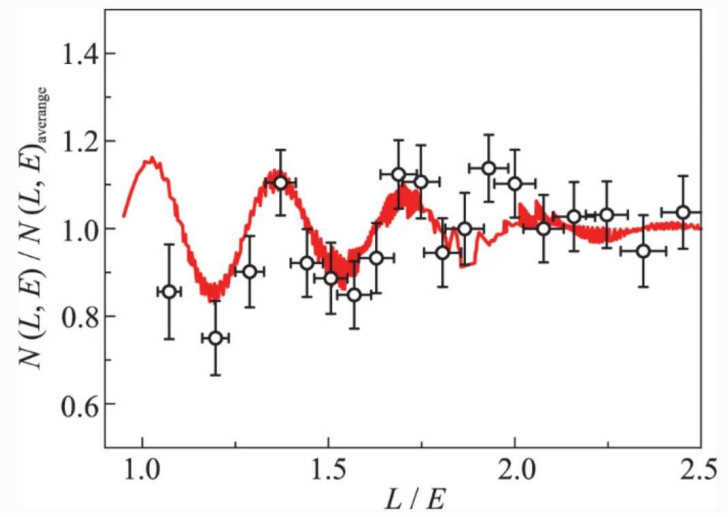

Figure 1.10: Neutrino signal oscillation curve from Neutrino-4 experiment. More details in [20]

1.3.2 Sterile neutrino phenomenology

It is possible to explain all the anomalies mentioned above by considering the existence of at least a fourth neutrino type, the sterile neutrino. Sterile neutrinos are theoretical fermions that exist as singlets within the gauge groups of the Standard Model. They do not have electric, color, or hyper-charges, making them unable to engage in electromagnetic, strong, or weak interactions. However, they could potentially interact through gravitational forces. In order to include the sterile neutrinos in the SM, the neutrino description should be extended to a minimal 3+1 model. In this case, the mixing matrix shown in 1.1 becomes a 4x4 matrix $U_{\alpha i}$ with $\alpha = e, \mu, \tau, s$ and $i = 1, 2, 3, 4$ where the fourth neutrino has the largest mass. Possible signatures of the presence of sterile neutrinos can be identified studying both the appearance and disappearance channels. In this section, the oscillation probability are reported for each channel, together with the present status on the measurements.

ν_e / $\overline{\nu_e}$ appereance channels

In the short baseline experiments, the oscillation probability can be written as an extension of the two-flavor model discussed before, indeed:

$$P_{\mu e}(L) = 4|U_{e4}|^2|U_{\mu 4}|^2 \sin^2 \frac{\Delta m^2_{41} L}{4E} \tag{1.9}$$

in which an effective mixing angle $\theta_{\mu e}$ can be defined as:

$$\sin^2 2\theta_{\mu e} = 4|U_{e4}|^2|U_{\mu 4}|^2 \tag{1.10}$$

and the effective mixing angle depends on the mixing of sterile neutrinos with electron and muon neutrinos. Figure 1.11 shows the constrain of the mixing angle and mass difference combining the results from different experiments: the preferred parameters are approximately $\sin^2 2\theta_{\mu e} = 0.01$, and $\Delta m^2_{41} = 1$ eV^2. The parameter range observed by both MiniBooNE and LSND also aligns with the absence of negative results from the other experiments. This leads to the conclusion that, if only the electron neutrino appearance measurements are considered, these results appear to be consistent with the presence of a sterile neutrino in the eV mass range.

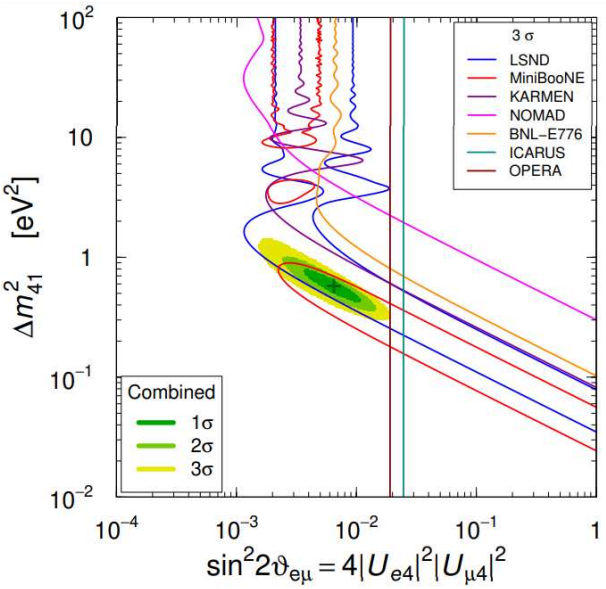

Figure 1.11: Global constraints on $\nu_\mu \to \nu_e$ (and corresponding anti-neutrino) oscillations at short baseline in the 3 + 1 framework.

ν_e/ $\overline{\nu_e}$ disappereance channels

The electron (anti) neutrino disappearance signals have been observed mostly by the reactor and by the Gallium experiments. Considering again short baseline approximation, the oscillation probability can be written as:

$$P_{ee}(L) = 1 - 4|U_{e4}|^2(1 - |U_{e4}|^2) \sin^2 \frac{\Delta m^2_{41} L}{4E} \tag{1.11}$$

in which the mixing angle is:

$$\sin^2 2\theta_{ee} = 4|U_{e4}|^2(1 - |U_{e4}|^2) \tag{1.12}$$

Figure 1.12 shows the compatibility of the results from the reactor experiments (represented by blue ellipses) with the constraints derived from various other sources, in particular the solar neutrinos (black dashed lines) and the atmospheric neutrinos (in green). The red ellipses represent the best fit region based on a combination of all ν_e and anti-ν_e datasets.

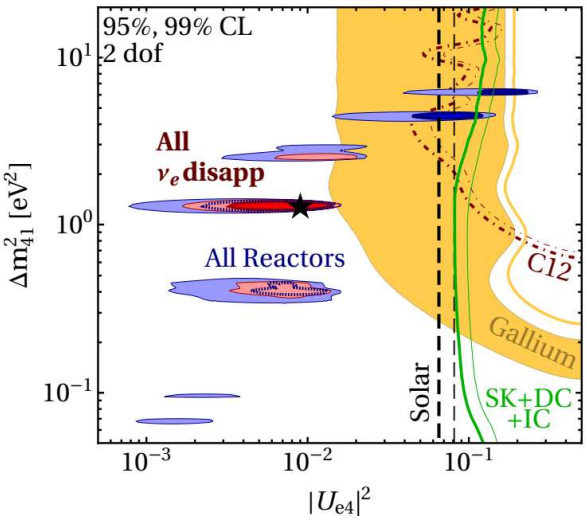

Figure 1.12: Global constraints on short-baseline ν_e and anti-ν_e disappearance, shown as a function of the mass squared difference Δm^2_{41} and of the ν_e–ν_4 mixing.

ν_μ / $\overline{\nu_\mu}$ disappearance channel

The oscillation probability associated with a muon neutrino disappearance can be written as:

$$P_{\mu\mu}(L) = 1 - 4|U_{\mu4}|^2(1 - |U_{\mu4}|^2)\sin^2\frac{\Delta m^2_{41}L}{4E} \tag{1.13}$$

and the mixing angle can be expressed as:

$$\sin^2 2\theta_{\mu\mu} = 4|U_{\mu4}|^2(1 - |U_{\mu4}|^2) \tag{1.14}$$

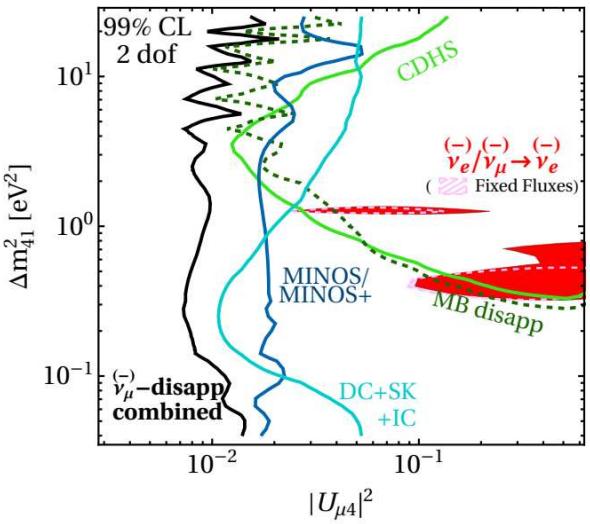

Figure 1.13: Global constraints on short-baseline ν_μ and anti-ν_μ disappearance in the 3 + 1 scenario, as a function of the ν_4–ν_μ mixing $|U_{\mu 4}|$.

The present status of the measurements related to a muon (anti) neutrino disappearance is shown in figure 1.13. It can be noticed that the defined mixing angles are strongly related so, for example, if an electron neutrino appearance signal is observed, a muon neutrino disappearance and an electron neutrino disappearance signal should be also detected. Even if there are evidences of ν_e appearance and disappearance, there are presently no evidences for ν_μ disappearance: the parameter region suggested by the electron neutrino appearance is ruled out by the absence of signals in the muon neutrino disappearance. This strong tension still needs to be solved and a conclusive experiment, that can study simultaneously all the mentioned channels, is required.

Chapter 2

SBN program and the ICARUS project

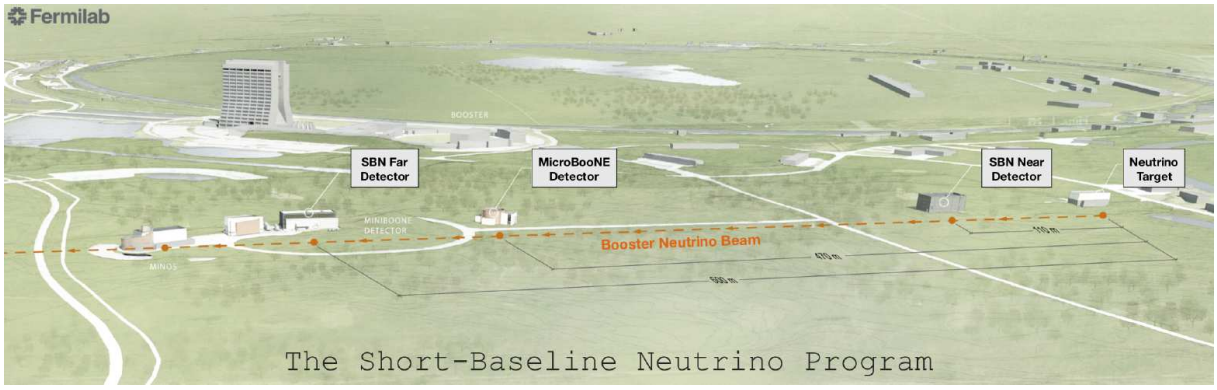

Figure 2.1: Representation of the detectors involved in the SBN project.

The Short-Baseline Neutrino experiment at Fermi National Acceleration Laboratory (USA) is devoted to investigate the results of LSND anomaly indicating the possible existence of sterile neutrinos at 1 eV mass scale. In the SBN program, three different detectors that exploit the same detection technology are exposed on-axis to the Booster Neutrino Beam (BNB), at different distances from the source to study any variation in the neutrino spectra and to clearly identify the oscillation phenomena of neutrino. The simultaneous study of the ν_μ disappearance and the ν_e appearance channels will finally provide a definitive clarification about the sterile neutrinos. In section 2.1 the main properties of the BNB beam will be briefly described, while in section 2.2 the three SBN detectors will be presented in detail, focusing in particular on the ICARUS T600, whose data analysis is the main topic of this thesis.

2.1 Booster Neutrino Beam

The Booster Neutrino Beam (BNB) at Fermilab is the main neutrino beam studied by the SBN program to solve the anomalies related to the possible existence of sterile neutrinos.

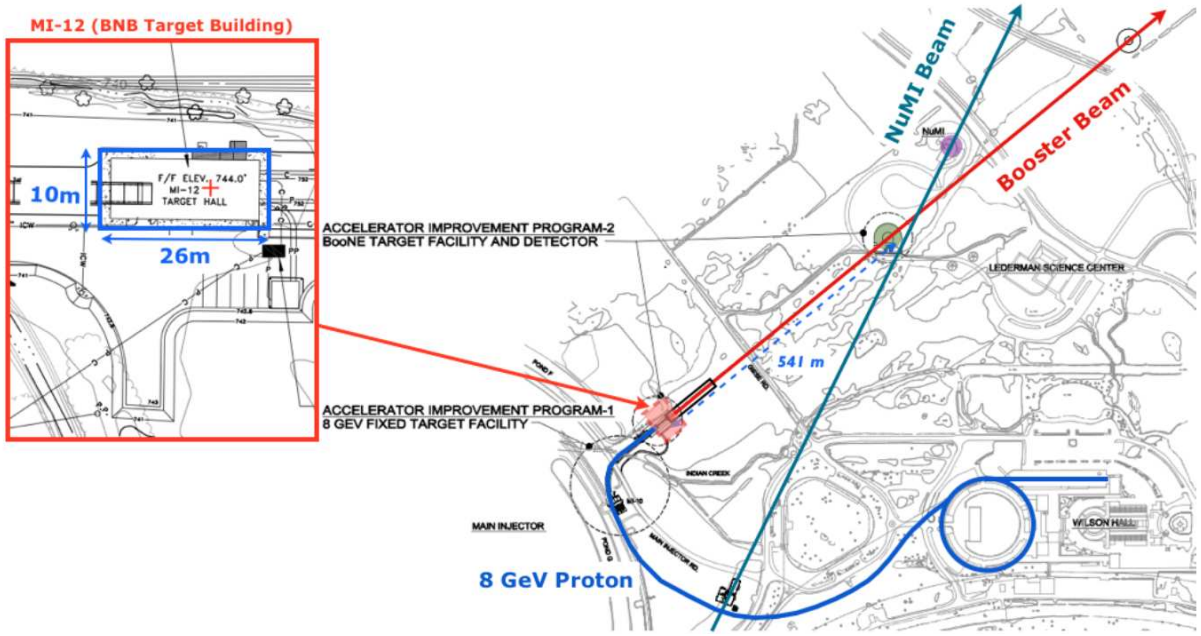

Figure 2.2: In the figure: on the right the blue line represents the accelerated proton beam; the BNB is the red line and the NuMI beam is the green line. The figure on the left shows the BNB target configuration[21].

The BNB beam is now operating for more than a decade in both neutrino and anti-neutrino modes. It is generated by protons accelerated at 8.89 GeV of kinetic energy from the Booster accelerator at FERMILAB, which is a synchrotron of 474 m in circumference. Protons impact a 71 cm long beryllium (Be) target, split into seven cylindrical sections about 10 cm long and with a 1 cm diameter. The interactions produce a secondary beam of hadrons, mainly composed of pions and with a small percentage of kaons. Around the target, there is a toroidal aluminium alloy focusing horn, which is an electromagnet that can pulse in both polarities: this allows to discriminate and to focus positive (or negative) charged particles and to de-focus the particles with the wrong charge sign. The focused mesons are then propagated for 50 meters in the decay region, where they can decay producing neutrinos. At the end of the decay region, there is a beam stop that absorbs all particles but neutrino.

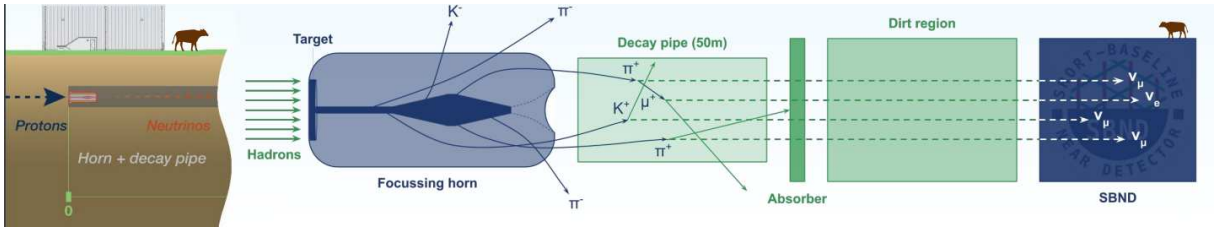

Figure 2.3: Schematization of the stages of the beam in BNB from the FNAL website

The composition of the neutrino flux for positive focusing is dominated by ν_μ (about 93.6%)

generated from the pion decay in flight, with the decay channel $\pi^+ \rightarrow \mu^+ + \nu_\mu$. In the beam $\bar{\nu_\mu}$ are also present (about 5.9%) while the contamination of ν_e and $\bar{\nu_e}$ results about 0.55%. The ν_e component comes mainly from the pion decay into muon $\mu^+ \rightarrow e^+ + \nu_e + \nu_\mu$ and from the decay of kaons $K^{+,0}$.

The BNB has been already stably operated for about 20 years and it is a well-understood beam: in figure 2.4 are shown the spectrum of the Booster neutrino beam fluxes at the SBN three detector.

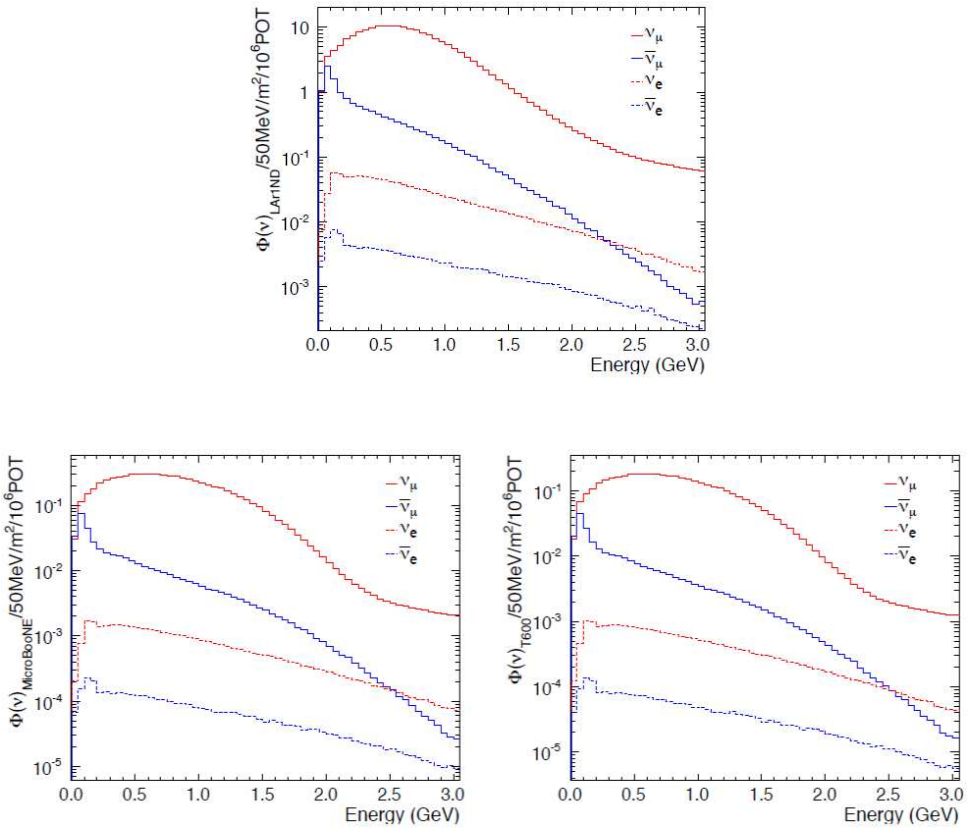

Figure 2.4: BNB flux at SBND (up), MicroBooNE (left), ICARUS (right). The rate in the near detector is higher than MicroBooNE and ICARUS [22].

An essential characteristic for the realization of the physics program is also the structure of the beam. The duration of the beam spill for the Booster results 1.6 microseconds with a maximum repetition rate of 5 Hz. In each beam spill, there are at maximum about 5×10^{12} protons delivered to the target. This number, which is indicated also as the number of POT (Proton On Target), is strictly connected to the number of interactions that occur on the target to produce neutrinos and can be used for example to evaluate the expected number of neutrinos in one of the SBN detectors.

2.2 The detectors in SBN

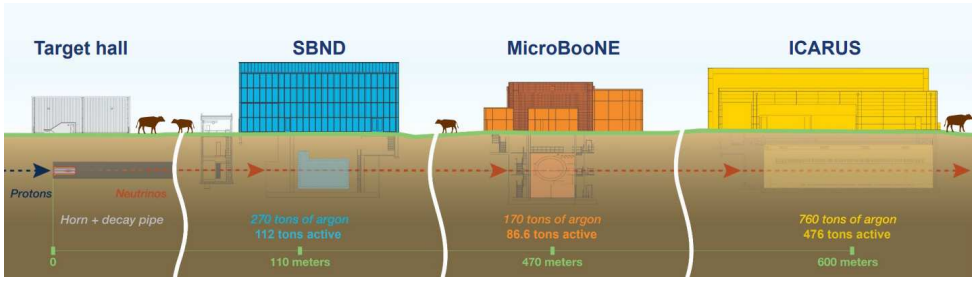

Figure 2.5: Schematization of the detectors of the SBN program from the FNAL website

The SBN program consists of three large Liquid Argon Time Projection Chamber (LAr-TPC) detectors placed on-axis at different distances from the neutrino source (see table 2.1).

Detector	Distance from BNB target	Total mass	Active mass
SBND	110 m	220 t	112 t
MicroBooNE	470 m	170 t	89 t
ICARUS T-600	600 m	760 t	476 t

Table 2.1: Summary of the characteristic of the three detectors at FNAL

The LAr-TPC is a sophisticated particle detector that employs a large chamber filled with liquid argon as detection medium.
The motivations for the use of Liquid Argon as the favorite element for the detection of neutrinos were described by Carlo Rubbia in 1977. As charged particles traverse the liquid argon, they undergo ionization, exciting the argon atoms and causing the emission of scintillation light. In his paper [23], Rubbia highlighted that highly purified Liquid Argon do not attach electrons produced by the ionization tracks, and permits their long drift under a uniform electric field, generated by an array of electrodes positioned at the detector's ends and sides. Moreover, liquid argon is the ideal medium because of its high density, high ionization and scintillation yield and its low cost that permits the creation of massive detectors[24].
When neutrinos interact with the liquid argon in the detector, the charged particles produced in the interactions, as they progress along their paths, emit scintillation light and ionize the argon atoms, leading to the liberation of ionization electrons. In the presence of a 500 V/cm drift field in the TPC (as in ICARUS T600 detector) $\simeq$ 4000 scintillation photons and 5000 free ion-electron couples per mm are produced by a minimum ionizing particles in liquid argon. The electric field within the TPC induces the liberated electrons to migrate towards the anode electrode, while the positively charged argon ions migrate towards the cathode electrode. Consequently, as the electrons and ions drift, they generate a distinctive pattern of electric signals along their trajectories that can be recorded at the anode. In particular, it is possible to do precise imaging reconstruction of tracks using three wire planes at different orientations, at the end of the drift path of electrons. Setting appropriate voltages on the wires, the first two planes facing the drift region provide signals in a non-destructive way and for this reason they are called Induction wires planes. The ionization charge is finally collected in the last wire plane which is usually called

Collection View. The signals generated by the drifting electrons are then read out and used for the spatial and calorimetric reconstruction of the event. Each wire plane gives the possibility to create a 2D representation of the particle track in the detector, while the drift time coordinates of the track (that is in common in the three wire planes) give the possibility to match the signals in the different wire planes and to reconstruct a 3D image of the event. In addition, the integral of the signal recorded on each wire is strictly related to the energy deposited by the particle: the reconstruction of the wire signal can then provide a calorimetric measurement of the event. Finally, the scintillation light produced by the particles propagates inside the highly transparent liquid Argon and can be detected by Photo-Multiplier Tubes located behind the wire planes, which prompt signal can be used for the trigger of the detector.

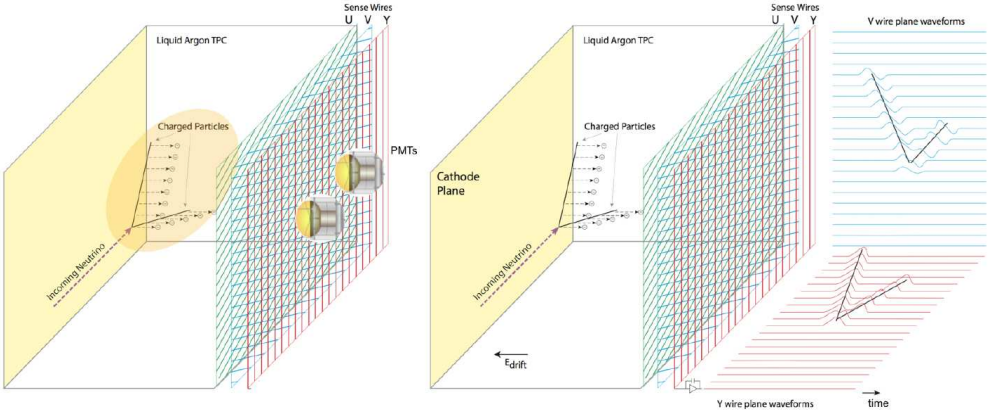

Figure 2.6: Representation of TPC detection principle with wire planes and PMTs

2.2.1 SBND

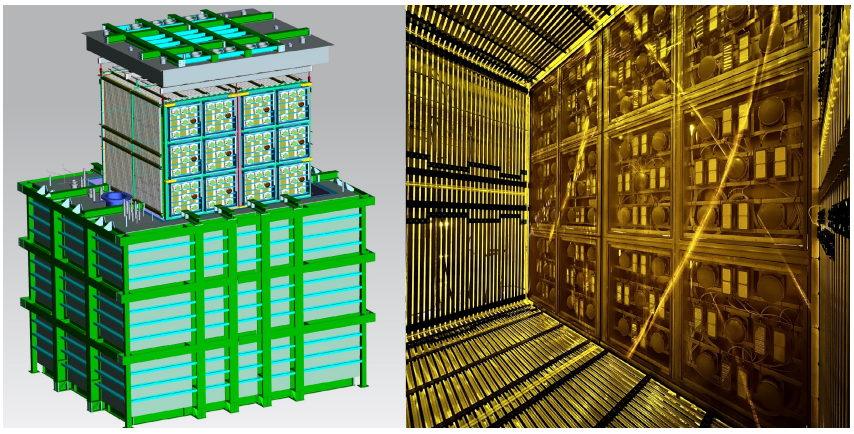

Figure 2.7: (left) rendering of the SBND detector and (right) internal part of the detector with the PMTs modules installed. Image from FNAL website

The Short-Baseline Near Detector SBND contains 112 tons of liquid argon with an active TPC volume of 4.0 m x 4.0 m x 5.0 m and a central cathode. The interacting particles in the liquid argon are detected with three wire readout planes with 3mm wire spacing. SBND is positioned approximately 74 cm off the beamline, allowing neutrinos to enter from numerous off-axis angles

(OAA). The detector can be divided into segments based on these OAA. Each segment is expected to observe over 10000 ν_μ for a total of 10 x 10^{20} protons on target.

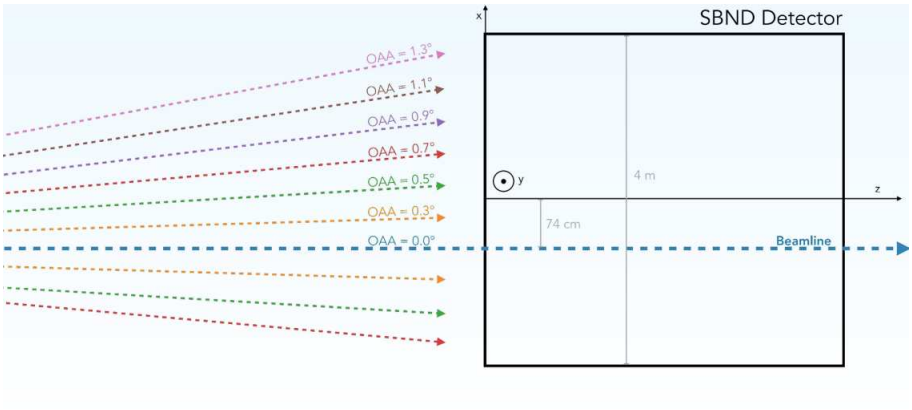

Figure 2.8: Visualization of the OAA section on the SBND detector from the FNAL website

SBND is expected to be operating from January 2024. It will provide a large data sample of neutrino events (about 2 million ν_μ CC per year) for the neutrino-argon cross-section measurements giving precise studies of neutrino-argon interactions in the GeV energy range. It will provide valuable insights for future neutrino experiments based on Liquid Argon Time Projection Chamber (LArTPC) technology, such as the Deep Underground Neutrino Experiment (DUNE). Understanding the physics of these interactions is important for advancing our knowledge of neutrinos and optimizing the design of future experiments in the field.

2.2.2 MicroBooNE

Figure 2.9: MicroBooNE detector (picture from the FNAL website)

The main purpose of the MicroBooNE detector is to provide an explanation for the anomalous results observed by the MiniBooNE experiment. It was exposed to the beam in the same configuration as the MiniBooNE experiment but it used a different detection technology to obtain a better identification and reconstruction of the electromagnetic showers.
MicroBoone is a liquid argon TPC (170 ton) with a rectangular active region with a volume

of 2.33 m x 2.56 m x 10.37 m located on BNB axis. The TPC is composed of a three-plane wire chamber: one with 3.456 wires in the vertical plane and the other two with 2.400 wires per plane oriented at ±60 degrees with respect to vertical. Behind the wire planes, 32 PMTs are placed to detect the scintillation light produced in the Argon. The MicroBooNE data set was collected entirely in BNB neutrino mode. Their latest study includes all the charged-current ν_e and ν_μ interactions considering all possible appearance and disappearance effects within the 3 + 1 active-to-sterile neutrino oscillation framework [25].

2.2.3 ICARUS experiment

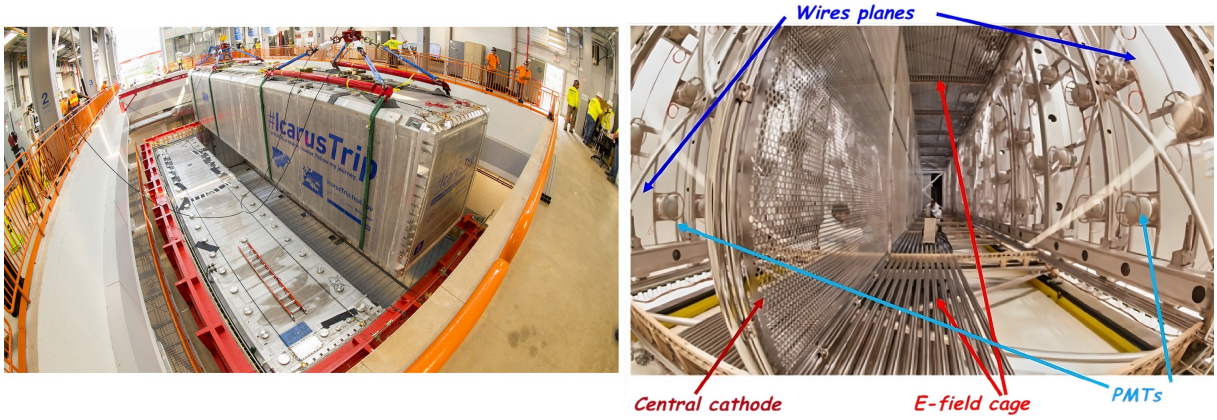

Figure 2.10: (left) Movement of the T600 during the installation at FNAL and (right) picture of the interior of the TPC, from FNAL website.

The ICARUS (Imaging Cosmic And Rare Underground Signals) T600 is the first large-scale LAr-TPC detector ever built.
The primary aim of the ICARUS T600 experiment is to study neutrinos and their properties and to identify signatures of neutrino oscillations. In fact, the LAr TPC technology allows to reconstruct the topology and the calorimetry related to the neutrino interactions with high resolution and precision. By detecting and studying these neutrino interactions, ICARUS can provide valuable data for understanding neutrino-nucleus interactions and improving the accuracy of neutrino oscillation measurements.
After three months of data taking on the surface in Pavia during 2001, the full ICARUS T600 detector was exposed for the first time to the CNGS neutrino beam between 2010 and 2013 in the Laboratori Nazionali del Gran Sasso (LNGS) in Italy. In this underground location, the detector was protected by 1400m of rocks that reduced cosmics muon flux by a factor of about 10^6. For each triggered event, the signals produced by a single particle crossing the detector (cosmic muon or neutrino interaction) were recorded. The events recorded in this first physics run demonstrated the effectiveness of the LAr-TPC detecting system, leading the way toward the construction of more giant detectors, as the Deep Underground Neutrino Experiment (DUNE), a detector under construction for the study of the neutrino oscillations. In fact, ICARUS serves also as a prototype for future large-scale liquid argon detectors. By operating and testing this technology, it aims to provide valuable insights into the construction, operation, and performance of such detectors, which are crucial for future neutrino experiments.
Between 2014-2020 the detector was moved from LNGS through CERN to FNAL. In particular

starting from December 2014 the T600 has been transported to CERN and underwent a significant overhauling phase in order to prepare the detector for the new data taking at Fermilab within the SBN experiment. This process was concluded in 2017 and the two modules were transported to FNAL and safely arrived at the far site during the summer 2017. The detector installation started soon after and it has been completed at the beginning of 2020. Between February and April the detector has been filled with Liquid Argon and the recirculation systems, needed to purify the Argon in the detector, have been activated. The final T600 activation and the new data taking, initially only with cosmics, was in August 2020.
ICARUS is currently taking data in the SBN far detector location, documenting interesting events both related to the Booster neutrino beam and to cosmic rays. In addition, ICARUS is also exposed to the off-axis neutrinos from the NuMI beam, in the 0÷3 GeV energy range, with an enriched component of electron neutrinos (a few per cent levels). ICARUS project will collect around one million BNB neutrino interactions in 3 years of data taking. One of the most important challenges for the study of these neutrino interactions is related to the T600 detector taking data essentially on the Earth's surface without the natural cosmic ray shield provided by the mountain at the Gran Sasso location. The cosmic rays continuously crossing the detector present a significant obstacle, especially in the quest to find electron neutrinos, because they can generate electromagnetic showers that mimic genuine neutrino events. Additionally, primary cosmic photons and neutrons can induce interactions in the detector that mimic electron neutrino-like behaviour. To tackle these cosmic background sources, it is used simultaneously a layer of 2.85 meters of concrete (added to the top part of the detector) and a Cosmic Ray Tagging system which surrounds the detector (see the CRT section). In the next subsections, a brief introduction and an explanation of all the parts that compose the ICARUS detector will be provided. For a more complete description of the detector and of the commissioning activities see [26], [27].

TPC modules and cryogenic system

ICARUS is composed of two large identical modules filled with 760 tons of ultra-pure liquid Argon with an active mass of 476 t. The two modules have internal dimensions of (3.6 × 3.9 × 19.6) m^3 and each module hosts two separate LAr-TPC with a common cathode.
The cathode is built in stainless steel and has an optical transparency of 58% between the two modules, while the anode is made of three parallel wire planes at 3 mm apart, placed at different angles between each other. Considering the inclination with respect to the horizontal direction, the Induction 1 plane is at 0°, while Induction 2 and Collection are at +/-60°. The total number of wires in the detector is 53248 and inside each wire plane the distance between two consecutive wires, as well as the distance between two adjacent wire planes, is 3 mm. The applied 500V/m electric field between the cathode and anode requires for electron $\simeq$ 1ms to drift over 1.482 m distance ($v_{drift} \simeq 1.6 mm/\mu s$ velocity). The signals collected on the wires are then recorded using the read-out electronics that are installed outside the detector. In this system, which has been upgraded with respect to the Gran Sasso run during the overhauling phase at CERN, the analogue and digital electronics are integrated into a single new CAEN board with a compact design. Each board can record the signals from 64 wire channels (32 wires from Collection+32 wires from Induction 2 or 64 channels from the same wire plane). In these boards, all the

amplifiers have the same filtering, preserving the bipolar characteristic of the signals that are recorded on the Induction 1/2 wires. Each amplifier is then followed by a serial 12-bit ADC, one per channel, with 400 ns synchronous sampling. The TPC wire signals are conveyed to the front-end amplifiers through special boards (DBBs) that are also used to provide the proper biasing to the wires. Finally, nine boards serving 576 channels are hosted in a custom small mini crate that is installed externally on a feed-through flange and globally 96 mini-crates are mounted on the top of the detector.

In the liquid argon TPC detectors, one of the main technological challenges is the purification of the Argon itself. The presence of electronegative impurities such as Oxygen (O_2) can absorb the ionization electrons producing an exponential decrease in the signal observed on the wires along the drift coordinate. To avoid this problem, which can make the wire signals associated with the passing particles too low to be identified above the wire noise, the Argon must be continuously filtered and recirculated both in the liquid and in the gas phase. In the ICARUS detector, pure Argon is maintained at low temperatures and continuously purified by a dedicated cryogenic system, which has been stable and functioning effectively since the detector was filled with liquid argon (LAr). The purity level of the liquid argon in both modules is consistently and automatically monitored in real time by studying the attenuation of the charge signal along the drift time on cosmic muon tracks. This continuous measurement allows to correct the attenuation effect improving the precision in the calorimetric measurement (figure 2.11).

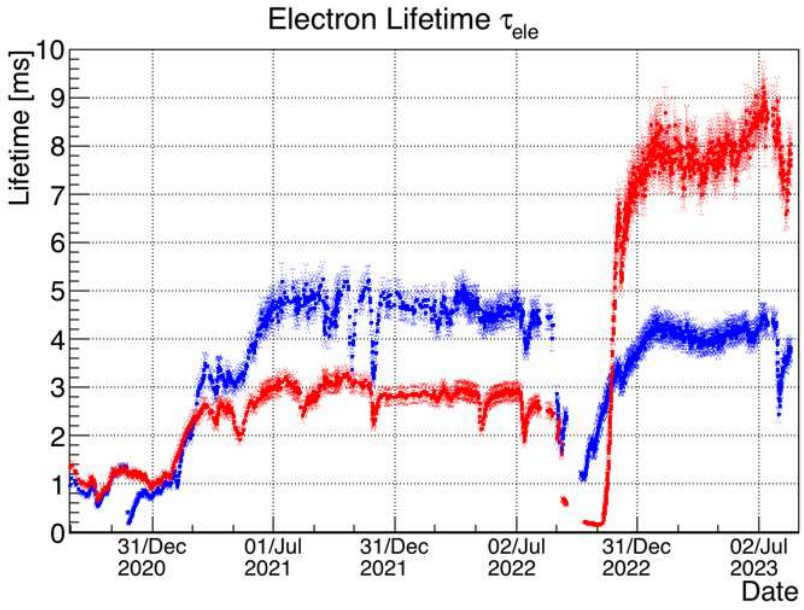

Figure 2.11: Purity behaviour since the activation of the ICARUS TPC detector. The measurements in the WEST cryostat are shown in red, while the measurement for the EAST cryostat are in blue.

During the commissioning of the T600 the TPC electronic noise levels have been continuously measured calculating the RMS of the waveforms from the TPC readout. The presence of a large coherent noise component, affecting groups of 64 channels recorded by the same board requires a dedicated noise subtraction study of the wire signals, to identify the physical energy deposition. The level of the measured noise before and after the coherent noise removal is shown in figure 2.12. In addition, considering runs with sufficiently high purity, the study of tracks crossing both

the anode and the cathode in one TPC allowed for an evaluation of the peak signal-to-noise ratio for minimum ionizing particles. This measurement demonstrates that the detector conditions allow for efficient identification of the physical ionization signals: more than 99% of the signals associated to muon tracks have a signal-to-noise ratio greater than four (see figure 2.13) [26].

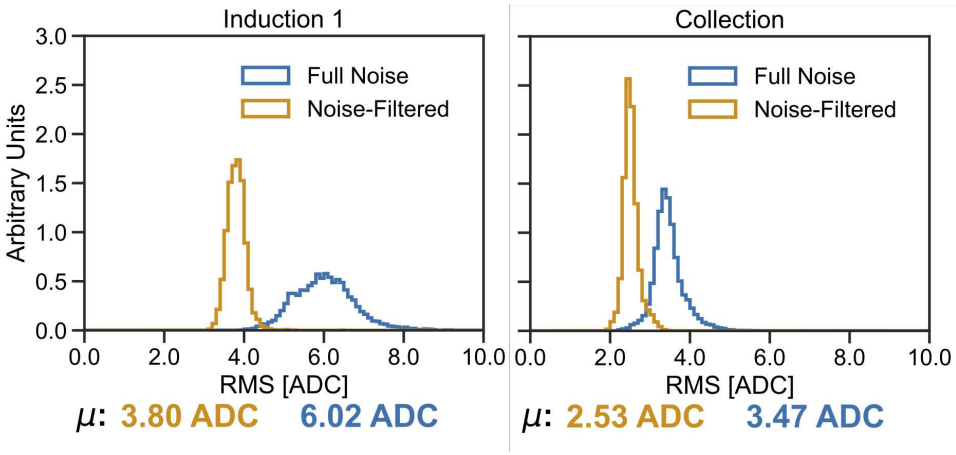

Figure 2.12: Before and after filtering of coherent noise in TPC.

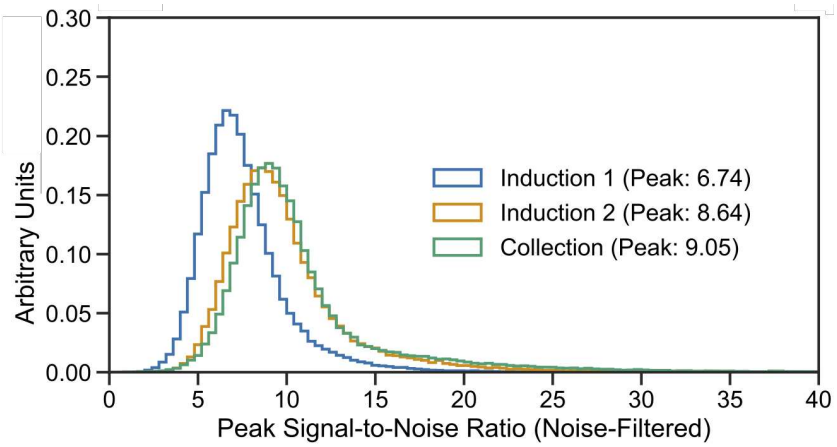

Figure 2.13: Signal-to-noise ratio of ionization signals after the coherent noise removal in TPC.

PMTs and the Trigger system

The light detection system consists of 90 photomultipliers (PMT) located behind the wire planes within each TPC. Its primary purpose is to generate a trigger signal based on light and accurately determine the timing of each interaction with high precision (time resolution $\simeq$ 1 ns). Collecting an average of 15 photoelectrons per MeV of deposited energy, this system enables the triggering of the neutrino events, providing a high sensitivity for events with low deposited energy events (around 100 MeV). Furthermore, with a localization capability better than 0.5m, this system allows for the classification of various signals, such as cosmic rays or neutrino events, by analyzing the arrival time of prompt photons and the intensity of the collected light signal.
During the overhauling phase at CERN, all the new 360 PMTs have been tested. The PMT glasses have been coated with $\simeq$ 200 µg/cm^2 of tetra-phenyl butadiene (TPB) to convert the 128-nm wavelength scintillation light generated in liquid argon to visible light. By applying

TPB, the PMTs can effectively capture and detect the scintillation light emitted in liquid argon, enabling the measurement of relevant signals in the visible light spectrum. This light detection system reached completion in 2019 and was subsequently activated following the successful filling of the detector with liquid argon.

The PMT system is presently the basis for the trigger of the detector. Originally, at the very beginning of the data taking at Fermilab, the trigger system was developed to record every beam spill associated with the BNB and NuMI beams. Then, it was implemented a new system that involved detecting the scintillation light captured by the PMTs in coincidence with a proper beam gate that is centered around the beam spill window. The generation of beam spill gates relies on the reception of "Early Warning" (EW) signals for the BNB and NuMI beams. These EW signals are received 35 ms and 730 ms in advance of proton-on-target, respectively. The timing of these signals is crucial to start the readout process, ensuring that the detector collect data at the appropriate moments aligned with the beam operations. To generate the trigger a specific request in the light recorded in coincidence with the beam spill is applied. Each TPC is divided into 5 overlapped regions along the beam direction and inside each region, the 30 PMTs are grouped into pairs based on their spatial position (see Figure 2.14). A threshold on the recorded light signal of 13 photo-electrons is applied to each PMT. The presence of at least 5 PMT pairs over the threshold in coincidence with the beam gate, generates a global trigger signal and the event is fully recorded. All the TPC wire signals for about 1.6 ms are recorded with a sampling time of 400 ns, while the PMT signals around the trigger and corresponding to 26 μs are saved with a sampling time of 2 ns. In addition, the PMT signals are also saved for an interval of 10 μs inside a 2 ms window around the global trigger, if at least 9 PMT pairs in a 6 m slice are over the threshold. This allows the study of the light signals corresponding to the cosmic rays crossing the detector during the TPC event recording. The events can be recorded also under additional different trigger conditions: for example, a trigger gate with the same requirements as the ones associated with the beam spill, can be generated when the beam is not present or between two physical beam spills ("off-beam" events). In addition, events can be also recorded without any specific requests on the light both in coincidence with the beam spill (on-beam min-bias events) or between two physical beam spills (off-beam min bias events). These particular kinds of events can be recorded only for a sub-sample of spills. Since no light is required, each time the gate is opened, the event is automatically recorded. These events allow to study of the trigger performance, to analyze possible background events for the analysis of cosmic-only events and to record events for calibration purposes. All these recorded events then underwent careful analysis to identify and reconstruct the recorded neutrino events and the crossing cosmic muon tracks.

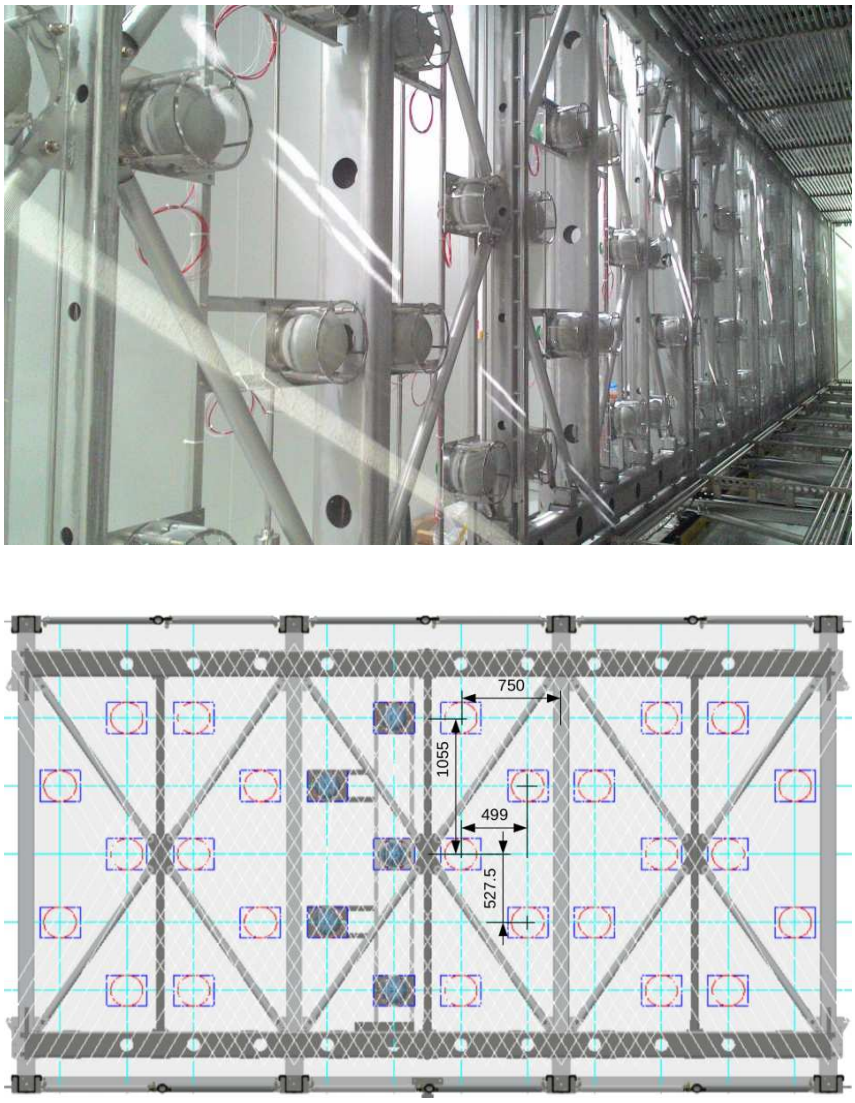

Figure 2.14: Top: View of PMTs positions inside the TPC. Bottom: visualization of PMT configuration Each purple circle represents a PMT [28]

CRT

The ICARUS-T600 detector is taking data at shallow depth, protected by a 2.85 m concrete overburden as previously discussed. With this shield, it is possible to eliminate all primary photons and reduce neutrons by a factor of 200. Moreover, it will suppress primary muons and their associated showers by approximately 25%. Consequently, the overall number of cosmic-induced backgrounds reaching the active liquid argon in the detector is significantly reduced.
To ensure an accurate identification of the residual incoming cosmic charged particles in the detector, the T600 is surrounded also by an external Cosmic Ray Tagging System (CRT). Three distinct subsystems, the top, the side and the bottom (not operating yet) each one featuring two layers of plastic scintillators, cover a total surface area of approximately 1100 square meters. The CRT enable precise tagging of these cosmic particles in terms of their time (resolution of the order of ns). The signals from this external detector combined with the signals from the T600 internal PMT system, will allow to unambiguously identify cosmic rays entering the detector and will allow measurement of the direction of the particle propagation via time of flight discriminating

between the incoming/outcoming particles. At the same time, an effective method to select an enriched sample of fully contained neutrino events is the requirement that no signal is recorded in the CRT in coincidence with the beam spill. In figure 2.15 the suppression of the rate for horizontal and vertical modules of the top CRT before and after the installation of the concrete overburden is evident.

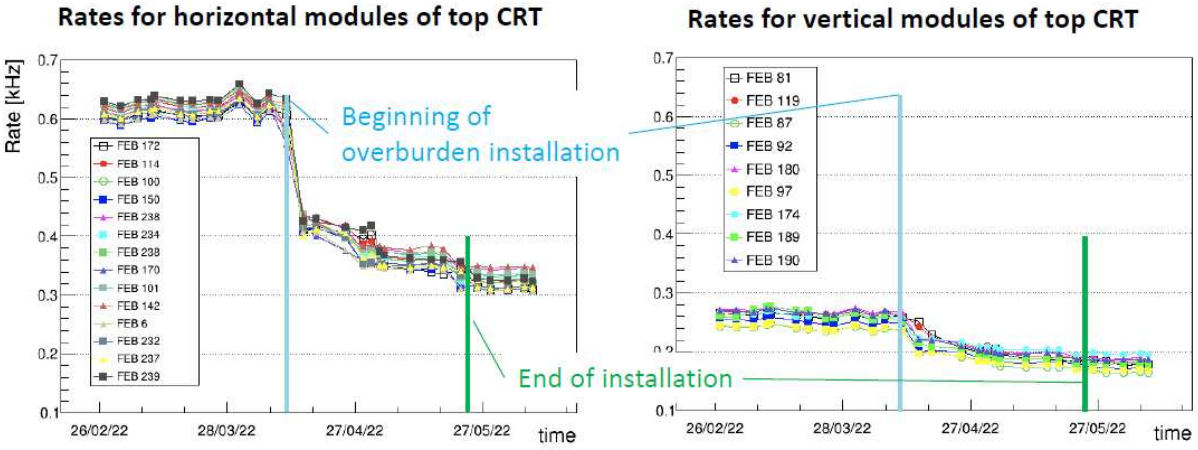

Figure 2.15: CRT rates before and after the installation of the concrete overburden.

Icarus initial operations

The ICARUS-T600 detector was first fully operational in June 2021, before the summer beam shut down. In particular, a full-time ICARUS neutrino beam run as BNB primary user ("Run0" data taking) has been performed during June 2021, collecting approximately 2.8×10^{19} proton on target (p.o.t) from the BNB and 5.2×10^{19} POT from the NuMI beam with a 95% efficiency. In this initial stage, the events recorded in the BNB and NuMI beam were carefully examined, focusing on selecting tracks within the cryostat where the trigger signal was generated. Figures 2.16 and 2.17 shown two types of neutrino events collected by ICARUS. Muon neutrino Charge Current events were chosen based on the presence of a long track (at least 0.5 m) originating from the primary vertex. In figure 2.16 a short track with high ionization (proton), and a longer track (muon) stopping inside the detector is clearly visible. This indicates a ν_μ CC quasi-elastic event. Instead, the electron neutrino event associated with the NuMI beam is characterized by the presence of a clear electromagnetic shower connected to the primary vertex, as shown in figure 2.17.

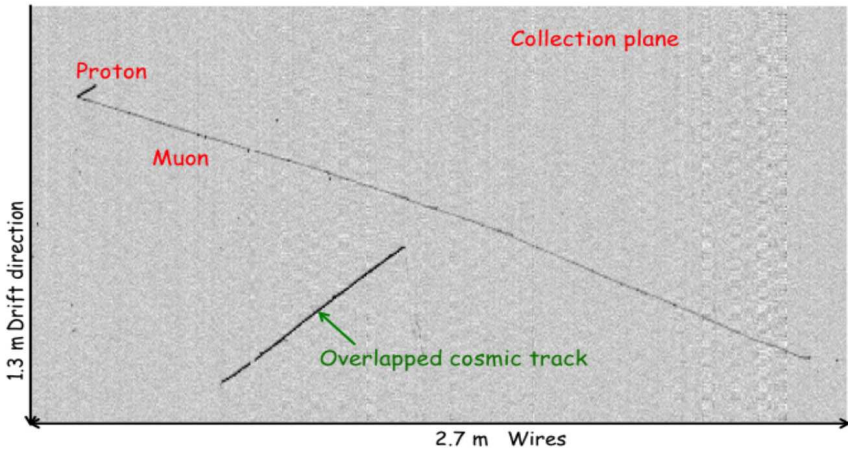

Figure 2.16: ν_μ event

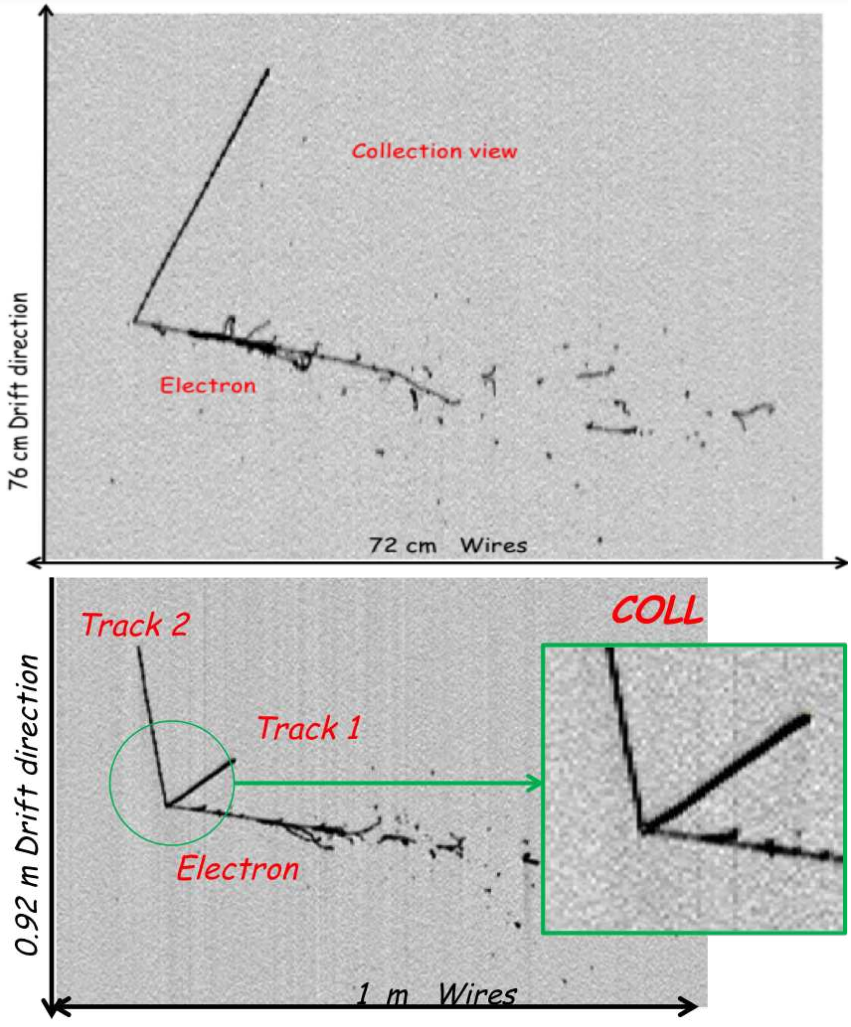

Figure 2.17: ν_e event from NuMI

After this first Run0 data taking, the TOP CRT installation was carried out and it was completed in December 2021. During spring 2022 the 2.85 m concrete overburden was also deployed above the TOP CRT concluding the installation and commissioning phases. The ICARUS Run 1 officially began on June 9 2022 and lasted until July 10 2022 when the beam summer shutdown

started. The data acquisition was largely successful: during Run 1 about 6.8×10^{19} POTs from the BNB beam and about 4.1×10^{19} POTs from the NuMI beam has been recorded. A second physics run (Run-2) started on December 20th after additional detector improvements were introduced: in particular the interventions on the cryogenics and purification systems allowed to increase the purity of the Liquid Argon, as shown in figure 2.11. This Run-2 data taking was completed in July 2023 with a detector lifetime exceeding 95% (see figure 2.18).

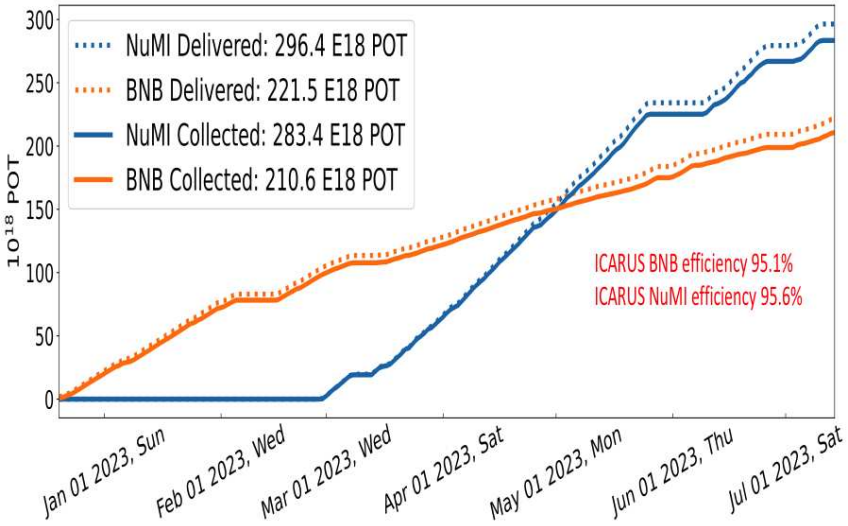

Figure 2.18: BNB and NuMI POT collected during the RUN-2 in ICARUS

2.3 Physics at SBN

The SBN program aims to conduct a sensitive search for high-Δm^2 neutrino oscillations over a period of 3 years, achieving a 5σ sensitivity on the parameter space indicated by LSND. Neutrino interactions corresponding to approximately 6.6 x 10^{20} proton on target from the BNB will be collected in the detectors. The detection of oscillation signals relies on the utilization of LAr-TPC detector technology, which offers excellent performance in tracking, electromagnetic shower reconstruction, and calorimetric measurements, enabling an efficient identification and reconstruction of ν_μ and ν_e interactions. Employing multiple stations on-axis along the beamline will allow simultaneous measurement of the appearance of electron neutrinos and the disappearance of muon neutrinos.

Oscillation signals can be identified by comparing the measured spectra at near and far locations. The choice of LAr-TPC detectors also facilitates effective control of backgrounds and systematic effects that may affect the analysis. The expected sensitivities of the SBN experiment are presented in figure 2.19.

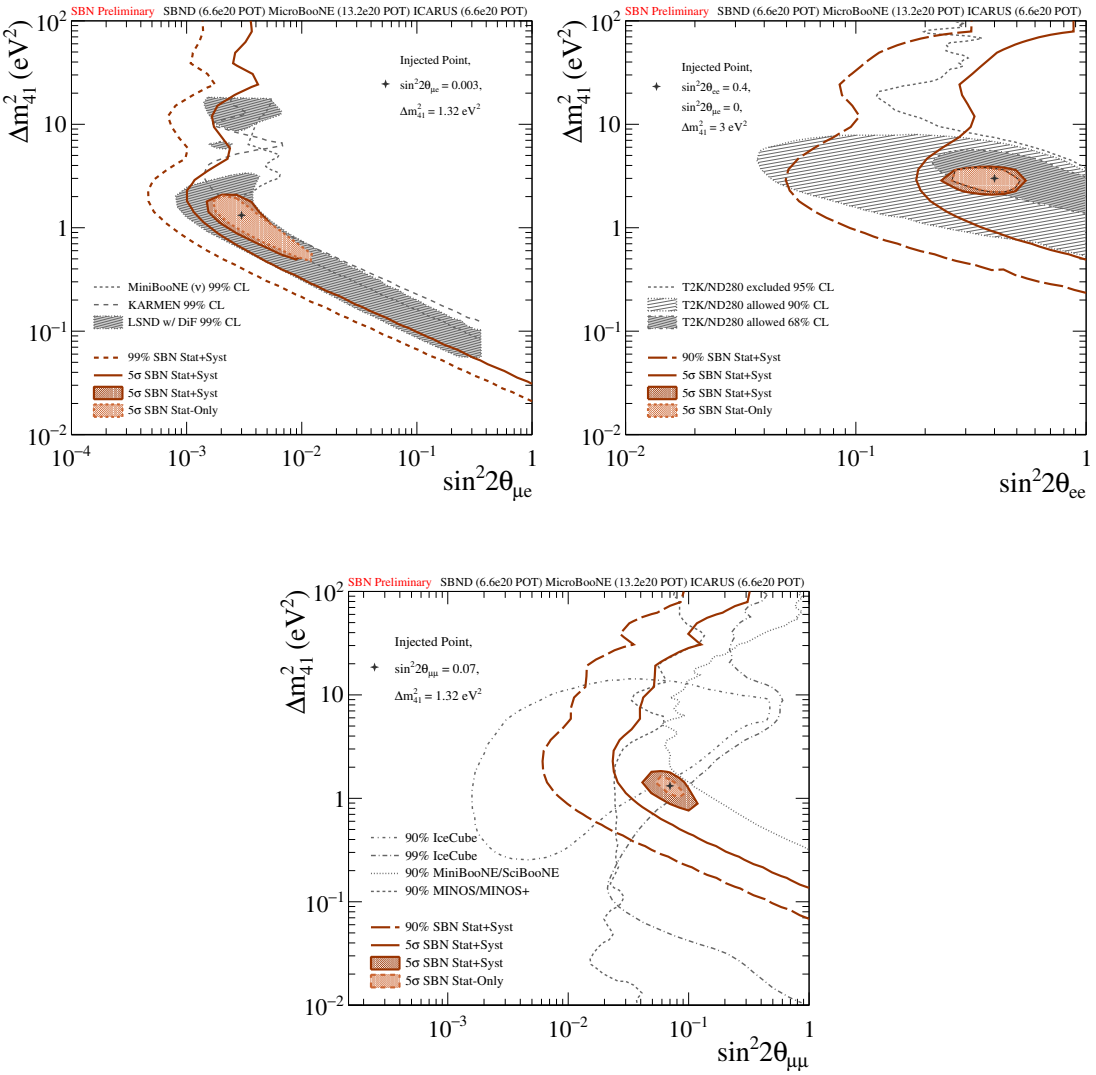

Figure 2.19: Expected sensitivity for three years of data taking.

As previously mentioned, the ICARUS T600 experiment is exposed to the off-axis flux of the NuMI neutrino beam. The analysis of ν_e and ν_μ events originating from the NuMI beam will enable ICARUS to measure with high statistics cross sections for neutrino-argon interactions (10^5 ν_e events/year) and enhance the reconstruction and identification of neutrinos. In figure 2.20 the event spectrum from the NuMI beam in ICARUS is shown.

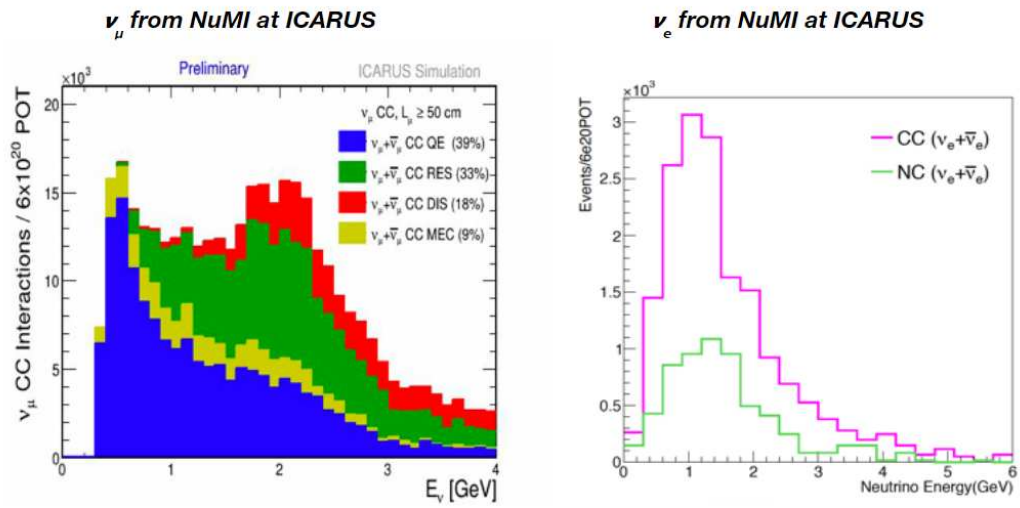

Figure 2.20: Expected ν_e and ν_μ events in ICARUS from NuMI

The ICARUS experiment can independently verify or disprove the Neutrino-4 oscillation signal using the neutrino events recorded in less than one year of data taking. The Neutrino-4 collaboration reported a modulation in the neutrino disappearance signal with a characteristic L/E (distance over energy) of approximately (1 - 3) m/MeV, corresponding to a Δm^2 of around 7.5 eV^2. ICARUS will have the capability to test this oscillation limit within the same L/E range, utilizing two separate channels associated with the exposure to BNB and NuMI beam. Firstly, it will search for a ν_μ disappearance signal in the BNB, focusing on quasi-elastic fully contained interactions where the primary muon has a length exceeding 50 cm. Additionally, ICARUS will investigate a ν_e disappearance signal in the NUMI beam, specifically selecting quasi-elastic contained events.

Figure 2.21 illustrates a comparison between the survival probability, assuming the best-fit value of oscillation parameters of Neutrino-4, and the expected measurement in ICARUS. This comparison is made in the presence of an oscillation signal for both muon neutrinos and electron neutrinos. Studying these two channels would provide the necessary confirmation of the modulation associated with the oscillation parameters suggested by Neutrino 4.

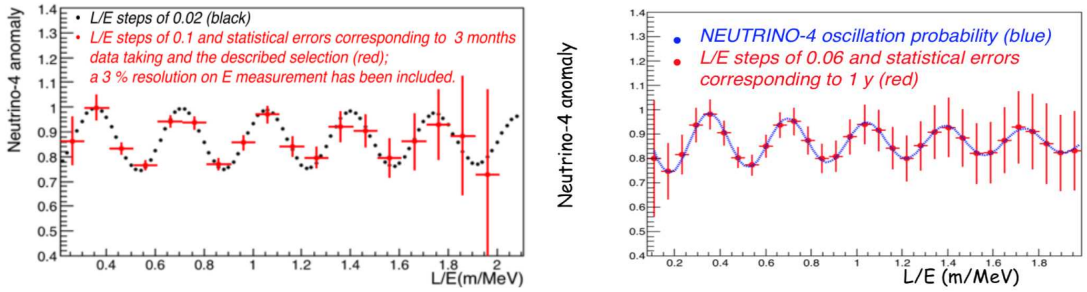

Figure 2.21: Expected survival probability of ν_e (right) and ν_μ (left) assuming three months (for ν_μ) and one year (for ν_e) of data taking, $\Delta m^2 = 7.25 eV^2$ and $\sin^2 2\theta \simeq 0.26$

Chapter 3

Data recostruction

Simulation and reconstruction of the recorded signals constitute a crucial phase in the study of particles crossing the detector, with particular attention to neutrinos. In this section some details on both the simulation and the reconstruction of the events in ICARUS will be briefly presented.

3.1 Simulation of the events in ICARUS

The simulation begins with the generation of the primary particles inside the detector, specifying their positions, directions and energies. This phase, known as the **"Icarus Gen Stage"**, strongly depends on the type of event that should be simulated. In particular, for the analysis described in this thesis, two different type of simulated events has been considered: the neutrino events and the so-called "in-time" cosmics.
For the simulation of the neutrino events, the **Genie**[29] generator is used, which provides all the information about the neutrino interaction (for example if the interaction is Quasi Elastic) and of the particles produced at the interaction vertex. Genie takes into account the cross sections and also it takes advantage of the expected flux and composition for the BNB neutrino in the T600 location. Finally, Genie also provides information about the equivalent protons on target that are simulated and provides a time distribution of the neutrino events similar to the expected beam spill.
For the simulation of the "in-time" cosmics, the **CORSIKA** [30] simulation program is used. It generates the cosmic particles that should reach the detector with the expected energy and time distribution, in a time window of 2.2 μs to match the usual gate opened for the trigger of the detector associated with the BNB beam. The simulation program then verifies that a cosmic particle reaches ICARUS sub-detectors (in particular the program verifies if there are signals in the PMTs) in order to store the produced event. On average only 1 simulated gate every 40 is not empty and then stored and fully simulated.
When the "gen stage" has been completed for the event, the particles are propagated inside the detector, taking into account all the physical processes for the particle in liquid argon (hadronic interactions, particle decays...). For example, the track for a muon produced in the neutrino interaction is propagated taking into account the energy loss along the propagation, the multiple coulomb scattering and all the other physical processes. Energy deposits are estimated point by

point along the particle tracks in all the regions of the detector, allowing the determination of the amount of energy deposited for each three-dimensional coordinate inside it.
Using the event information and exploiting the energy deposited point by point, it is possible to calculate how many scintillation photons and how many ionization electrons are generated along the track. These signals are then propagated inside the detector in order to evaluate the amount of scintillation light detected by each PMT and the signal induced on each TPC wire by the ionization electrons. By integrating the signals over all 3D points with deposited energy, the total number of photons collected in the various PMTs and the charge signal collected on each wire of the TPC are obtained. This phase of the simulation process, known as the "**G4 Stage**", is powered by the Geant4 [31] simulation program and is referred to as "truth" in our analysis. These *truth information* are stored not only for the simulation of the signals in the different sub-detectors but also for a comparison between the reconstructed quantities and the expectations before introducing any other effects.
After obtaining the "truth" signals produced by the G4 Stage the simulation of the detector is introduced. During this phase, called "**DetSim**" (Detector Simulation), the signals are formatted with all the characteristics of the acquisition electronics used, including the electronic noise, for all the sub-detectors. The produced signals are equivalent to the one detected in real data and after this stage, the MC events can be treated essentially as the real event.

3.2 Reconstruction of the events in ICARUS

The reconstruction of the events in ICARUS is performed in two stages which produce the data used for subsequent analyses. In the first **stage 0** physical signals are identified in all sub-detectors while in the following **stage 1** more complex analysis are done, such as the reconstruction of the tracks in TPC. At the end of these two stages, all the reconstructed objects and the results from the different analysis tools are stored in dedicated analysis files: in particular, for the studies performed on this thesis the calibration ntuples format has been used. These files contain all the information related to the TPC tracks reconstructed, with the associated information in each wire plane, and to the signals recorded on the PMT and CRT. It Is important to mention that in this work, only the basic information related to the TPC reconstruction are used, with a focus exclusively on tracks information, omitting more high-level reconstruction details such as the neutrino, the vertices, and the showers object provided in the stage1. This approach is adopted to avoid potential biases or issues arising from the high-level reconstruction process applied in the stage1 and described in the following section. The neutrino events preselected using the criteria outlined in this thesis can serve the purpose of testing, validating, and improving the reconstruction performance.

TPC reconstruction

The first step for the identification and reconstruction of the signals in the TPC wire planes is the removal of the coherent noise component that is observed over 64 electronic channels in the same TPC read-out board. This technique facilitates the identification of the physical hits drastically reducing the number of fake signals and improving all the following reconstruction steps. However, there is a possibility that the removal of the noise can slightly impact the

reconstruction of the real tracks. The presence of segments of tracks that are parallel to the wire plane and whose signals are recorded at the same time on the wires can be partially misidentified as noise as well as in general part of the physical wire signals may be subtracted together with the coherent noise component. All these effects result in the potential loss of valuable information, translating then in a small reduction of efficiency for the identification of the physical signals.
The following step for the TPC reconstruction is the deconvolution process of the wire signal to extract the ionization signals on the wires by eliminating effects linked to the electric field between wire planes and to the signal shaping introduced by the front-end electronics. There are four primary factors at play: when the particle trajectory traverses the detector, electrons are generated not exclusively in the vicinity but within a confined area surrounding the trajectory. Additionally, there's electron diffusion in argon that enlarges the cloud of ionization electrons while drifting to the wire planes; upon reaching the wire plane and in the passage near the wires, an electric signal is induced in the wires and finally, the signals are recorded by the front-end electronics. The deconvolution process allow to remove the last two effect and for this reason, the physical signals in the wires are expected to have, after this treatment, a Gaussian shape.
Subsequently, the physical hits are recognized on a wire-by-wire basis. In this scenario, the requirement is for a signal above the baseline, whose height exceeds a threshold that is plane-dependent. The identified hits are fitted with a Gaussian and to each hit the information about wire, time, and hit area is stored.

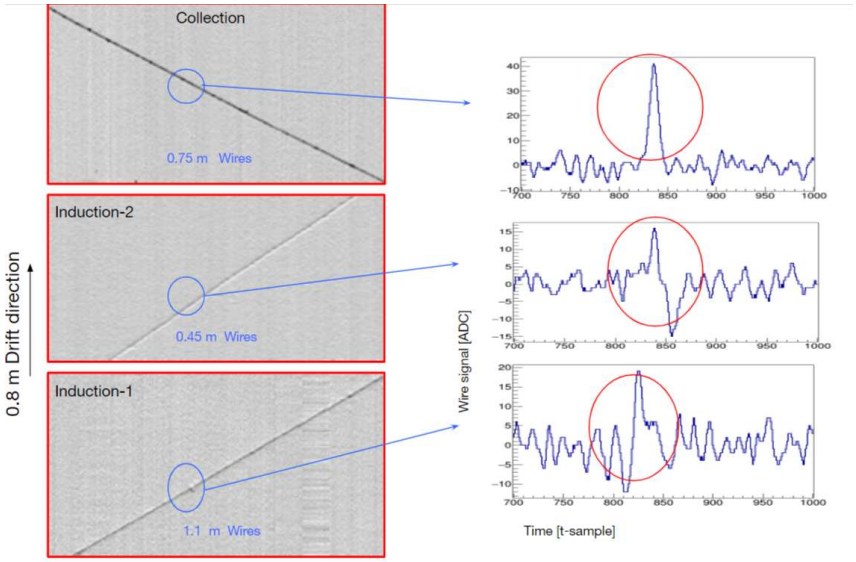

Figure 3.1: Wire signal (on the right) taken from the corresponding wire plane in the TPC, for a crossing muon.

Once the physical signals are found in each wire plane, the hits from different wire planes in the same TPC are combined to create 3D space-points. The association is made on the basis of the hit time: the hit signals in the 3 wire planes should have the same drift time if corresponding to the same deposited energy. The requirement to create a space point is reduced to at least 2 hits from two different wire planes when it is impossible to cluster together a point in the three views. This approach ensures that informations related to physical points are maintained even in presence of some inefficiency in one wire plane. Finally, only the hits associated to a space

point are considered for the analysis while the remaining hits are removed.
After collecting all the space points in the so-called "**cluster 3D**" phase, this information is provided to "Pandora" in order to obtain the final reconstruction of the TPC recorded signals. Pandora is a pattern recognition multi-algorithm tool that aims to group together adjacent hits into clusters related to the same particle and to classify the cluster properties, discriminating for example the tracks from the showers. A depiction of the functioning of the reconstruction tool can be seen in Figure 3.2.The first applied stage is defined PandoraCosmic: in this phase Pandora considers all the 2D signal hits available and it identifies all the track that are candidates to be cosmic-ray muons and separate them from the other particles. These track candidates highlighted as possible cosmic rays are also flagged as “Clear Cosmic”. In the second step, defined as "PandoraNu", the algorithm starts from the residual 2D hits and it is devoted to the reconstruction of all the neutrino candidates interactions. The tool will reconstruct and save the information about the presence of vertices, tracks, showers, etc. In fact, this reconstruction process detects a vertex corresponding to a neutrino interaction candidate and facilitates the reconstruction of all particles exiting from this vertex location, classifying them as tracks or showers.
Through reconstruction using Pandora, it is also possible to define important characteristics of the identified track signals. In general the recorded time of the hit is related to both the crossing time (t_{cross}) of the particle and the drift time of the ionization electrons t_{drift}

$$t_{hit} = t_{cross} + t_{drift} \tag{3.1}$$

The t_{cross} time is usually unknown for particle crossing the detector at a time different from the trigger time. The x-coordinate, which depends only on t_{drift}, is calculated using the available hit time and so it is usually wrongly estimated for these out-of-time particles because the reconstruction is assuming $t_{cross} = 0$. If a track passes through the cathode, the program will attempt to connect the two track segments to the right and left side of the cathode. This connection will use the 3D direction of the two segments, and the requirement that the y and z coordinates and the hit time of the crossing points in the two TPCs should be similar. Once the algorithm recognizes that the two segments belong to the same particles, a unique track is reconstructed. In addition, since the x-coordinate of the cathode is well defined, it is possible to obtain a direct evaluation of the crossing time of the particle and the corresponding correction of the x-coordinate along the track. These particular tracks are usually defined as cathode crossing "t_0-tagged" tracks and the t_{cross} is often indicated as t_0 of the track.
It is also important to notice that depending on the t_0, a track crossing the detector can not be fully visible in the recorded TPC waveform, which is about 1.6 ms long. Let’s take for example a track crossing the detector at t_0 and crossing both anode and cathode: the ionization signal produced near the anode will be recorded in the waveform at the time $t_{hit-anode} = t_0$ while the signals produced near the cathode are recorded at $t_{hit-cathode} = t_0 + t_{drift}$ with t_{drift} corresponding to the maximum drift time in the TPC (about 0.94 ms). The track would be fully visible only if both $t_{hit-anode}$ and $t_{hit-cathode}$ are inside the time window recorded in the TPC waveform. Taking into account that for the TPC wires about 846 samples (400 ns each) are recorded before the trigger (pre-sampling) and globally 4096 samples are recorded, a t_0 tracks results fully visible

only if t_0 is between -338 μs and 357 μs.

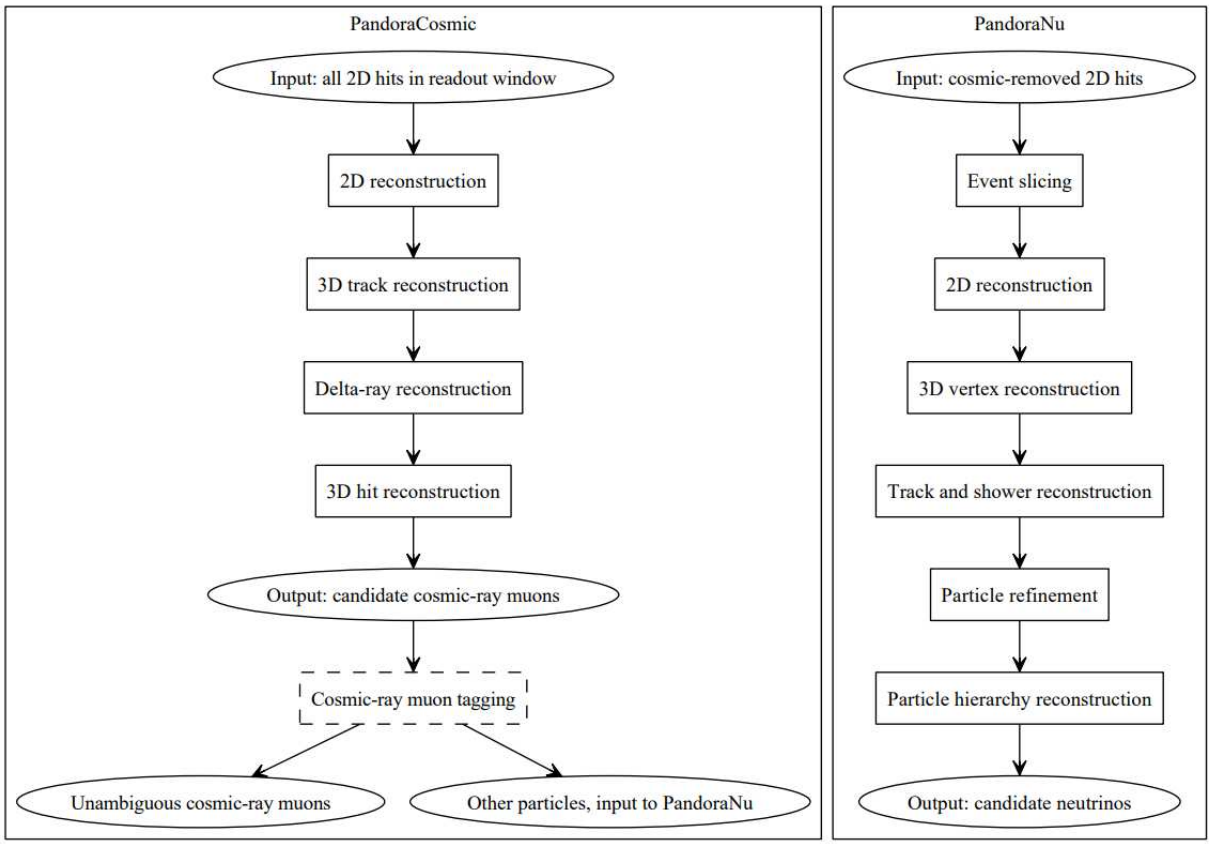

Figure 3.2: Description of the Pandora algorithm [32].

PMT and CRT reconstructions

The first step in the reconstruction process involves identifying the physical signals from PMTs, referred to as "Optical Hits." Each PMT waveform is analyzed individually, and signals above the baseline are detected using a low threshold of 0.5 photoelectrons (phe). Information such as start time, amplitude, and integrals of the hit is recorded. In a second step, time intervals of 100 ns are considered, and the optical hits from different PMTs collected within each interval are examined. If the sum of the integrals of optical hits that start within a time interval exceeds a defined threshold, a "flash" is created, and all the optical hits within a 1 μs window are grouped together. In this way, optical hits that coincide in time, which means that are related to the same particle, can be studied in a unique object. For each flash, the associated time (corresponding to the time of the first optical hit in the flash), integral (sum of integrals of all hits), and barycenter in the y and z directions are then determined.

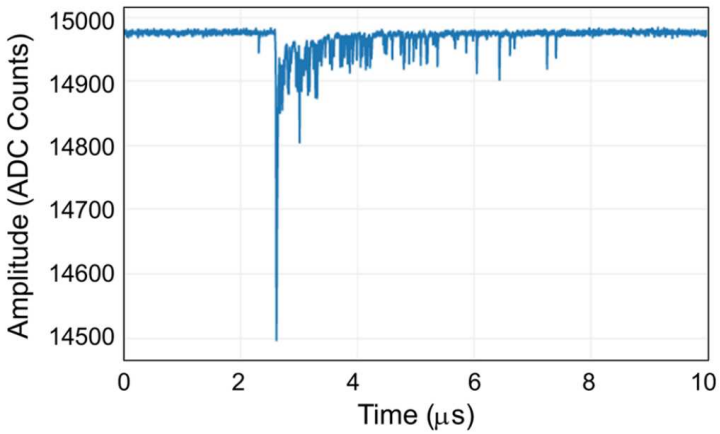

Figure 3.3: Recordered PMT signal by the detection system [26]

Similarly to the PMTs signals, the CRT signals detected by the SiPMs connected to the CRT scintillation bars are studied separately. Presently the main goal of the CRT reconstruction is the identification of the physical signals related to the passage of cosmic particles. When the recorded charge amplitude exceeds a defined discriminator threshold, a CRT hit is recognized and the used algorithm associates to this hit the position in space, the recorded time and the information about the signal amplitude.

3.3 Simulated event samples

For the development of the analysis described in this thesis, two different Monte-Carlo events have been considered, simulating the neutrino interaction and the cosmics passing in coincidence with the trigger gate. Some details about these events will be presented in this section.[1]

In-time cosmics

These events represent the possibility that a cosmic ray particle traverses the detector inside the trigger gate time window. In particular, in these MC events, only the particles "in-time" are simulated, while all the possible additional cosmics crossing the detector in the drift window of ±1 ms (out-of-time particles) are not simulated. These "in-time" particles could be the only source of trigger for the off-beam data. For the on-beam events, a fraction of the triggers is generated by neutrinos interaction in the active liquid argon or in the surrounding materials (case of the "dirt events")[2] while the majority of triggers is due to in-time cosmic rays. Figure 3.4 shows the deposited energy of the simulated "in-time" cosmic events in the detector. The peak at about E=800 MeV corresponds to vertical cosmic muons that are minimum ionizing particles and that transverse $\simeq$ 317 cm in the detector, that is the vertical size of the detector. The region of the spectrum below this peak represents the energy deposition of muons that stop

[1] An additional sample of MC events named "Single μ" has been also studied in the preliminary phases of this analysis: these events simulate only the muons that are produced in a BNB neutrino interaction and so with a direction strictly related to the BNB beam. This sample has been used in particular to set up the initial analysis. Since these events are not so "physical", no results from this sample will be shown in this thesis.

[2] This category of event will be explored in the conclusion part of Chapter 4

inside the detector or that partially transverse it while the region above the peak is enriched also by longer muons with a much more "horizontal" direction.

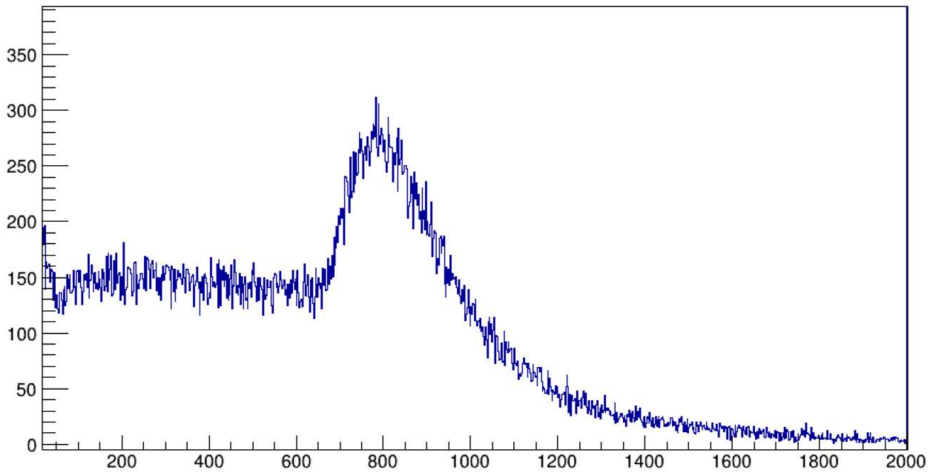

Figure 3.4: Distribution of the deposited energy in the detector by the simualted in-time cosmics events. The deposited energy is measured in MeV.

In this simulation, only a minimal request on the light collected by the PMTs has been applied to store the event. For this reason it is possible to have events that induce a light signal in the PMTs but are not crossing the active volume: in this case, there is a stored event in the MC but with no deposited energy in the detector. All these events produce a huge peak near the zero, which is removed in figure 3.4: these are $\simeq$ 30000 events, $\simeq$ 20% of the events simulated.

Neutrino events

These events simulate neutrino that interacts in the active liquid Argon. All the particles produced by the neutrino interactions are propagated inside the detector and produced tracks and showers emerging from the primary vertex.
In this sample, all the ν_μ CC interactions will be studied with a specific emphasis on quasi-elastic (QE) type, involving a muon produced with a length L_μ exceeding 50 cm and stopping within the active volume of the detector (that means the μ end-point is inside the active volume of the detector). These events correspond to $\simeq$ 20% of the total neutrino interactions and are distributed as shown in figures 3.5, 3.6 and 3.7. Table 3.1 summarises the Monte Carlo statistics available for this thesis.

Neutrino	$5.73 \cdot 10^{19}$ POT	66658 neutrino events
In-time cosmic	3732500 gates	91500 cosmic events

Table 3.1: Information on simulated Monte Carlo events.

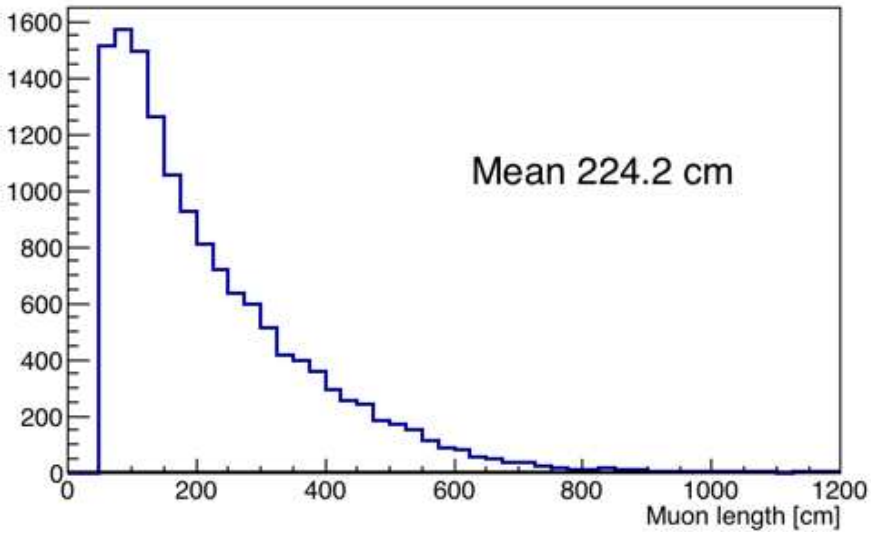

Figure 3.5: Muon length distribution for contained ν_μ CC QE neutrino interactions with a muon length starting from L_μ>50cm on MC neutrino events.

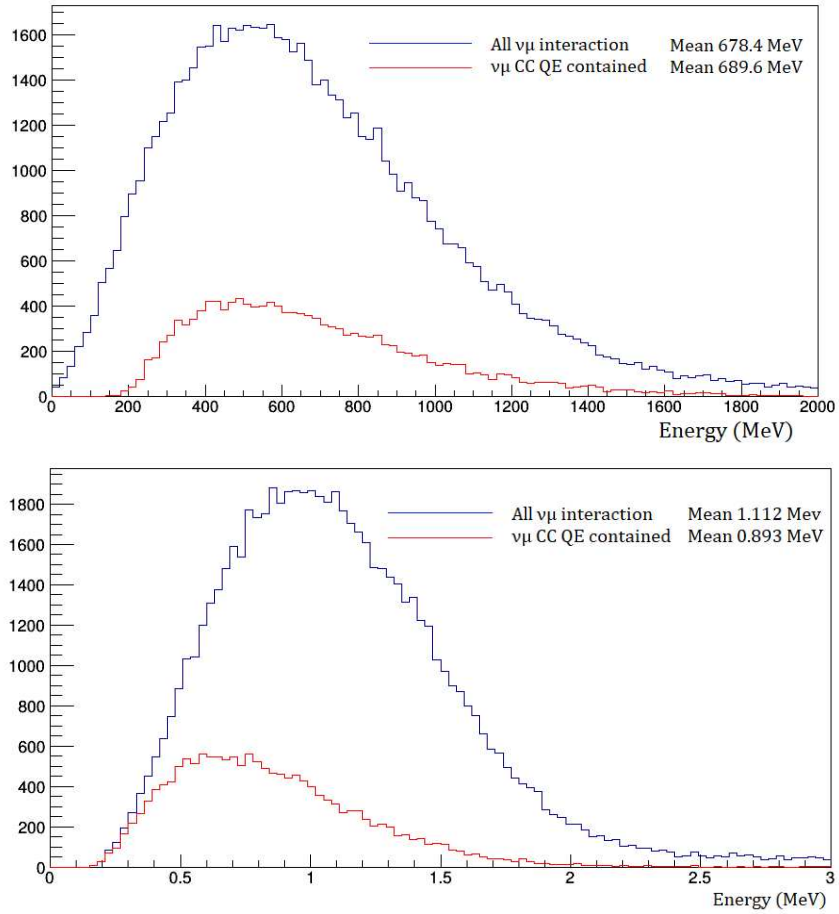

Figure 3.6: Distributions of the neutrino energies (top) and of the total deposited energies (bottom) for all the simulated ν_μ CC interactions (blue) and for the simulated quasi-elastic CC interactions fully contained in the detector and with a muon length L_μ>50cm (red).

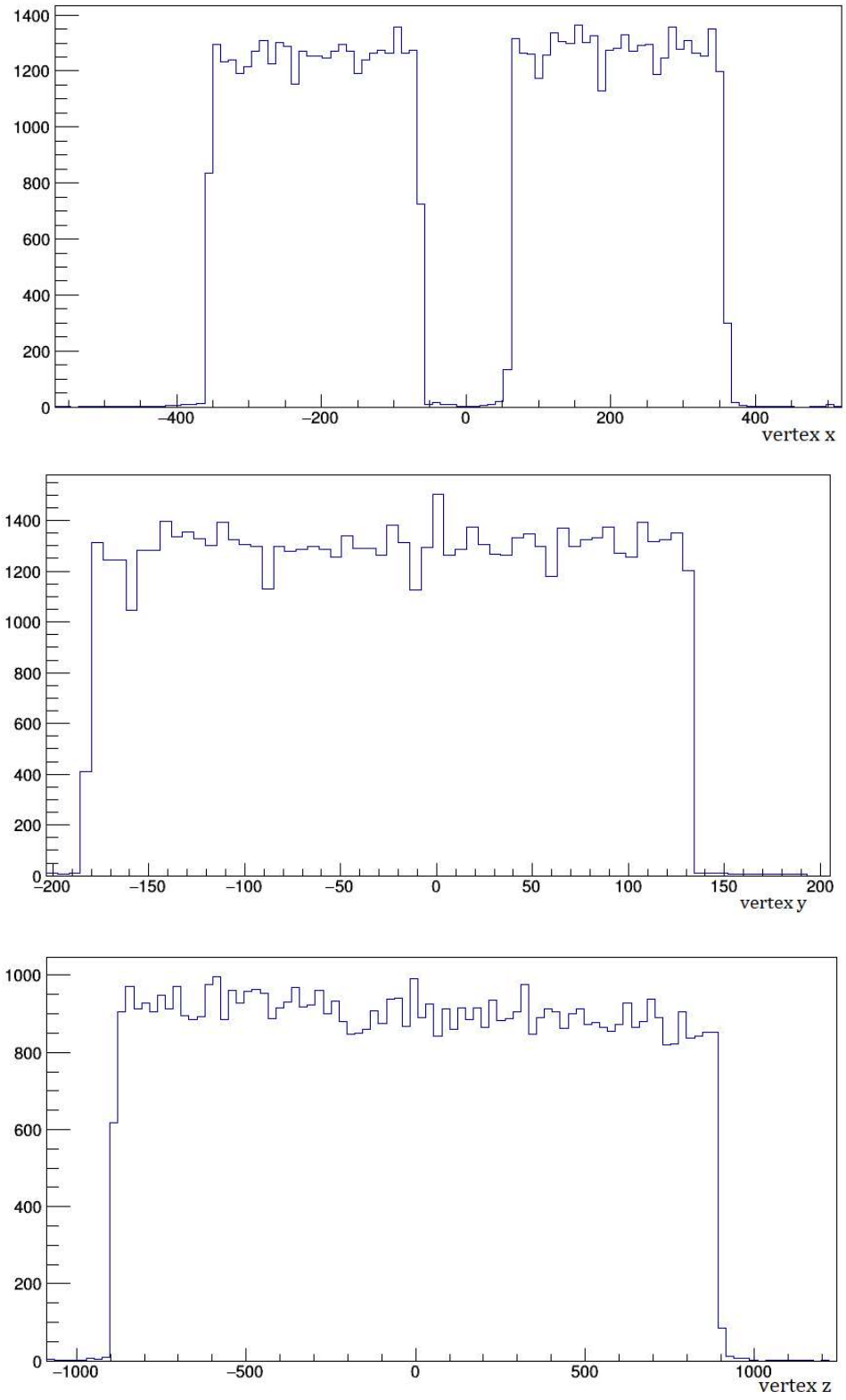

Figure 3.7: Vertex distribution for all ν_μ CC interactions along the drift (top), the vertical (middle) and beam (bottom) directions.

3.4 Analyzed data sample

The real events used in this thesis are collected in the detector under two distinct trigger conditions referred to as the "on-beam" and "off-beam" conditions. For on-beam events, the trigger opens a beam gate synchronized with the arrival of the BNB neutrino beam spill. In contrast, in the off-beam events, the trigger logic is identical but applied in a fake beam gate opened between two successive beam spills, to ensure that no beam interactions are present in the detector. This thesis analyzed the events collected by the so-called Majority trigger requiring a minimal multiplicity of 5 PMT pairs in coincidence with the trigger gate, as previously described. The "on-beam" and "off-beam" are recorded in parallel during the data taking and for each gate opened in coincidence with the beam spill, an additional gate is opened "off-beam". The data used in the analysis were acquired by the detector in two runs, summarized in the table 3.2.

RUN	**Date (dd/mm/yyyy)**	**P.O.T.**	**Spill**	**Available evt**
8460 (on-beam)	08/06/2022	$5.64 \cdot 10^{17}$	127638	3788
8460 (off-beam)	08/06/2022	$5.64 \cdot 10^{17}$	127638	2952
9435 (on-beam)	29-30/01/2023	$1.025 \cdot 10^{18}$	224369	7372
9435 (off-beam)	29-30/01/2023	$2.038 \cdot 10^{18}$	448994	10577

Table 3.2: Information on the run used for the analysis. For run 9435, only half of the available statistics has been considered for the study of the on-beam events.

As previously discussed, in real events are present contributions from both in-time and out-of-time particles. In the selection procedure it is possible that an out-of-time cosmic particle could be misidentified as an in-time one and consequently included in the selected sample. The impact of the out-of-time cosmics particles can not be directly evaluated using the MC simulations used in this thesis since in the simulation these particles were not included. To mitigate this potential issue, off-beam events will be employed. This offers a direct estimate of the expected cosmic background by both in-time and ou-of-time cosmic rays. Furthermore, given an identical number of open gates for both on-beam and off-beam triggers, the count of events selected by the filter linked to cosmic backgrounds in the two samples should be statistically equivalent, indicating a method to estimate their number.

Relevant differences between MC and real data

It is important to notice that the reconstruction procedure applied to the Monte Carlo events and to the real collected events is exactly the same, but there is a substantial difference related to the time reference within the events. The trigger time is the reference time in the data but not for the MC, since the trigger simulation is not implemented in the studied samples. For this reason, the t=0 reference time in the MC events is the starting time of the gate (for the in-time cosmics) or of the beam spills (for the neutrino events). This implies that when considering elements such as flash time or CRT hit time, these temporal differences have to be accounted for and the analysis modified accordingly. Figures 3.8 and 3.9 show the time differences between MC neutrino and real data from the CRT and from the PMT respectively. The in-time cosmic experience a similar behaviour as neutrinos.

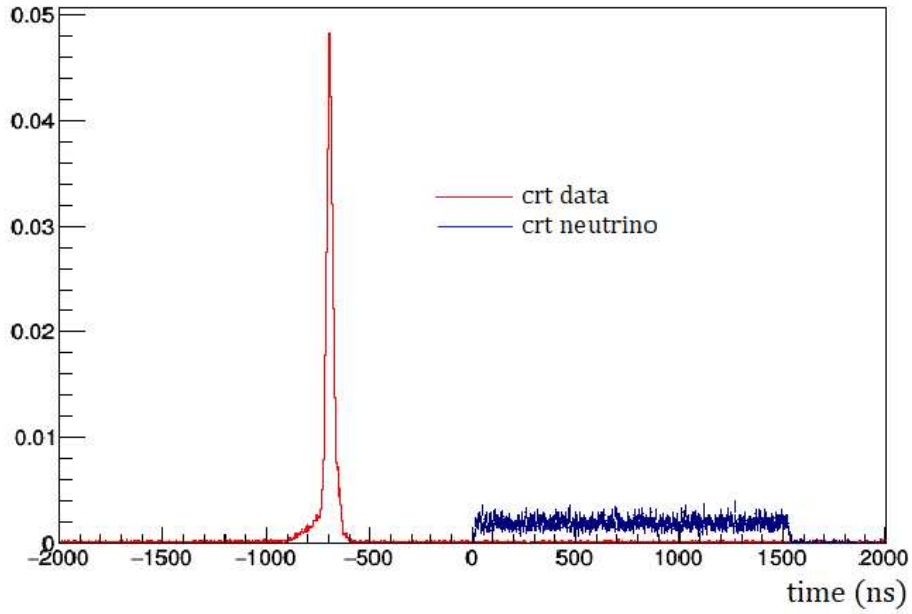

Figure 3.8: CRT hit time for real data (red line) and for neutrino MC events (blu line). See text for the discussion on the reference time.

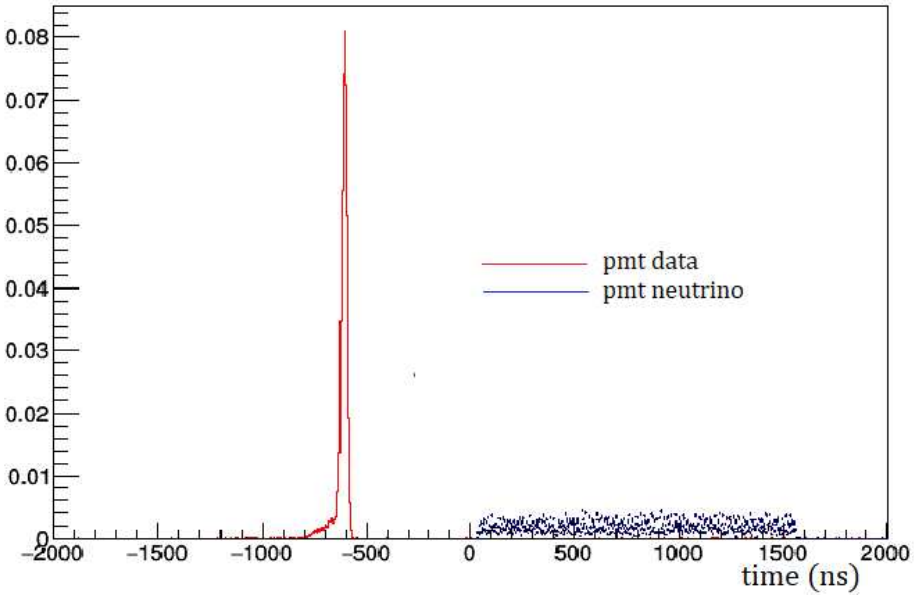

Figure 3.9: Time of the flash acquired by the PMTs for real data (red line) and for neutrino MC events (blu line). See text for the discussion on the reference time.

Table 3.3 summarizes the time window that has been considered to identify in particular the signals recorded by the PMTs for all the data sets studied in the analysis. If more than one flash is acquired, the first one that occurs temporally has been chosen for this analysis.

Dataset	Starting RT	Ending RT
Neutrinos	-0.1 μs	1.8μs
In-time cosmics	-0.5 μs	2.5μs
Real Data	-0.68 μs	-0.54μs

Table 3.3: Reference time used for the search of Δz in the PMT flash time.

For real events, the presence of the particles crossing the detector just before the gate opening and whose scintillation light has produced a trigger should be also taken into account[3]. These possibilities are represented by the tail at low t_{flash} shown in figure 3.10. To reject these events, a restricted time interval is used considering only flashes with a $-0.68 < t_{flash} < -0.54$.

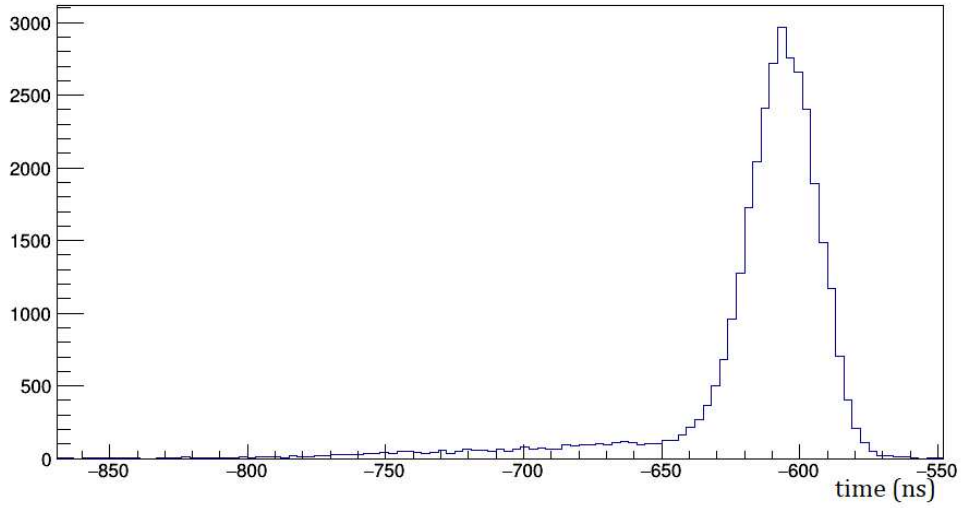

Figure 3.10: Focus on the peak of the curve already shown in figure 3.9 for the pmt data. The chosen interval for the analysis is between -0.68 to -0.54.

[3]This effect is essentially related to the fact that the emitted scintillation light in liquid Argon is characterized by characteristic time constants: the fast component (time constant ∼6 ns) and a slow component (1.5 μs)

Chapter 4

Studies on the light-charge association

4.1 Preliminary studies

The tools for the automatic identification of the interesting events recorded in the LAr-TPC should take advantage of all the available signals recorded in the detector: the charge signals collected on the wires, the light signals by the PMTs behind the wire planes and the hit signals recorded by the external Cosmic Ray Tagging system (CRT). The combination of these signals is fundamental in particular to reject the background from the cosmic rays. The TPC wire signals are recorded for at least the maximum drift time of 1 ms to collect the ionization electrons over the full drift volume, as determined by the 1.55 mm/μs drift velocity and by the 1.482 m maximum drift distance of the TPC. The detector is operating at shallow depth, protected only by 2.85 m concrete overburden, subject to a large flux of incoming cosmic rays, so the recorded TPC images for any collected event include tracks produced by randomly overlapped cosmic rays in $\pm$1 ms around the trigger. The DAQ is also recording the PMT and CRT signals in a $\pm$1 ms time interval around the trigger, to be used in the reconstruction and analysis pahse to reject these out-of-time cosmics.
Since the time of traversing the LAr of these cosmic tracks is unknown, tools are needed to discriminate the acquired signals associated with the possible neutrino interaction from the tracks associated to other sources (like cosmic rays muon, noise, and others). A possible way is based on the association of the light signals recorded by the PMTs with the corresponding spatial correlated signals in the TPC that are essentially produced along the path of the ionizing particles. In particular, matching the light recorded in coincidence with the trigger with the corresponding charge signals recorded on the wires, would allow identifying the particle generating the trigger or at least the region where the particles generating the trigger is located.
This chapter describes a simple association between the PMT light signals and the charge acquired in the TPC wires and evaluates the corresponding efficiency. The matching is based on the comparison of the barycenters along the beam direction z of the signals recorded by the wires and by the PMTs. The PMT signal barycenter allows to localize the longitudinal slice of the detector which contains the triggering event and consequently to remove the most part of the overlapped cosmic rays muon tracks that arrive on the detector in the same acquired event.
Preliminary studies to develop this PMT-TPC association and to verify its performance have been done using the real data collected in the detector. I studied the distributions of the track

inside the detector considering only the track crossing the cathode. Then, I proceeded with the calculation of the tracks barycenter along the longitudinal direction z in the TPC, defined as:

$$z_{TPC} = \frac{\sum_i z_i \cdot A_i}{\sum_i A_i} \tag{4.1}$$

in which z_i is the z coordinate of the spatial 3D point associated with the i-th hit of the track and A_i is the associated hit area. In a similar way, also the PMT barycenter is calculated as:

$$z_{PMT} = \frac{\sum_i z_i \cdot PE_i}{\sum_i PE_i} \tag{4.2}$$

in which z_i represents the z coordinate of the photo-multiplier detecting the i-th optical hit in the studied flash, while PE_i is the signal integral in photo-electrons.

In the analyzed data, the TPC hit area was obtained in two different ways: 1) the sum of the ADC counts between the beginning and the end of the hit signal or 2) the integral of a gaussian fit of the hit signal. For the purposes of the present analysis, the two options are equivalent and the barycenters calculated in either way agree within few centimeters. For this reason, it was decided to use the gaussian integral that should be the more precise hit area estimator. Similarly, the calculation of the charge barycenter has been tested using the hits of a single wire plane or combining the hits recorded in all the wire planes. Also in this case the barycenters result in agreement within a few cms except when the track direction results in only a very small number of wires occupied by the track in the considered wire plane. For the moment I use only the Collection plane, but the analysis can be easily extended to use all three wire planes[1].

The reason for the emphasis on studying barycenter along the z-axis is due to its high sensitivity, because the PMTs are approximately equally spaced in columns along the full length of the detector, while along the vertical axis, they are only present in 5 horizontal rows (see Figure 2.14). Additionally, cosmic rays passing through the detector tend to cover the entire vertical range, so the barycenter along the y-axis would mostly be at the centre of the detector, like neutrinos. By focusing on the z-axis, the particle's location along the longest dimension of the detector can be effectively identified. As a result, the detector volume to be analyzed is significantly reduced, indicating specific regions of interest, greatly rejecting the contribution from out-of-time cosmic rays.

The testing and validation of this PMT-TPC association is performed with a sample of recorded cosmic muons crossing the cathode between two adjacent TPC. For these tracks the TPC itself can determine the time t_0 of the entrance of the muon[2] within a few μs precision so for them the correct correspondence between the TPC and the PMTs signals is confirmed by this independent measurement. The correctness of the association can be then obtained by comparing the corresponding measured times:

$$\Delta t = t_0 - t_{flash} \tag{4.3}$$

where t_0 is the track time measured by the TPC and t_{flash} is the time associated with the signals acquired by the PMTs. Given the $\simeq 10^4$ Hz rate of cosmic rays crossing the detector and the

[1] In this first part, the barycenter of the tracks was calculated in all three wire planes only for the west cryostat, but the complete study is done in both the west and east cryostat.

[2] We can refer to all the track that crosses the cathode, so with a defined t_0 as "t_0 tagged"

$\sim \mu$s resolution of the t_0 measurement it is expected that the TPC-PMT association based on Δt have only a few % probability of wrong random association.
Similarly, the distance between the z barycenter associated to the track in the TPC, z_{TPC}, and the one estimated from the signal recorded by the PMT, z_{PMT} is defined as:

$$\Delta z = z_{TPC} - z_{PMT} \tag{4.4}$$

Each "t_0 tagged" track can be then associated with each PMT flash signal recorded in the same event: if the TPC track and the PMT flash signal are not associated with the same particle, their barycenter difference Δt and Δz will be large, otherwise, when the two signals correspond to the same particle, the difference should be small, $\simeq 0$. Considering only tracks with a small Δt and Δz would guarantee the proper association between track and flash signals.
The distribution of the Δt is characterized as expected by a clear peak around $\Delta t = 5\mu s$ as shown in figure 4.1, which corresponds to the proper association between the charge and light signals. The peak emerges more clearly from random coincidence after a request on Δz is also applied. The offset of Δt from 0 is probably related to an artifact in the reconstruction of the TPC signals that is still under investigation but that doesn't impact this analysis.

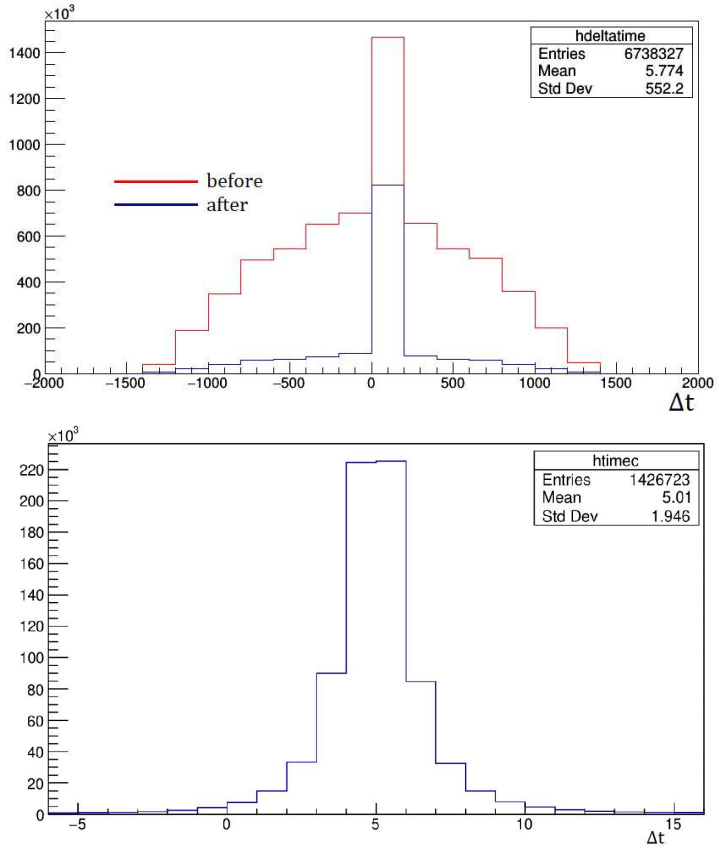

Figure 4.1: Δt (in μs) distribution before and after (top) and only after (bottom) imposing a limit on the differences between the TPC and PMT barycenters, with -100<Δz<100.

In the same way the distribution of the Δz exhibits a clear correlation peak and random TPC-PMT combinations disappear by requiring an agreement between the t_0 and the flash time, as shown in figure 4.2. (bottom). As expected, the distribution of Δz is centered around zero and

the TPC and PMT barycenters agree within tens of cm (RMS of Δz is about 30 cm).
Finally the same analysis can be performed by imposing bounds on Δz to see how the distribution of Δt changes. Also in this case the improvement of the distributions is evident (see Figure 4.1 bottom). If only the associations characterized by a small difference in their charge-light barycenter are considered, the temporal coincidence between the TPC track and the light signal is confirmed.

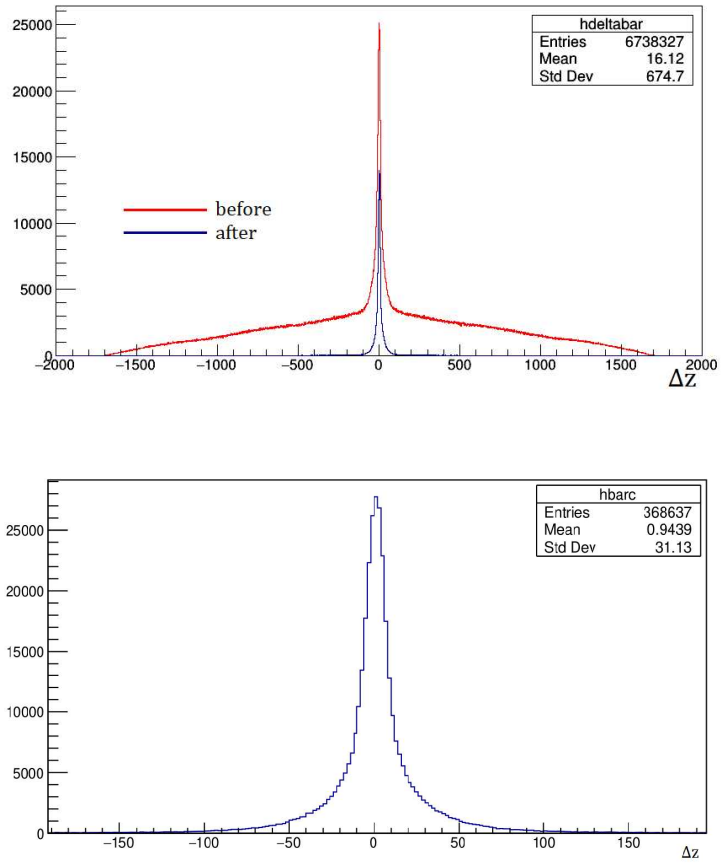

Figure 4.2: Distribution of Δz (in cm) before and after (top) and only after (bottom) imposing the limit on the time interval of the hits, with 1 μs$<\Delta t<$ 9 μs.

In conclusion Δz and Δt allow to unambiguously identify the correct association between a track in the TPC and the corresponding light signal detected by PMTs. These preliminary studies have shown that the TPC-PMT barycenters can provide a good way to obtain an efficient charge-light association or, more in general, the light barycenter can be used to define a region of interest along the z direction where the particles generating the trigger are located.

4.2 Development of the method on MC and real data collected events

In this section I discuss the optimization of the filter using the track-light barycenter comparison to pre-select events to be later visually studied. The filter should select with high efficiency the interesting events while reducing the total number of events to be studied. The tuning of the method should also take into account the differences between the neutrino interactions that

should be recognized and the cosmic rays that are similar to the single tracks crossing the cathode considered in the previous section. In the neutrino interactions more tracks are generated at the primary vertex; in addition, while the cosmic particles are propagating mostly along the vertical direction y, the neutrino interactions tend to develop along the horizontal beam axis z direction. The available MC simulations of the neutrino interactions and of the so-called in-time cosmics were used for this study. In these simulations only the particles generating the trigger are present and for this reason all the tracks identified in the TPC are clearly associated with the light signal recorded on the PMTs. The same method applied to the cathode crossing tracks can be used. The barycenter of the light signal for all the available MC events is identified in the time interval discussed in section 3.4 table 3.3. Then, all the tracks acquired in the same event are considered: the barycenter of the signal in the TPC is calculated and the corresponding Δz determined. In figure 4.3 the distributions of the Δz for the neutrino and the in-time cosmics events are shown.

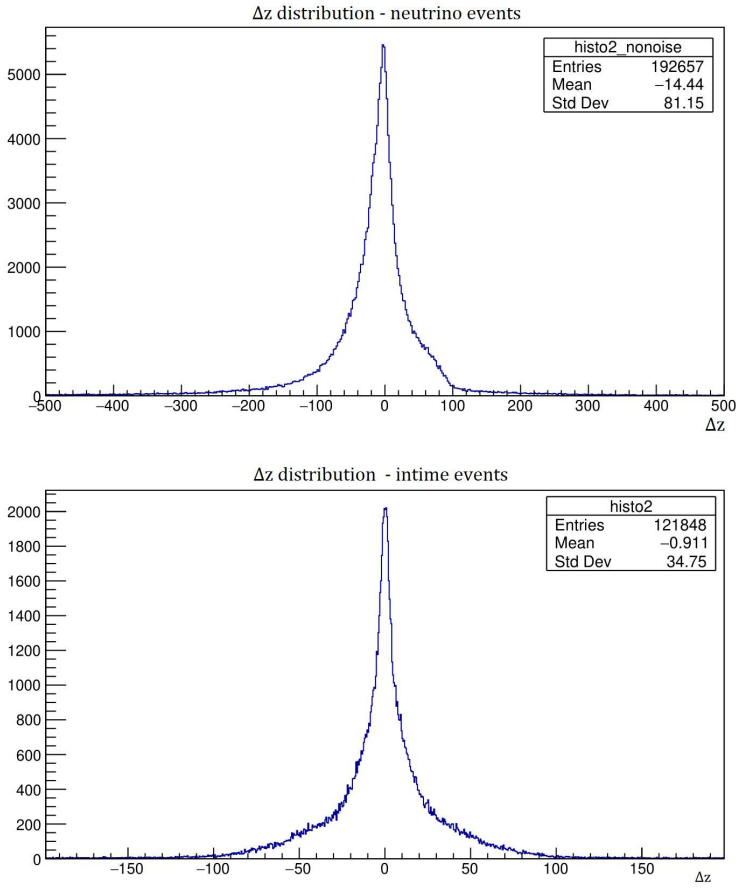

Figure 4.3: Δz (cm) distributions for the simulated BNB neutrino interactions (top) and for the in-time cosmics (bottom).

These distributions are characterized by a clear peak around zero and two symmetric tails at large Δz. A peculiar pattern near the border of the detector, at large |z|, has been also observed when studying the relationship between Δz and the barycenter z_{TPC}. As shown in figures 4.4, 4.5, and 4.6 the Δz distribution deviates significantly from zero along the detector's edges as consistently observed across all data sets.

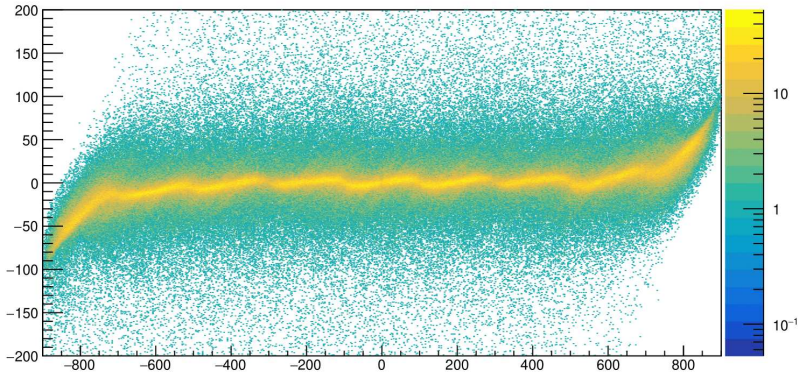

Figure 4.4: Δz (y-axis) as a function of z_{TPC} (x-axis) for the "t_0 tagged" tracks in the collected events.

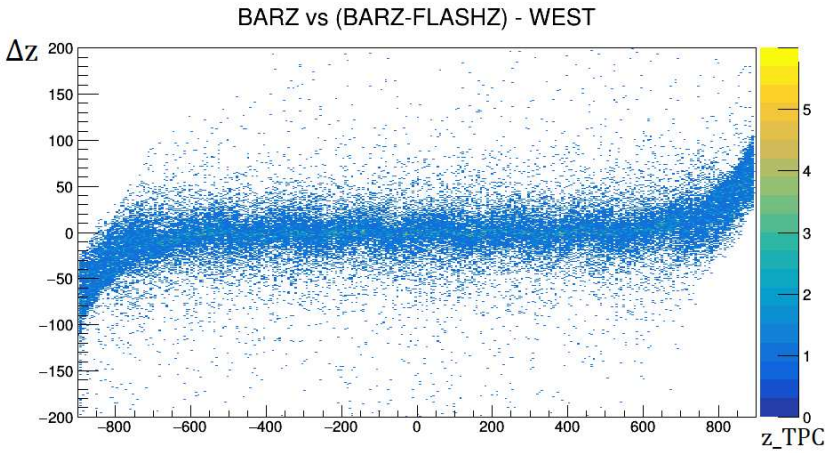

Figure 4.5: Trend of Δz as a function of z_{TPC} for the MC in-time cosmic events.

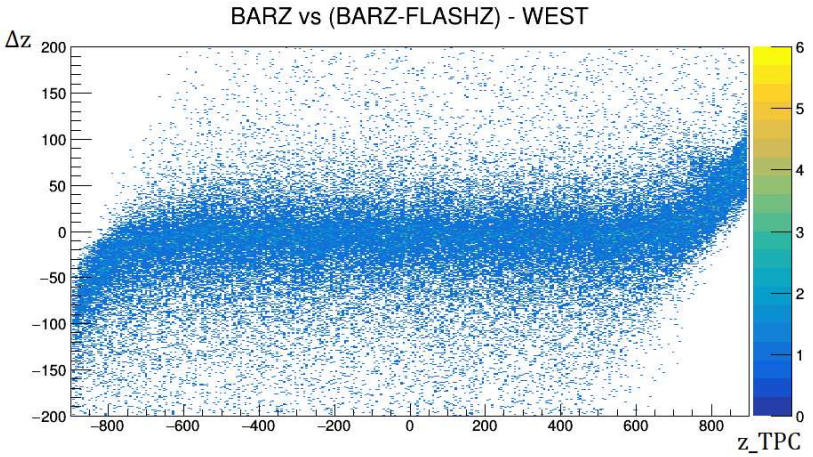

Figure 4.6: Trend of Δz as a function of z_{TPC} for the simulated neutrino events.

This border effect is due to the geometry of the detector and of the PMT system. While for tracks crossing the detector far from the upstream and downstream walls the emitted ligth can be detected on both sides of the track along z, the light can be detected only on one side, with a consequent bias, when the track is close to the border in z. To better illustrate this effect, a

schematic representation of the detector is sketched in figure 4.7. The yellow circles represent the light signal acquired by the PMT for a track (grey) passing through the detector.

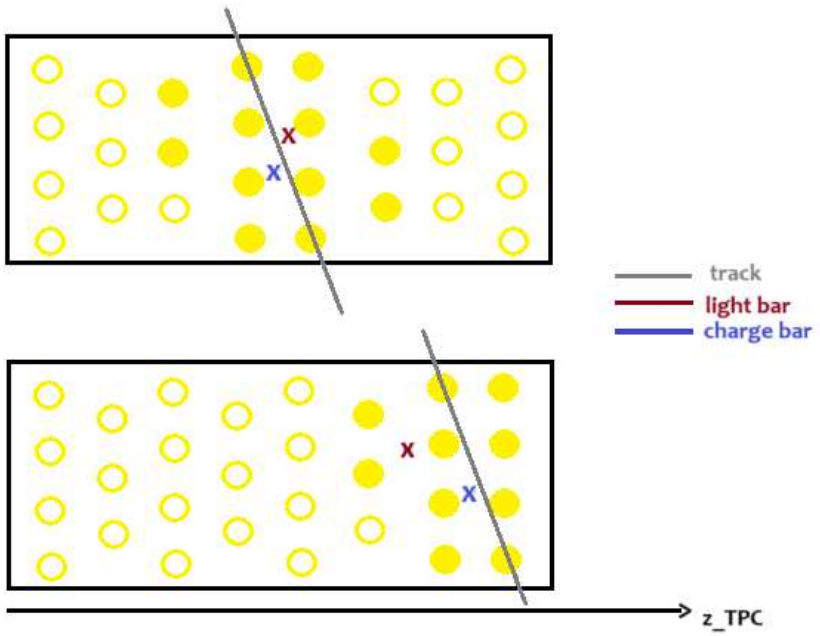

Figure 4.7: Graphical representation of the track (grey line) that passes through the detector and of the signals acquired by the PMTs (yellow circles). The activated PMT are full yellow circles, the empty yellow circles represent PMTs that are not activated by the track passage.The position of the ligth and charge barycenters is also shown.

To correct this border effect, the average Δz is computed as a function of z_{TPC}[3]. The Δz profiles have been studied for the simulated events by computing both the barycenters using the truth information provided by the Monte Carlo and the barycenters obtained using the reconstructed signals. The Δz profile based on the truth and on the reconstructed signals present similar trends, confirming that the deformation of the profile at the z edges is a detector effect.
Figure 4.8 represents the reconstructed and truth variable for MC in-time cosmics and for the neutrino events. Both variables show the same trend within 10-20 cm. Figure 4.9 shows the border effect profile for the cosmic tracks in collected events, for the simulated neutrino and for the MC in-time cosmics using the reconstructed objects. Also in these cases, the behaviour is similar for all the data sets, showing deviations from 0 up to 80 cm at the two z edges.

[3]The plots studied to obtain the correction are obtained from the distributions of Δz as a function of z_{TPC} using the function *profileX* provided by ROOT .

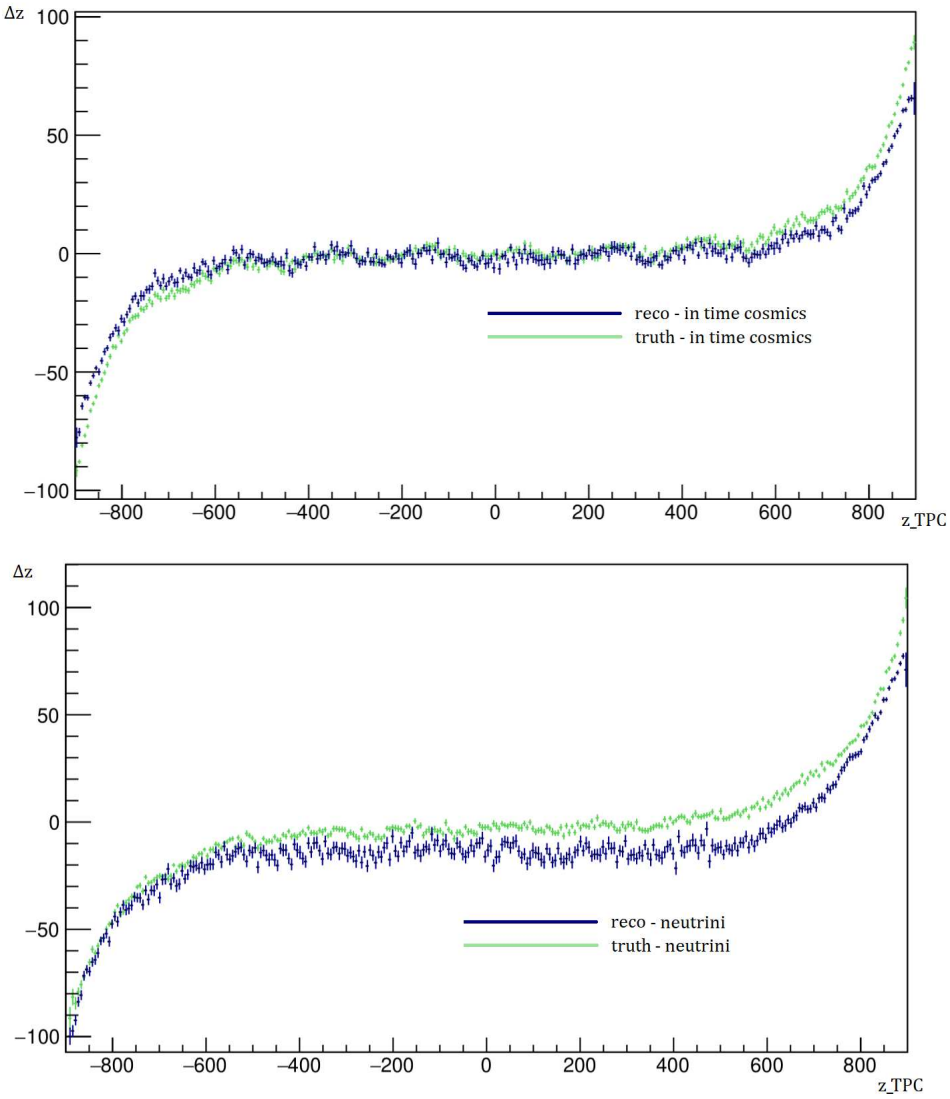

Figure 4.8: Average Δz as a function of z_{TPC} for the in-time cosmics (top) and for the neutrino events (bottom). The trend is obtained using both the reconstructed objects and the truth variable from the MC.

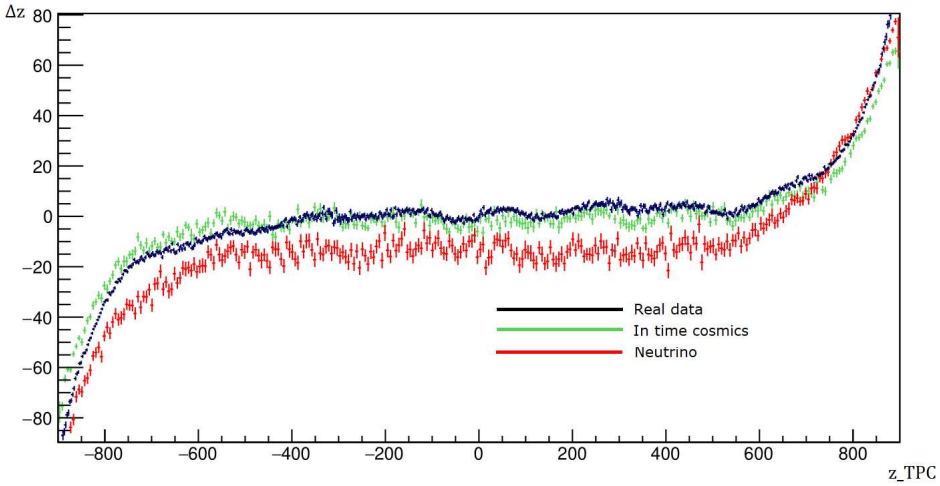

Figure 4.9: Average Δz as a function of z_{TPC} for all the MC data sets and for real data, obtained from the ones shown in figures 4.4, 4.5, 4.6 .

The Δz profile for neutrino is similar to the ones for in-time cosmics simulation and real data but presents a small bias toward negative values of Δz. This difference, which is present only for the reconstructed quantities and not for the truth MC variables, should arise from the methodology employed in calculating the barycenter. Specifically, for in-time cosmic events, a single long track is present, whereas neutrino events may consist of multiple tracks originating from the same vertex. The light barycenter takes into account all the tracks produced in the events while each track from the primary vertex is considered separately[4] in the TPC reconstruction. It means that the comparison between the light and charge barycenter performed for each TPC track is biased because the two barycenters could refer to two different topologies. Since the neutrino beam propagates along the positive z direction, the charge barycenter of longer tracks (e.g., the muon) would largely align with the light barycenter of the entire neutrino event. However, the Δz difference tends to be negative for shorter tracks emitted at the vertex. In fact, the charge barycenter will be in close proximity to the vertex while the light barycenter can be at the highest z, resulting in a negative Δz. Since in this analysis for each track a Δz is calculated, the average Δz results biased by the presence of these short tracks. Two different actions should be then performed: a correction for the effect seen at the borders of the detector and the introduction of a simplified tool to merge multiple tracks associated to the same particle interaction (the methods used to do this merging will be discussed in section 4.3).
In order to correct the distortions observed at the edges of the detector along z, the average Δz was fit as a function of z with a polynomial of fifth degree[5] at the two extremities, i.e. for z>500 cm and z<-500 cm, as shown in figure 4.10[6]. The fit was performed for all the simulated cosmic events combining the two cryostats while for the real events the fit was performed separately for

[4] As previously mentioned the Pandora reconstruction provides not only the track reconstruction but also the full reconstruction of the neutrino candidates, connecting the tracks coming from the same interaction vertex. In this analysis, only the tracks are used, discarding the other available information, to avoid possible biases introduced by the high-level Pandora reconstruction.

[5] The *pol5* function provided by ROOT has been used for the fit.

[6] A more accurate study would involve using a three-dimensional mapping that corrects each z-value pointwise. As a first approximation the fitting function can in any case provide a rough correction that is sufficient for the purposes of this thesis.

the two cryostats obtaining a correction that is cryostat dependent. The fit function $z_{correction}(z)$ has been then applied to obtain a corrected estimate of the TPC-PMT barycenter difference:

$$\Delta z_{NEW} = z_{TPC} - z_{FLASH} - z_{correction}(z) \tag{4.5}$$

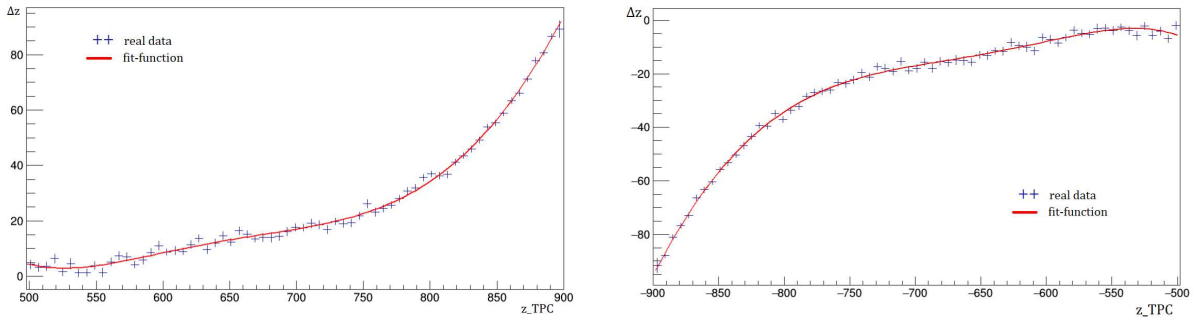

Figure 4.10: Polinomial fit of the Δz profile at the extremities of the detector, starting from the data reported in figure 4.4 for the t_0 tagged tracks in the west cryostat.

The obtained corrections have been then applied to the available data showing that the barycenter distributions are positively affected. Figure 4.11 shows the Δz distribution before and after the correction on the barycenter for the west cryostat in real data for the tracks whose barycenter $|z_{TPC}| > 500$ while the distribution of Δz as a function of z_{TPC} is shown in figure 4.12 for all the tracks in real data.

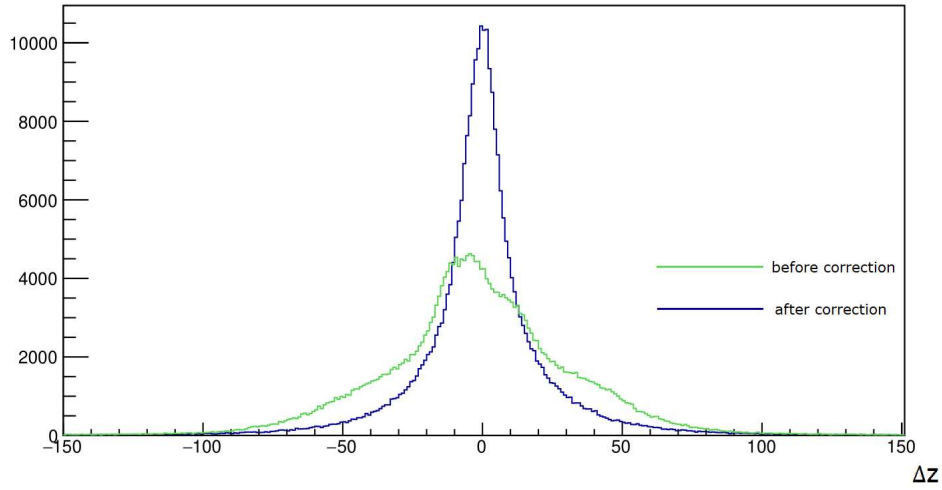

Figure 4.11: Δz (cm) distribution before and after the border effect correction applied on the real data shown in figure 4.2 (top) for the tracks whose barycenter $|z_{TPC}| > 500$.

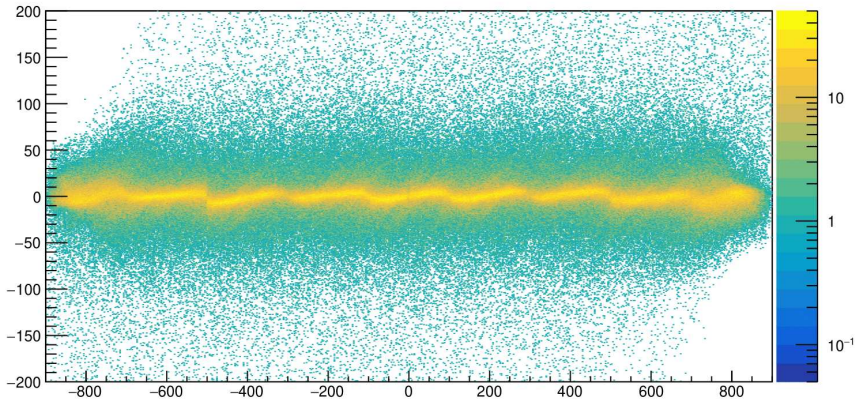

Figure 4.12: Corrected behaviour of Δz (cm) as function of z_{TPC} (cm) shown in figure 4.4

Noise elimination

A group of wires with exceptionally high noise are introduced in the Monte Carlo events to simulate the occurrence of malfunctioning channels in the detector. As a result, "fake" tracks are created by the reconstruction process by combining noise signals from channels in two different wire planes within the same TPC. The two distinct vertical lines between z=-600 and z=-400 in figure 4.13 (left) are traced back to the corresponding noisy TPC readout boards.
To identify and eliminate these unwanted tracks it is checked if the TPC barycenter of all the "candidate noise" tracks consistently align with the same 3D point. In addition other properties of these tracks, such as their start and stop points, remain consistent across numerous events. This behaviour is shown in Figure 4.14: for a large amount of tracks the start and end points are clustered in the same small region of the detector.

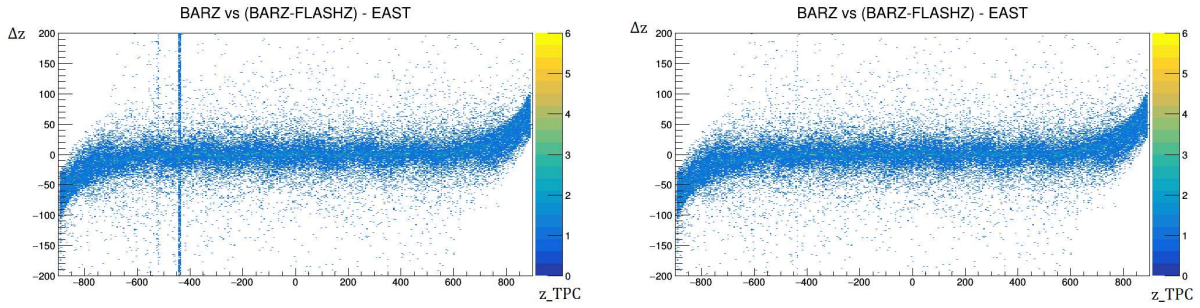

Figure 4.13: Δz as a function of z_{TPC} before (left) and after (right) the removal of the tracks associated to noisy cards introduced in the MC simulation.

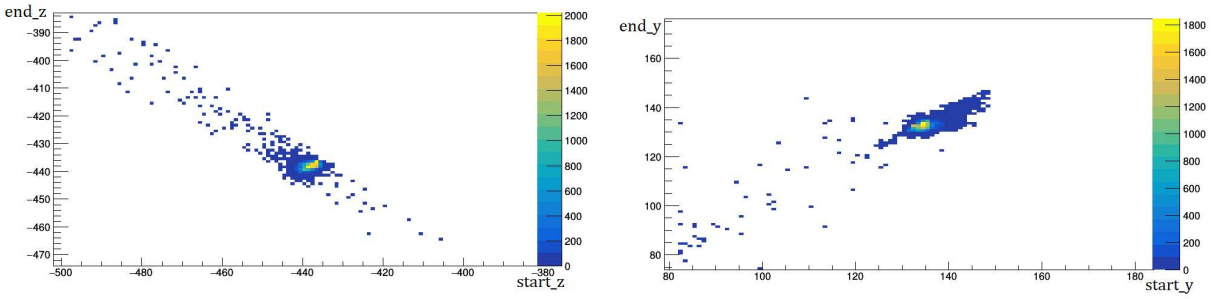

Figure 4.14: Start-end point in the y-axis (right) and z-axis (left) for the noisy track candidates in the east cryostat.

Starting from these plots, dedicated criteria, based on y and z coordinates of the start and the end points of the tracks, have been introduced to reject these noisy tracks. For example short tracks whose start and end points are within few centimeters from y=135 and z=-440 are rejected. After this noise removal, all the survinging tracks have been used in the following analysis.

4.3 Track merging and efficiency

As already indicated the main purpose of this thesis is the preparation of a pre-selection filter for the identification of the neutrino interactions collected in the T600. This pre-selection filter will be based first of all on the light-charge association in order to recognize the particle generating the trigger. The selected events will be then visually studied in details and used as a benchmark for the validation of the high-level reconstruction from Pandora, of the capability to recognize the vertices and to merge together the particles belonging to the same neutrino interactions. To avoid possible bias introduced by the Pandora identification/reconstruction of the neutrinos, this filter has been developed using the information available at the initial stage of the reconstruction. Each single reconstructed track is considered as a separate object in the analysis files used for the study of this thesis (calibration ntuples). For example, if a proton and a muon are produced at the same interaction vertex, two independent tracks are reconstructed and are available for this study. This can produce a bias in the search to associate the recorded light signal to the charge recorded by the TPC. The light signals are associated to both tracks while for the TPC each track is considered separately. This bias in the association can be reduced if the tracks belonging to the same interaction are merged using a very simple tool.
Two distinct merging models described in the next sections have been developed. The first method ("start-stop") is based on the distance between the start and end points of the tracks, while the second ("All-hits") is obtained studying the tracks point-by-point and imposing some boundary on the distance between the points belonging to two different tracks.

Start-Stop merge

The start and end points of each pair of tracks are considered, calling S_i, S_j the starting points of the two tracks and E_i, E_j the end points. The minimum distance d_{ij} between $S_i - S_j$, $E_i - E_j$, $S_i - E_j$, and $E_i - S_j$ is calculated and it is distributed as shown in figure 4.15. A peak at small distances (below 2 cm) is clearly visible, corresponding to tracks that are connected. Taking into account this distribution, if $d_{ij} < 4$ cm the two tracks are merged into a new track and its

barycenter and its start/end points are calculated starting from the corresponding quantities of the merged tracks. The new track is then added to the list of the tracks in the events while the two merged tracks are removed. The process is then iterated up to when no more tracks can be merged. The choice of the merging distance is a compromise between the request of an efficient grouping of the tracks belonging to the same interaction and the need to avoid to mix together different uncorrelated tracks.

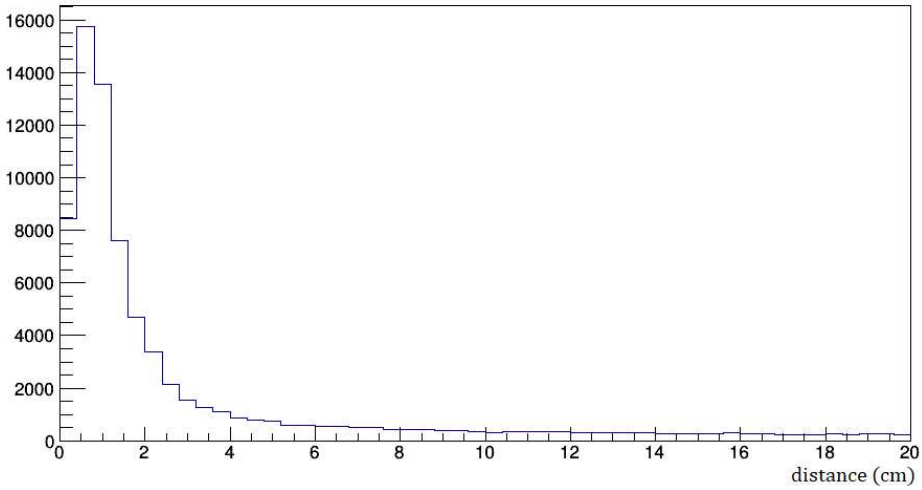

Figure 4.15: Distribution of the minimum distance used for the merging.

The merging procedure was first applied to MC events. Figures 4.16 and 4.17 show the impact of the start-stop merging on the barycenter definition, where the difference Δz_{TR} between the truth charge barycenter of the whole event and the barycenter of each TPC track recognized in the event is shown for the simulated neutrino interactions and for the "in-time" comics before and after the track merging.

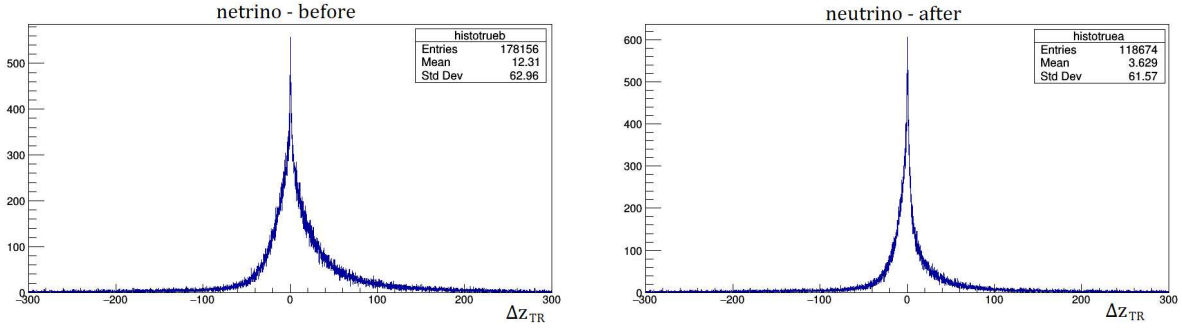

Figure 4.16: Δz_{TR} distribution (cm) before (left) and after (right) the application of the start-stop merging on neutrino MC events

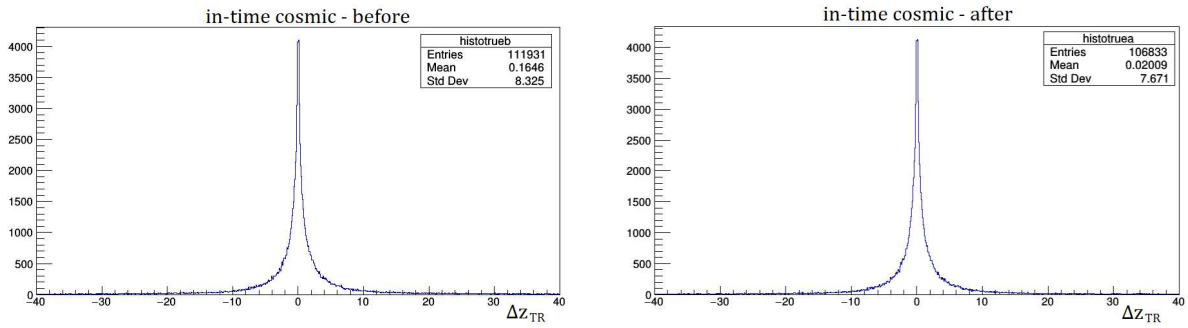

Figure 4.17: Δz_{TR} distribution (cm) before (left) and after (right) the application of the start-stop merging on simulated cosmic events

As expected, the Δz_{TR} mean value results centered to zero after the described merging procedure. This tool has a more significant impact on the simulated neutrino interactions, because the in-time cosmics MC are mainly formed by single tracks while in neutrino events more tracks are present and can be merged. Figure 4.18 shows the number of tracks before and after the application of the merging on all the neutrino events (left) and when only ν_μ CC QE neutrino events with a muon track longer than 50 cm are considered (right).

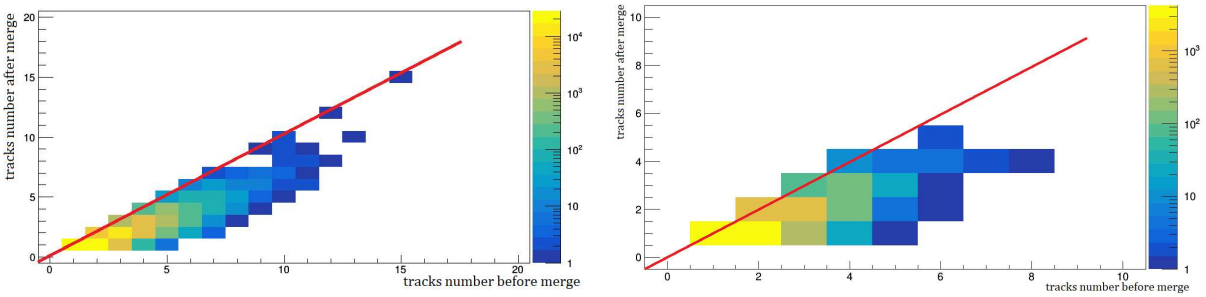

Figure 4.18: Comparison between the number of tracks in the simualated neutrino events before and after applying the start-stop merging for all neutrino categories and only for interesting neutrino

All-hit merge

This second approach has been introduced to take into account the possibility of having a track that is connected to another track at a point different from the start/end of the track. A typical example is the presence of delta rays along the muon: in this case, the Pandora pattern recognition can identify the delta ray as a different track close to its parent muon but distant from its start/end and then not merged by the previous approach. For this analysis, only the information in the Collection wire plane has been used. For each identified physical signal (hit) in a wire plane the number of the wire that has recorded that signal and the corresponding sampling time (in units of t-sample corresponding to 400 ns) are stored and this information used to calculate the distance between two physical signals in the wire plane projection. Each hit in a track in each simulated event is compared to all the hits of any other track in the same event and for each pair of hits the difference between the hits wire numbers, between the hits time-sample and their 3D distance have been calculated. The distributions for the obtained differences are shown in figures 4.19, 4.20 and 4.21. In particular, only the zoom on the region corresponding to small distances, where possible hits belonging to two connected tracks should

be present, are shown. Taking into account that the previous study on the "start-stop" merging has provided a maximum distance for the merge of 4 cm and taking into account also that if two tracks are connected, a small distance between the hit wires and the hit time is clearly expected, the following parameters could be adopted for this "All hits" track merging:

difference in wire ≤ 5	**difference in t-sample** ≤ 30	**3D separation** ≤ 4 cm

Table 4.1: Final parameters used in the analysis to merge tracks.

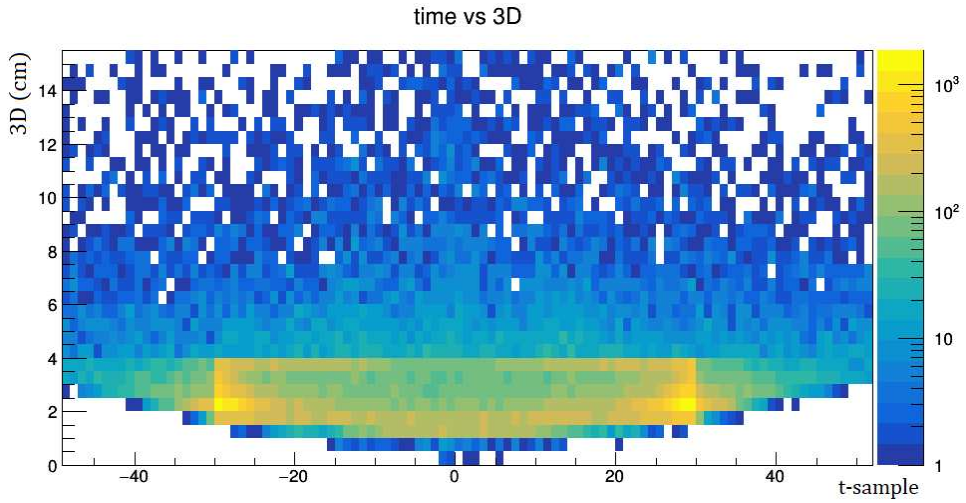

Figure 4.19: Relation between the difference of t-sample (x-axis) and the 3D distance (y-axis) for all the pairs of hits from different tracks. Each t-sample is 400ns (considering the drift velocity, it corresponds to a drift distance of 0.63 mm).

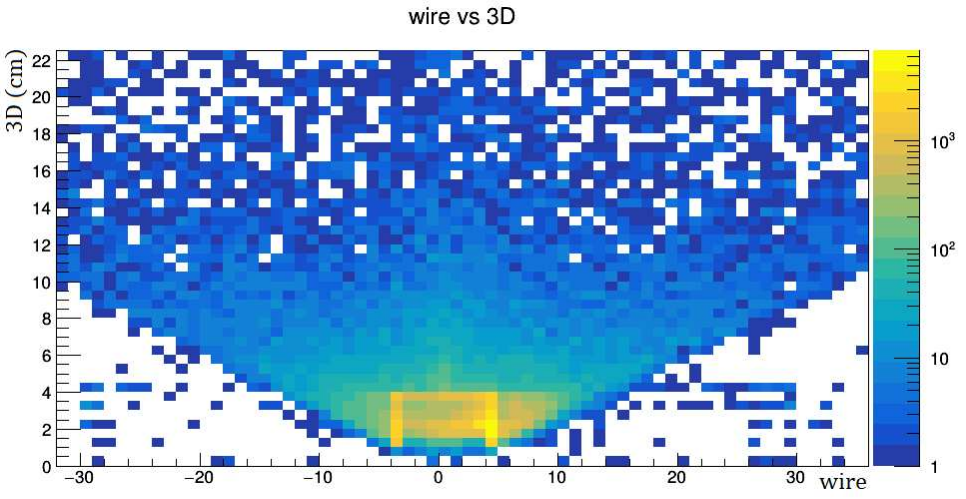

Figure 4.20: Relation between the 3D distance (y-axis) and the difference of the number of wires (x-axis).The distance between two wires is 3mm.

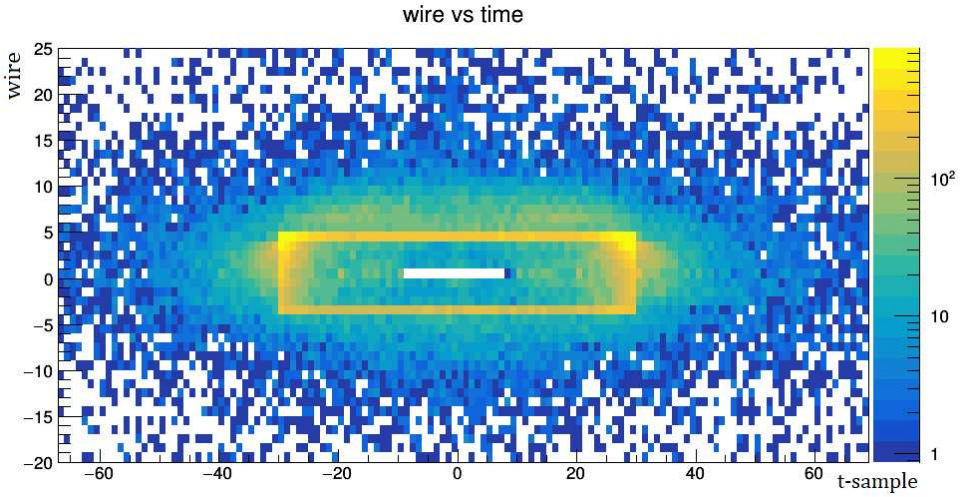

Figure 4.21: Relation between the difference of t-samples (x-axis) and the number of wires (y-axis). Each t-sample is 400ns (considering the drift velocity, it corresponds to a drift distance of 0.63 mm) and the distance between two wires is 3mm.

The impact of this merging tool results similar to the one obtained in the simpler merging based on the start-stop of the tracks as can be seen for example in figures 4.22.

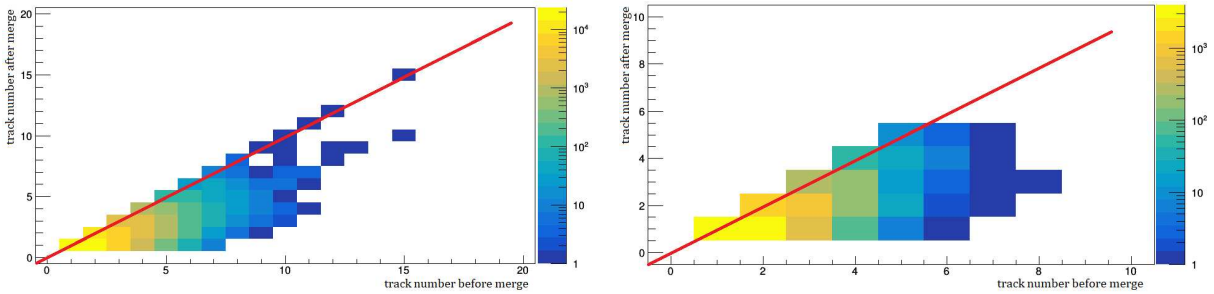

Figure 4.22: Comparison between the number of tracks in the simulated neutrino events before and after applying the merging for all neutrinos and only for ν_μ CC-QE neutrino with L_μ>50 cm.

Efficiency

After the noise removal (for MC), the border effect correction and the merging of tracks as discussed above, the efficiency of the selection based on the distance between the TPC and the light barycenters along z can be studied. The calculation is performed by considering all tracks in each event and verifying if in the event there is at least a track that is matched to the light signal within a given distance d. The efficiency has been then studied varying the distance "d" from 0 to 300 cm. Defining $N_{matched}$ the number of events with at least a track matched with the light within a distance d and N_{total} the total number of events with at least a recognized flash in the detector, the efficiency ϵ is calculated as a function of d as:

$$\epsilon = \frac{N_{matched}}{N_{total}} \tag{4.6}$$

while the error on the efficiency is calculated with the `TEfficiency` tool by `ROOT` with the Clopper-Pearson statistic[33].
The efficiency has been calculated for both merging methods, to see which one is eligible to be

applied to real data. Figure 4.23 shows the comparison between the efficiency for both methods applied on simulated neutrinos. Both methods exhibit comparable efficiency, saturating below 100%, and the merging method based on the usage of all hits seems to provide a better efficiency. Anyway, for practical reasons, in this study the start-stop merging method has been finally adopted to process real data. The "all-hits" method requires in fact to combine all the hits from all tracks but the number of tracks in the real events results too high due to the presence of cosmics. So this method demands substantial processing time and for this reason the usage of a simpler and faster start-stop merging method will be considered allowing in any case to yield a high efficiency more swiftly.

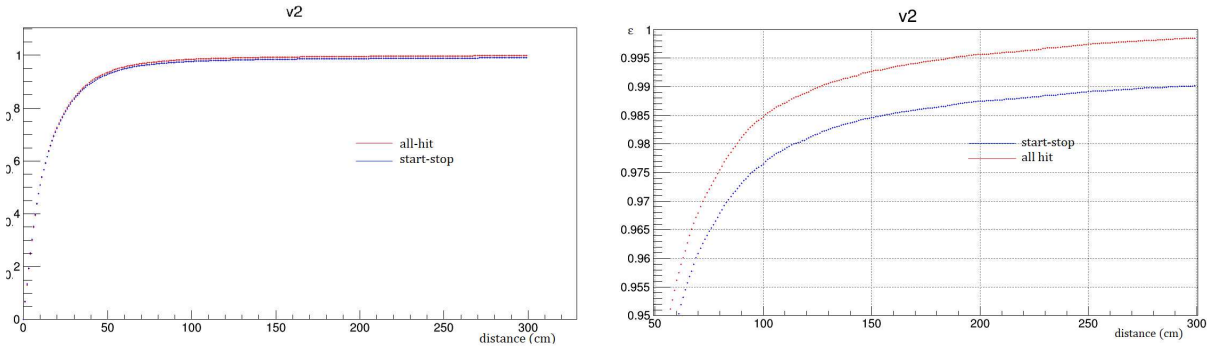

Figure 4.23: Comparison between the two merging strategies for the simulated neutrino interactions in the active liquid Argon.

It is interesting to notice that in both merging cases, even considering a large distance d, the association reaches an efficiency of ≃99%. Probably the residual tiny inefficiency is due to problematic events where the reconstruction still fails, as briefly described at the end of this section. The difference between the two merging methods becomes negligible for the simplest events with a ν_μ CC-QE neutrino with L_μ>50 cm and fully contained in the active volume (interesting event for the first physics analysis in ICARUS), as shown in figure 4.24. The better agreement between the two merging methods is due to the simplest topology of these neutrino events (a long muon and one or more protons at the primary vertex): the two merging procedure have similar performance on these events.

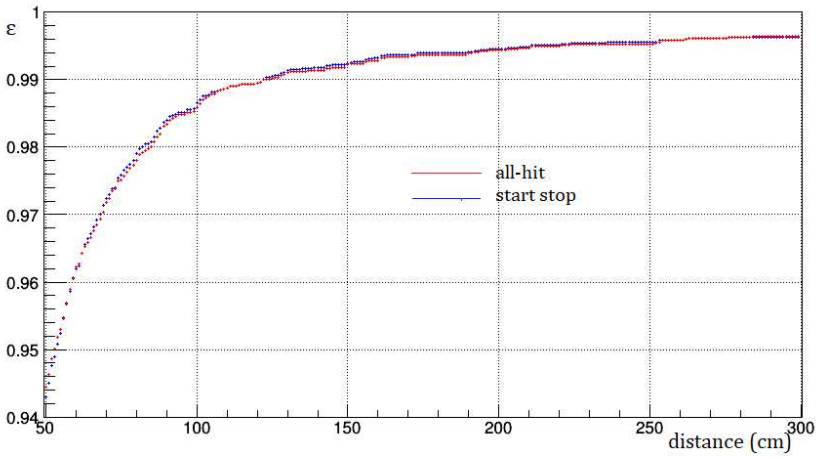

Figure 4.24: Comparison between start-stop and all-hit merging method for the ν_μ CC-QE neutrino with L_μ>50 cm.

The efficiency for the start-stop merging method is shown in figure 4.25 as a function of d for all the BNB simulated neutrinos before the merging (BLUE) and after the merging (RED) and for the fully contained ν_μ CC QE with a muon length of at least 50 cm after the merging (GREEN).

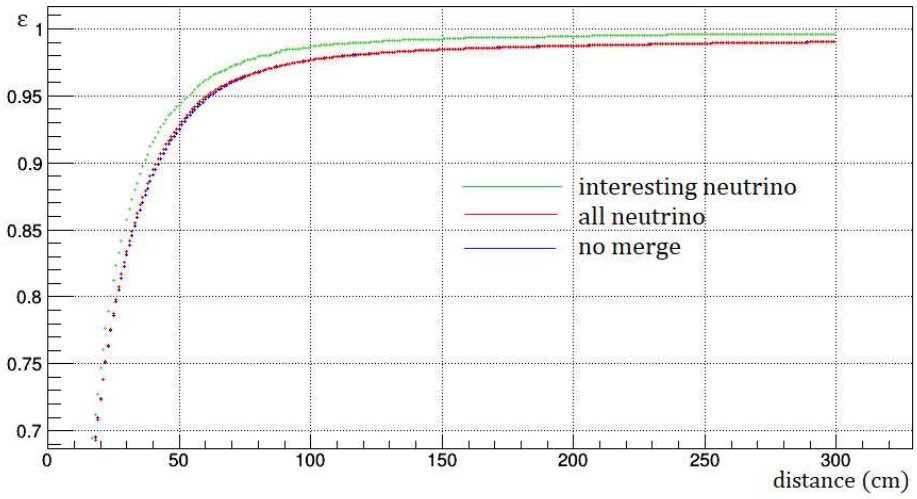

Figure 4.25: Comparison between the efficiency as a function of the distance between the TPC and light barycenter calculated for merged ν_μ CC-QE neutrino with L_μ>50 cm flagged as "interesting neutrino" (green), all the neutrino before the merging (blue) and after the merging (red).

In figure 4.26 the central part between 50 cm and 200 cm is also plotted: improvements in the efficiency become relatively small starting from 110-120 cm.

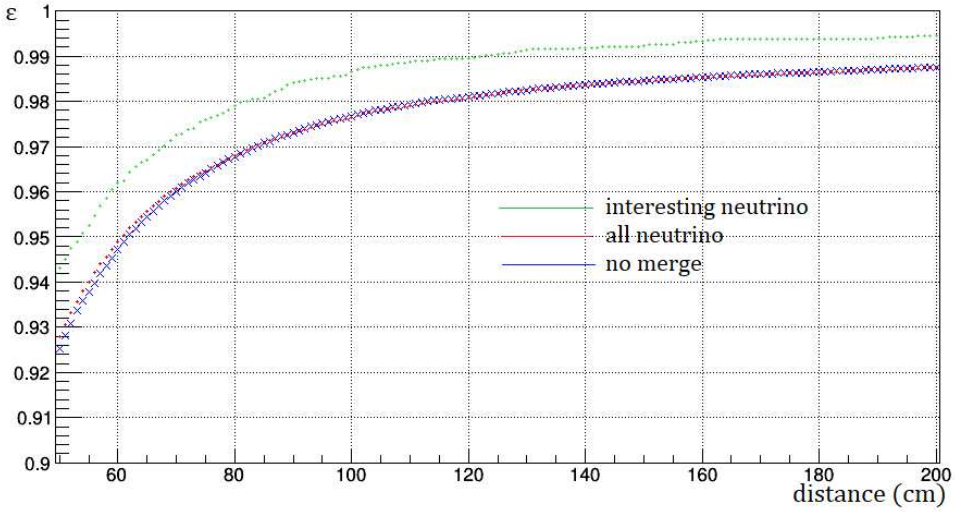

Figure 4.26: Comparison between the efficiency calculated for merged interesting neutrino (green), merged all neutrino (red) and no merging (blu), in the region between 50 cm and 200cm

It can be noticed that the impact of the merging is visible essentially only when a small distance between the charge and light barycenter is considered while the variation is extremely small considering higher distances. Even though the difference between merging and not merging is minimal, performing the merge provides greater completeness of information about the studied event and therefore it is still preferable to consider it. For example, in order to recognize if a neutrino interaction is fully contained, from the perspective of the light-charge association,

the matching with one of the tracks from the neutrino is sufficient to recognize the presence of an interesting interaction. However, to determine if the event is contained, it is necessary to establish whether all tracks of that interaction are contained inside the detector. Thus, clustering together all the tracks belonging to the same interaction allows for a more accurate study of the characteristics of the event. In addition, the usage of a very simple procedure for the merging should not introduce bias in the studied event selection.
In conclusion this study indicates that an efficiency above 98% can be obtained considering a distance d for the match between charge-light barycenter around 100cm. For the ν_μ CC-QE fully contained neutrino interactions with L_μ>50 cm a 99% efficiency can be reached selecting the tracks whose barycenter is within 1 m along the longitudinal direction with respect to the light barycenter as shown in figure 4.27.

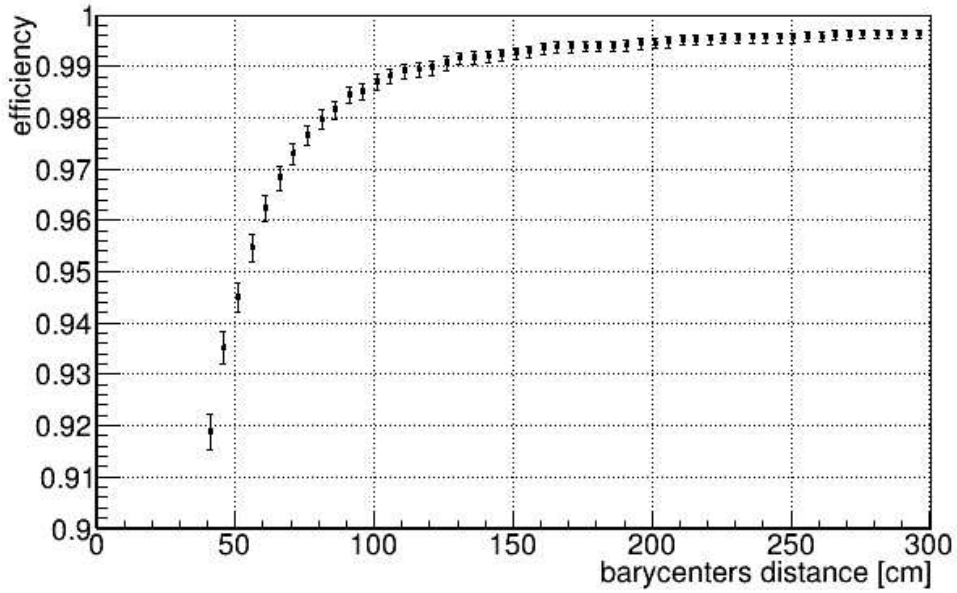

Figure 4.27: Efficiency with error bars for MC ν_μ CC-QE fully contained neutrino interaction with L_μ>50 cm.

It is possible to notice that even at distances exceeding 3 meters for the match of the barycenters, the curve doesn't reach the 100% efficiency.
Given the limited number of events that are not matched by the analysis (seven events over a total number of studied interactions of about 7000), it was possible to visually examine each of these events using the track visualization program.
In the following figures, three of these events are shown to illustrate the types of issues that can occur. There are two main reasons why a 100% efficiency is not achieved in this study.

1. Poor track reconstruction

To this category belong all events with tracks not well reconstructed by Pandora.
These tracks can be visualized using the viewer, but the hits are not accurately reconstructed. An illustrative example is provided in the figure 4.28. This specific type of track is clearly visible in the collection plane, while it becomes lighter in intensity on the induction 1 plane, due to the track direction along the drift direction. Since this effect is present on the two Induction wire

planes, consequently it is difficult to reconstruct the 3D track and Pandora's reconstruction fails and the event is not properly reconstructed.

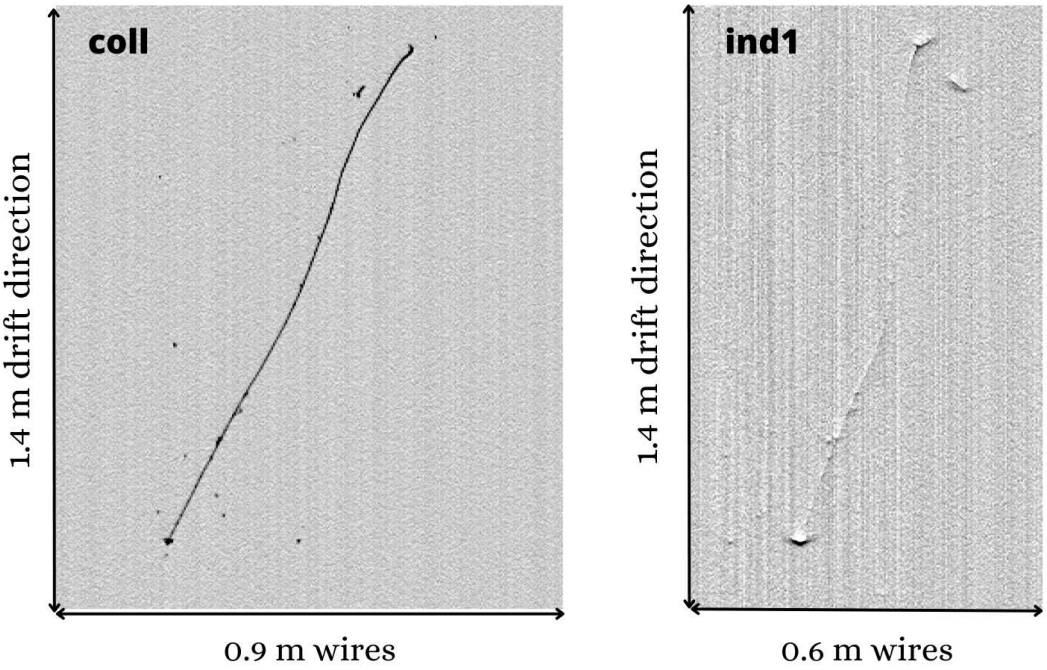

Figure 4.28: Two tracks are visible: a proton of 1 cm long and a muon of 130 cm long. In the induction 1 view, the track is hardly visible, making difficult the muon track reconstruction.

Another example is in figure 4.29: the muon in this case is only partially reconstructed. More specifically, the reconstruction process identifies two distinct tracks that effectively represent the muon's initial segment (near the vertex) as well as its last portion. However, a substantial fraction of the muon's central region is not reconstructed (this problem is still under investigation). The two reconstructed segments are too distant to be merged and the charge-light matching screwed up because the barycenters of the two isolated muon segments are notably distant from the light's barycenter, which is, in contrast, located at the muon's centre.

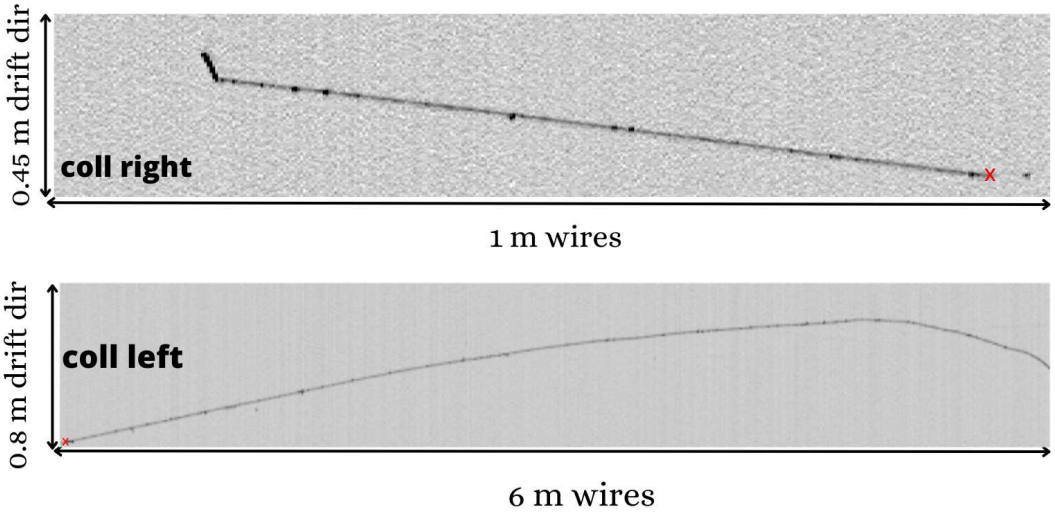

Figure 4.29: Example of a muon neutrino QE interaction. On the top the neutrino vertex is visible. Two tracks are produced: the muon is 7.8 m long and the proton is 4.8 cm long. In the figure at the bottom, the last segment of muon track that passed through the cathode and goes on the left collection view is visible.

2. Presence of other particles in the detector: the case of dirt events

In this last category event, two independent interactions occur at the same time and inside the same cryostat. An example is shown in figure 4.30. The first (in a blue circle) is a $\nu\mu$CC QE candidate from BNB that starts from the right collection plane region, while the muon crosses the cathode and stops in the left collection plane (the last part is in the small blue circle in the lower left area of the figure). The second interaction (red circle) corresponds to a muon track entering from outside, entering in the active volume through the wire planes and stopping inside. Because both interactions occur within the same cryostat and in a close time frame, the light signals generated by the two interactions merge together, resulting in a single light flash whose barycenter represents the average of the light barycenters of the two interactions. Therefore, even though the tracks are accurately reconstructed, neither of the two tracks has a charge barycenter that aligns with the light barycenter.

The second interaction shown in this event is a typical example of the so-called "dirt events" produced by neutrino interactions in the material surrounding the active liquid Argon (for example, in the passive liquid argon behind the wire planes or in the material that constitutes the detector). The particles produced in these neutrino interactions can reach the active volume, allowing their scintillation light to be recorded by the PMT, and their tracks become visible in the TPC. These events are important because they can generate a global trigger for the detector and represent an additional contribution that should be studied as a possible source of background. In fact, the external neutrinos interactions can produce for example some neutrons that can interact within the detector and mimic neutrino interactions in the active volume. These events have not been studied in detail in this thesis but their contribution should be taken into account in particular in the development of the selection and identification of the neutrino events.

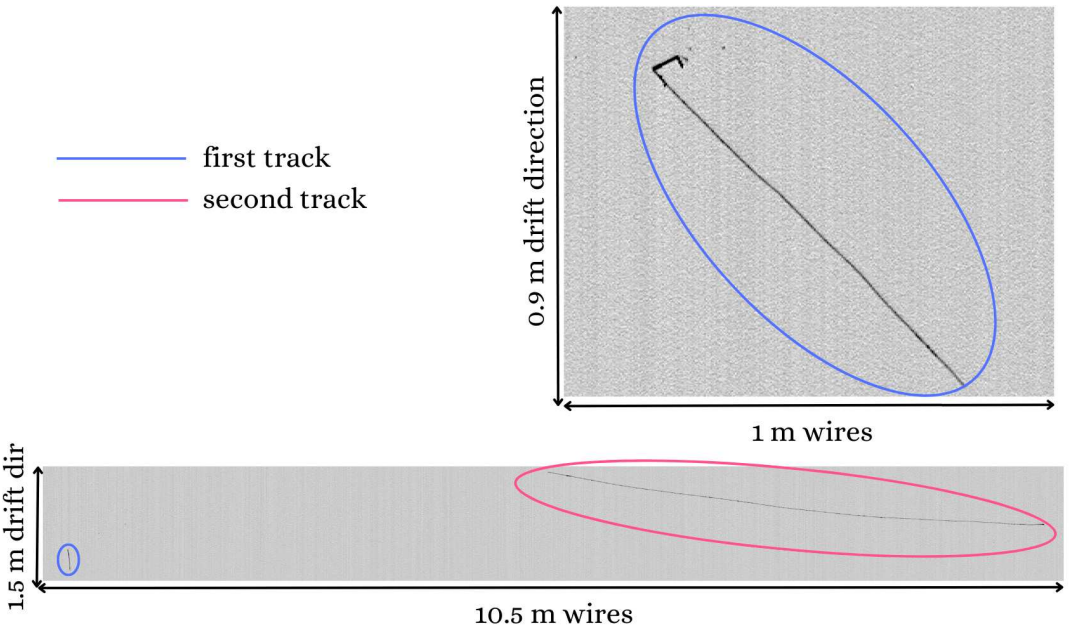

Figure 4.30: In this figure two separate interactions are shown. On the top figure, a muon neutrino CC QE interaction, with a muon and a proton in the same vertex, is visible; on the bottom figure, there is the final segment of the muon track (blue circle) and a second separate muon track (red circle) produced by a neutrino interacting outside the active volume. The two images are from collection view, right (top) and left (bottom).

Chapter 5

Selection of the contained neutrino events

In the previous section, I studied methods to improve the preliminary neutrino event selection by Monte Carlo simulations. As a result, the charge barycenter of the event generating the trigger can be localized within $\simeq$ 1 m from the barycenter of the light detected by the PMTs. In this section I focus on the analysis of collected events to find efficient neutrino selection criteria, minimizing at the same time the surviving background events related to cosmics. Furthermore, major attention is reserved to the selection of the fully contained ν_μ CC neutrino interactions from BNB, representing the channel exploited for the initial ICARUS stand-alone physics analysis, devoted to the investigation of the Neutrino-4 claim.

5.1 Track containment

The identification of the fully contained ν_μ CC events requires the capability to properly recognize if all the particle tracks produced in the interaction are inside the active liquid argon volume. Since the information related to the start/end points of each reconstructed track is provided by Pandora, an easy check on the containment can be directly performed using only these two extreme points. The performance of this track containment can be validated directly with the study of the cosmic muons recorded in the detector that are surely entering (and in many cases also exiting) through the active volume boundaries, to define the conditions that should be satisfied by the contained tracks.

The properties of the track start and end points have been studied for a sample of cosmic muons with a length L_μ>50 cm and that are t_0 tagged. For this sample the TPC allows to reconstruct with a precision of $\simeq$1 μs the time of the passage of the track in the detector and to obtain the correct position of the track along the x-drift direction. In addition, only tracks with a crossing time t_0 between -338 and 357 μs have been considered. This additional requirement allows us to see the full recorded track in the detector as previously described (see 3.2).

The distributions of start and end points in the detector in the x (drift) y (vertical) plane are shown in figure 5.1 and 5.2 for the tracks crossing the West cryostat. The conditions extracted from the tracks seen in the West cryostat will be in any case applied also on the East cryostat. In addition, a large sample of about $5.88 \cdot 10^5$ events has been used to produce these pictures, in

order to enhance particular effects in the detector. The expected boundaries and the coordinates definitions of the West cryostat active volume are summarized in table 5.1. Tracks produced by cosmics are mostly due to muons crossing the detector boundaries as visible in figures 5.1 and 5.2. The vertical coordinate distribution of track start and end points in figure 5.1 exhibits clear peaks at the top and bottom corresponding to the the entry and exit points of vertical muons.

Axis	**axis distribution (cm)**
x: drift direction	from 61.7 to 358.73
y: vertical direction	from -181.86 to 134.96
z: longitudinal/beam direction	from -894.95 to 894.95

Table 5.1: Coordinates (in cm) corresponding to the active volume of the West cryostat in the reference system used in ICARUS. The coordinates for the East cryostat are similar but the x coordinates are negative.

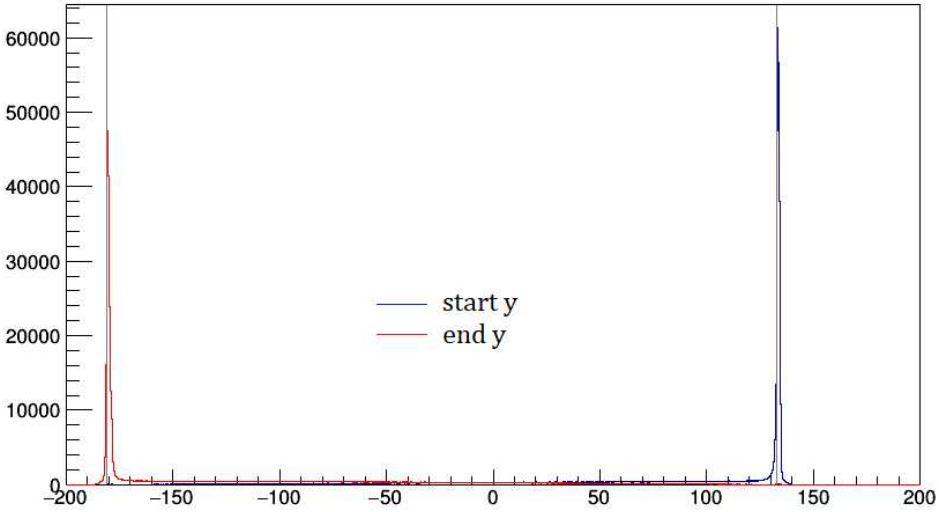

Figure 5.1: Y coordinate of the start (blue) and end (red) point for the t_0 tagged cosmic muon tracks longer than 50 cm in real collected events.

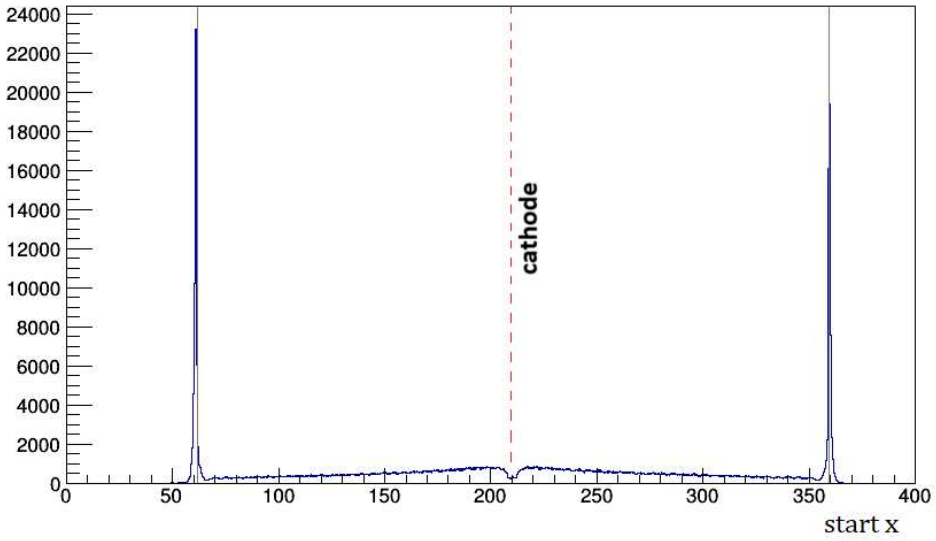

Figure 5.2: X coordinate of the start point for the t_0 tagged cosmic muon tracks longer than 50 cm in real collected events. The endpoints have a similar distribution.

Figure 5.2 shows also the presence of two peaks corresponding to the tracks entering from the wire planes. In addition, there are essentially no tracks starting at the cathode. The requirement for the track to be t_0-tagged implies that the track should cross the cathode: it is necessary to observe a segment of track on both sides of the cathode. If the track starts very near the cathode and crosses it, the segment of the track on one side results to be very short and the algorithm doesn't recognize it: this prevents flagging the track as cathode crossing and associating to the t_0. Another peculiar behaviour in real collected events was observed in the projection of the start and end points for example in the xy plane. The start/end point position at the top of the detector has a dependence on the x-drift coordinate, as shown in figure 5.4. This effect is produced by the accumulation of the positive argon ions in the active volume (*space charge effect*) [34]. When a charged particle crosses the liquid argon, it ionizes the Argon producing electron-ion pairs: while the electrons drift velocity is relatively high (maximum drift time about 0.94 ms), for the positive ions a longer time (several minutes) is required to reach the cathode. In addition, since the detector is continuously crossed by cosmic muons, an accumulation of positive charge is produced. This induces an alteration in the electric field, subsequently leading to a distortion in the particle trajectories recorded by the TPC. This electric field distortion is of the order of a few per cent, and is induced in particular at the TPC borders. The global effect in the observed muon tracks is the movement toward the central region of the TPC of the observed start/end point of the tracks. This effect is under study to introduce the proper correction at the reconstruction level. Also it is simulated in the studied MC events.

The track containment definition should necessarily take into account of this effect: for this reason, a track is defined as contained inside the detector only if both the start and end points of the tracks are at more than 5 cm from the boundaries of the active volume. This containment condition has been first of all applied to the track used in this study, to evaluate the performance of this request. The containment condition reduced the $\simeq$859000 available tracks to only about 76000 tracks. Only 9% of the cosmic tracks are classified as contained, demonstrating the effectiveness of this single requirement in rejecting the cosmic ray particles.

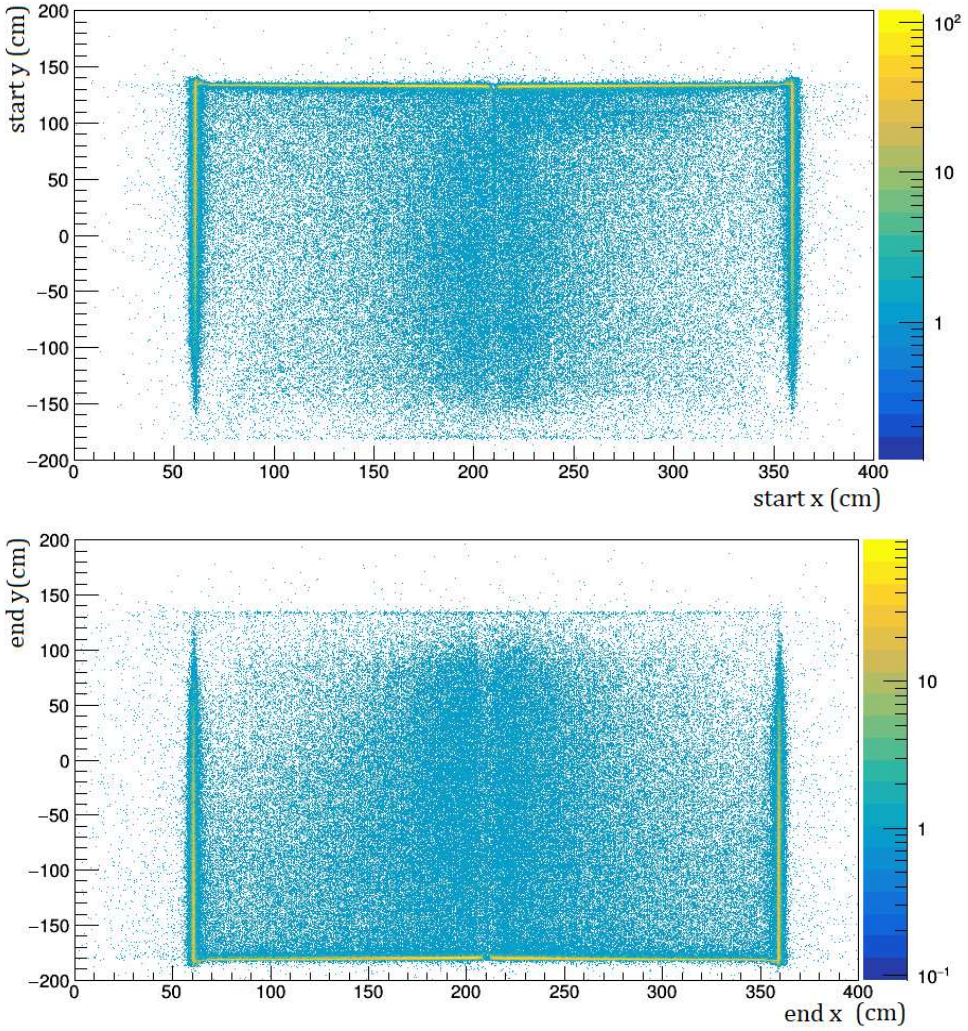

Figure 5.3: Start and end points in the xy-plane for f t_0 tagged cosmic muon tracks longer than 50 cm in real collected events

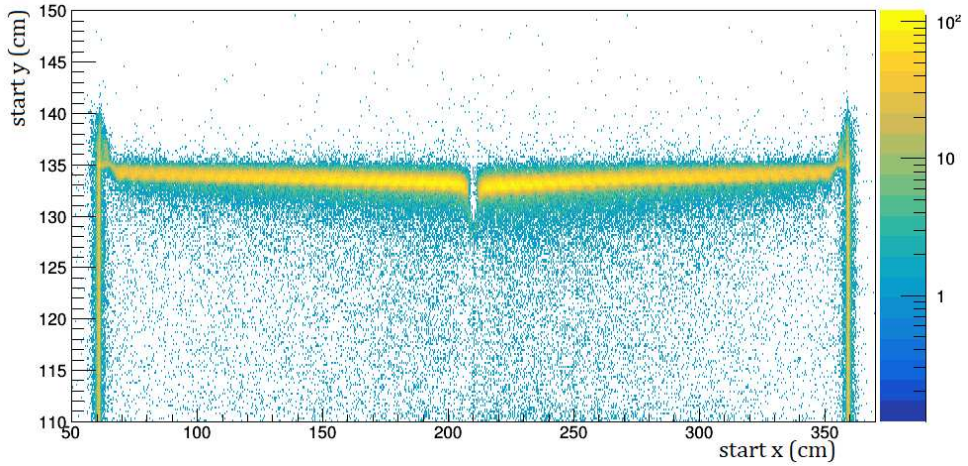

Figure 5.4: Zoom of the distribution shown in figure 5.3: the effect related to space charge is clearly visible. A similar effect can be also seen on the bottom region.

5.2 Preliminary selection studies in cosmic rays collected events

The identification of the fully contained neutrino events should be based on selection criteria that can strongly reduce the backgrounds from cosmics. For this reason, preliminary studies have been performed directly on the off-beam events collected in the detector in run 8460 (2952 events) and 9435 (10577 events). The distribution of the length of all the tracks in the studied events is shown in figure 5.5. The high number of tracks with a small length is related to the presence of short delta-rays and small electromagnetic showers that the TPC reconstructs as a track candidate. In addition a clear peak at around 320 cm is also visible: this is related to vertical cosmic tracks that are entering from the top and exiting on the bottom of the detector.

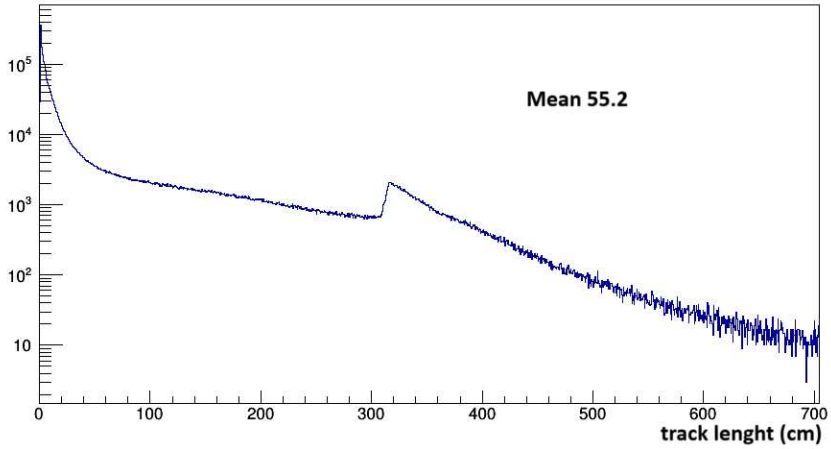

Figure 5.5: Length distribution of all the tracks reported in logarithmic scale.

For each event, the total number of reconstructed tracks with a length exceeding a minimum threshold L has been calculated: in figure 5.6 is reported the number of tracks with a length exceeding the minimum track length L as a function of L in the event; the color scale represents the number of events where a number of track corresponding to y has been found requiring the specific minimum track length corresponding to x. The average number of tracks per event rapidly decreases increasing the minimum track length L required, as expected.

	0 cm	**50 cm**	**100 cm**
Total track	119	29	22
Contained within 5 cm	71	7.5	4.4
No clear cosmic	27	6	4
No clear cosmic and contained	19.2	1.4	0.7
Match 150	12	4	2.5
Contained CC match 150 cm	2.3	0.2	0.1

Table 5.2: In this table the average number of tracks per event is reported with respect to the minimum track length considered; different additional requirements are also applied to select the tracks, as in the figures shown in this section.

Table 5.2 summarizes the average number of tracks per event considering different minimum track lengths for the selection and applying different requirements to the track. The impact of

the containment requirement can be seen comparing figure 5.7 with figure 5.6: a strong reduction is visible, in particular on longer tracks that are associated with cosmic muons that are crossing the detector, as described in the previous section. The information provided by Pandora can be used to discriminate between cosmics and neutrino candidates. As described in section 3.2, Pandora recognizes the clear cosmic tracks crossing the detector, providing a flag "clear cosmic" that is associated to the track and to all its secondaries. Figure 5.8 shows the corresponding reduction on the average number of tracks introducing the no-"clear cosmic" requirement. Since all the studied tracks are produced essentially by cosmic muons or by small showers produced by these muons, a strong reduction with respect to figure 5.5 is expected also in this case. The combination of the containment and the no-"clear cosmic" requirements results in a powerful tool to reject the cosmics. A factor 20 reduction is obtained for cosmic tracks longer than 50 cm (average number of tracks before any cut: 29; average number of tracks after these two requests: 1.4, as shown in table 5.2).

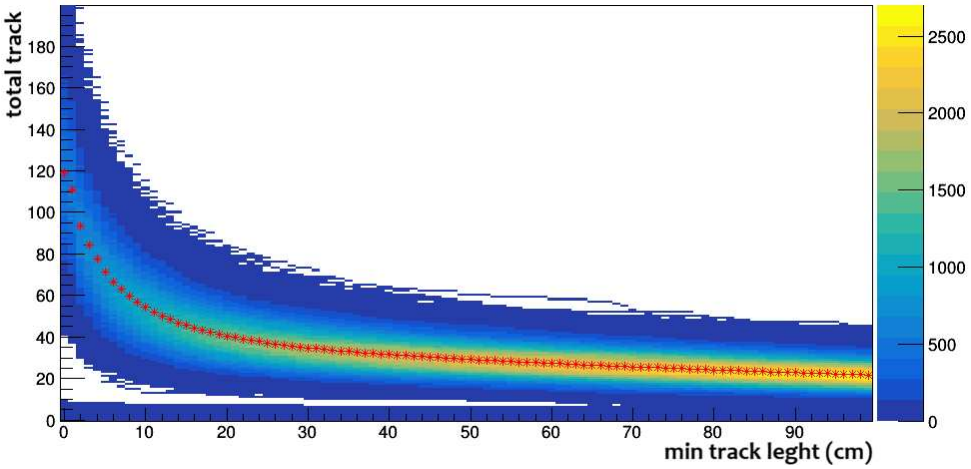

Figure 5.6: Total number of tracks in function of the minimum required track length without any filter.

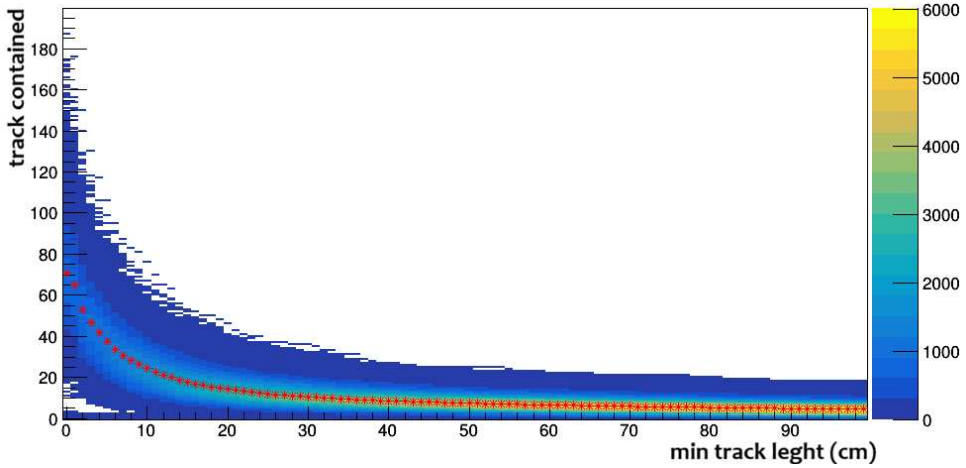

Figure 5.7: Number of tracks that are contained within 5cm from the active volume boundaries as a function of the minimum required track length.

The identification of the particle responsible for generating the trigger should also benefit from the correlation between light and charge, which was explored in the previous chapter. The im-

pact of the association has been studied requiring that a track is selected only if the distance between the charge and light barycenters is smaller than 150 cm (see figure 5.9) resulting in a large reduction in particular for long cosmic muons. In fact, the request of a track whose barycenter is within 1.5 m from the light barycenter implies a reduction of a factor $\simeq 6$ of the volume observed in each cryostat (along z the detector is 18 m long and a region of interest of 3 m is considered by this selection requirement). In addition in many events the light signals generating the trigger are present only in one cryostat, producing an additional factor 2 reduction of the observed detector volume.

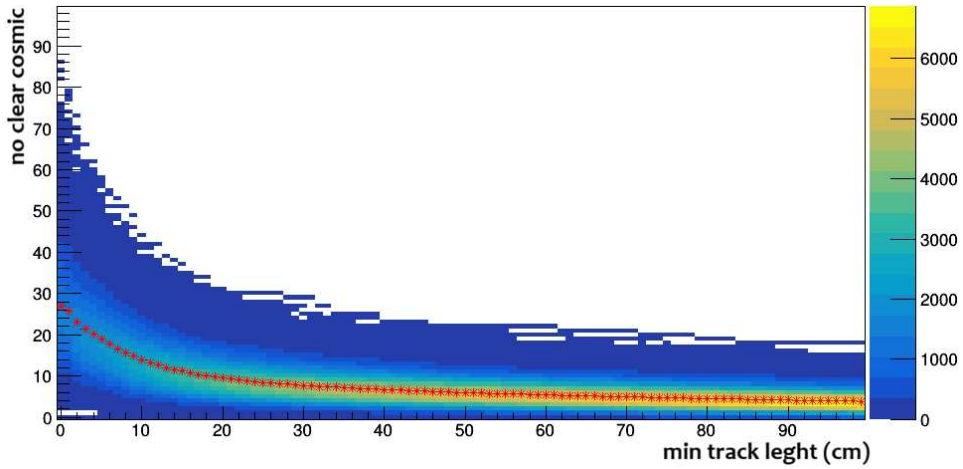

Figure 5.8: Number of tracks that are no clear cosmic as a function of the minimum required track length.

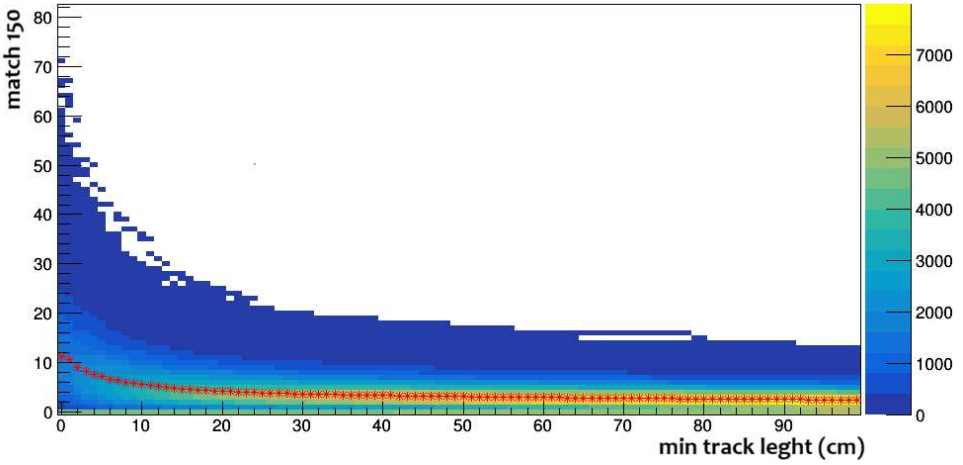

Figure 5.9: Number of tracks that have a charge-light match within 150 cm as a function of the minimum required track length.

All the mentioned requirements have been finally combined: a track is selected only if it satisfies the light-charge association, the containment requirement and if it is not tagged as "clear cosmic" by Pandora. For each event the total number of tracks that survive all the requirements is shown in figure 5.10 as a function of the minimum track length required. The reduction with respect to figure 5.5 is very strong. The application of these requirements results in a powerful cosmic

rejection filter and will be used to reduce the background from cosmics in the search for neutrino interactions.

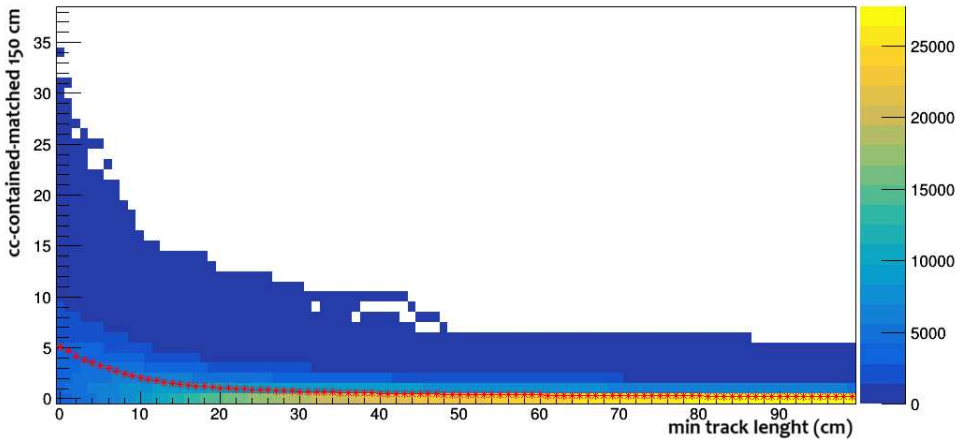

Figure 5.10: Number of tracks in each event that have a charge-light match within 150cm, that are contained within 5cm inside the detector and are flagged as no clear cosmic as a function of the minimum required track length.

5.3 Selection of the events

In this section, the development of a selection "filter" to identify possible neutrino candidates will be described. This analysis is applied to:

- the most recent MC neutrino simulation, to obtain a direct evaluation of the selection efficiency for the neutrino interactions;
- the real events collected off-beam, to obtain a direct evaluation of the expected residual cosmic backgrounds;
- the real events collected on-beam, where the trigger can be generated by cosmic rays or by neutrinos, to validate the selection performance for the neutrino interactions.

The focus of the proposed selection will be the muon neutrino interactions fully contained in the detector and with a muon track longer than 50 cm, and in particular the Quasi Elastic (QE) events.
The first goal of the selection is the identification of the particle that generates the trigger exploiting the PMT signals. To this purpose the differences between data and MC should be taken into account (see figure 3.9). The flash signals generating the trigger will be identified using the requirements already described in table 3.3. Once identified, the light signal associated to the trigger is associated to the TPC tracks as described in the previous chapter by selecting only tracks with a charge barycenter within ΔBar from the light signals barycenter along the longitudinal z-axis. This association is applied after the track merging procedure described in section 4.3.
To match the condition adopted for the identification of the muon in ν_μ CC interactions, the considered track should be longer than 50 cm. In addition, the selected track should not be tagged by Pandora as a clear cosmic track and has to be contained in the detector within 5 cm,

as discussed in paragraph 5.1. This track should also have a good 3D reconstruction, to allow additional analysis of the selected events as for example the measurement of the dE/dx along the track and the particle identification.
The last condition is related to the CRT: all the events with a CRT signal in coincidence with the trigger are vetoed as cosmic event and rejected. This criterion has been added since the filtering procedure is meant to select neutrino interactions fully contained in the active LAr. The presence of a CRT signal implies in fact that the particle generating the trigger is coming from outside the detector or is exiting from the detector.
This selection filter should be properly tuned and studied. Different values between 70 and 150 cm have been considered for the maximum allowed distance ΔBar between the light and charge barycenters, following the results previously described in Chapter 4.
In addition the number of 3D points associated with the hits of the track in Collection N_{HIT3D}, the length of the track L_μ and the average 3D distance between two reconstructed 3D points in the track $L_{3D} = \frac{L_\mu}{N_{HIT3D}}$ have been exploited to define the quality of the 3D track reconstruction. Different conditions have been tested for the selection of the track:

- case "N_{HIT3D}>0";
- case "N_{HIT3D}>50";
- case "L_{3D}<1";
- case "L_{3D}<0.75";
- case "L_{3D}<0.5";

The selection filter has been first applied to the simulated neutrino events. Table 5.3 reports the variation of the selection efficiency with respect to the different selection criteria for both the 3D track condition and the barycenter light-charge association. The filter efficiency has been evaluated for the ν_μ CC QE events fully contained and with a muon track longer than 50 cm. The efficiency as a function of ΔBar is reported in figure 5.11.

	70 cm	**90 cm**	**110 cm**	**130 cm**	**150 cm**
N_{HIT3D}>0	0,91	0,92	0,93	0,93	0,93
N_{HIT3D}>50	0,90	0,91	0,91	0,91	0,92
L_{3D}<1	0,88	0,89	0,89	0,90	0,90
L_{3D}<0.75	0,84	0,85	0,86	0,86	0,86
L_{3D}<0.50	0,69	0,70	0,70	0,70	0,70

Table 5.3: Selection efficiency for the ν_μ CC QE contained MC events with a muon longer than 50 cm as a function of the distance ΔBar and of the different request for the 3D quality of the track: these values are also shown in figure 5.11.

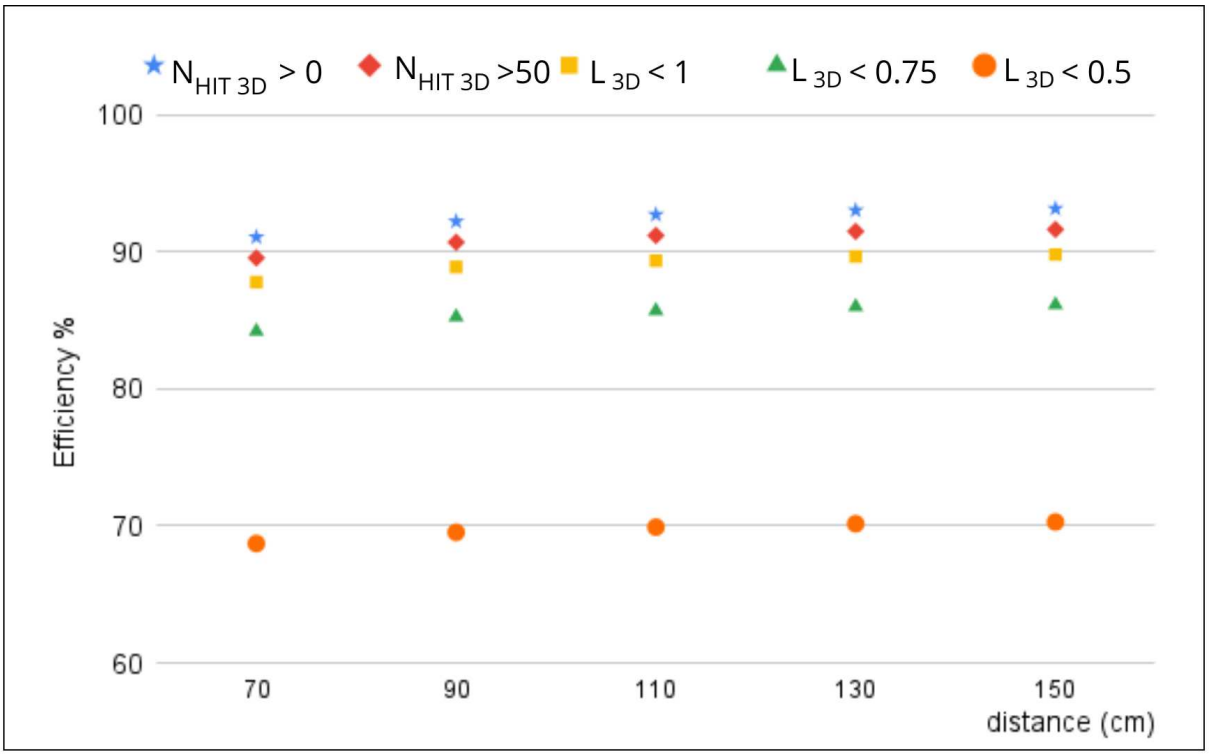

Figure 5.11: Selection efficiency for the ν_μ CC QE contained MC events with a muon longer than 50 cm: the dependency as a function of the distance ΔBar and of the different request for the 3D quality of the track is shown.

Then, to evaluate the impact of the different conditions on the cosmic backgrounds, the filter was also applied to the available 10577 off-beam events collected in run 9435. Figure 5.12 and table 5.4 show how the number of cosmic background changes as a function of the different criteria applied. In both cases, the graphs are reported as a function of the applied maximum ΔBar (x-axis) and of the 3D quality selection criteria (different markers).

distance (cm)	N_{HIT3D}**>0**	N_{HIT3D}**>50**	L_{3D}**<1**	L_{3D}**<0.75**	L_{3D}**<0.5**
70	130	95	78	69	42
90	148	108	91	79	49
110	166	116	99	86	53
130	176	121	103	89	55
150	183	127	110	96	59

Table 5.4: Number of background cosmic events selected among the off-beam events, as a function of the distance ΔBar varying the selection criteria, (see also figure 5.12). These backgrounds are selected among a sample of 10577 events.

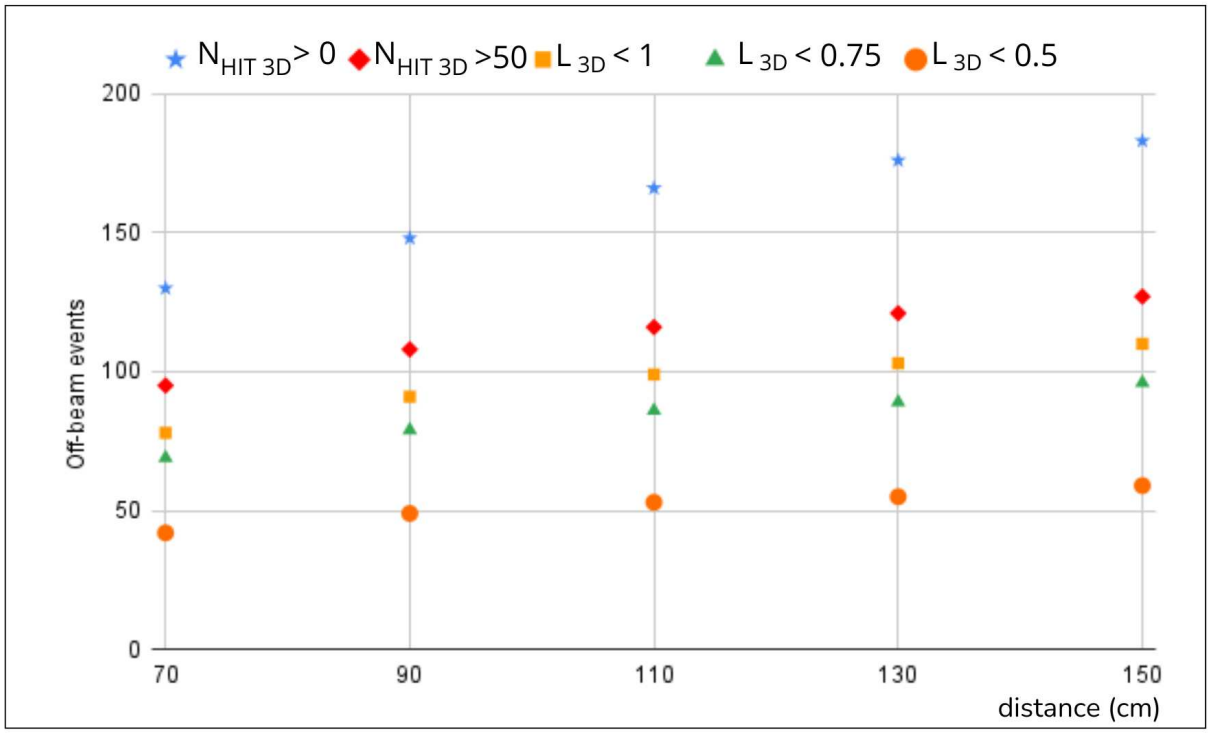

Figure 5.12: Number of background cosmic events selected by the filter in the off-beam event sample as a function of the distance ΔBar and varying the selection criteria applied for the quality of the track 3D reconstruction. These backgrounds are selected among a sample of 10577 events.

The comparison between these results shows that the request for the 3D quality of the track $N_{HIT3D}>0$ gives the highest level of efficiency at each distance ΔBar but also a large number of cosmic selected events. This is because the track can be selected even if it is badly reconstructed in 3D. This can happen quite frequently for the electromagnetic showers present in the cosmic rays interactions.

At the same time, the constraints $L_{3D}<0.75$ and $L_{3D}<0.5$ give the lowest number of backgrounds at the cost of a reduction of the efficiency on neutrinos. In fact, in these last two hypotheses, a larger number of 3D points should be associated with the hits in the Collection view. Since in Collection a 2D projection of the 3D track is visible this requirement translates into a requirement on the direction of the track[1]. Taking into account these results, I restrict the possible conditions for the 3D quality of the track to the request $L_{3D}<1$ or to the request $N_{HIT3D}>50$. Moreover, the selection efficiency for the neutrinos is only slightly increasing if the maximum distance ΔBar is increased (figure 5.11), as expected from the study on the ligth-charge association. This behavious is observed for all the different 3D condition criteria considered. The number of cosmic rays exhibits instead a more evident increase changing the distance ΔBar, as shown in table 5.4, suggesting to consider a reduced maximum distance between light and charge barycenters to select the neutrino candidates and reduce the backgrounds.

The final definition of the filter has been obtained by applying the filter to the real data recorded on-beam, where neutrino should also be present, from both run 8460 and run 9435. The different

[1]For example, if a track is 1 m long the request $L_{3D}<0.5$ implies that at least 200 hits in Collection associated with 3D points should be present: the average segment of the track seen by each wire (pitch) should be <0.5 cm. It is important to remember that since the distance between two wires is 3 mm, the pitch can not be smaller than 3 mm.

conditions on the charge-light barycenter matching and the request $L_{3D}<1$ or $N_{HIT3D}>50$ for the 3D quality of the track have been considered. Once the filter has been applied, the tracks in each selected event have been visually studied using the ICARUS event display. The main goal of this scanning phase is the recognition of the neutrino events, discriminating them from the cosmic particles. Neutrino candidates with a primary track with no hadronic interactions and a length[2] $L_{\mu}>50$ cm are classified as a "muon neutrino CC interaction". If all the tracks associated with the neutrino are contained, the neutrino is classified as contained.
The results obtained from the scanning are summarized in figure 5.13 and 5.14. The figure 5.13 shows the total number of events that have been visually studied (left) and the total number of neutrino candidates identified by scanning (right) as a function of ΔBar and for the two separate requirements $L_{3D}<1$ or $N_{HIT3D}>50$.
The purity of the selection is defined as the ratio between the identified contained neutrino candidates and all the events visually studied. This parameter is shown in 5.14 (left) together with the number of identified contained neutrino events (right). In tables 5.5 and 5.6 are also reported the corresponding numbers of events when the conditions $L_{3D}<1$ or $N_{HIT3D}>50$ are applied.

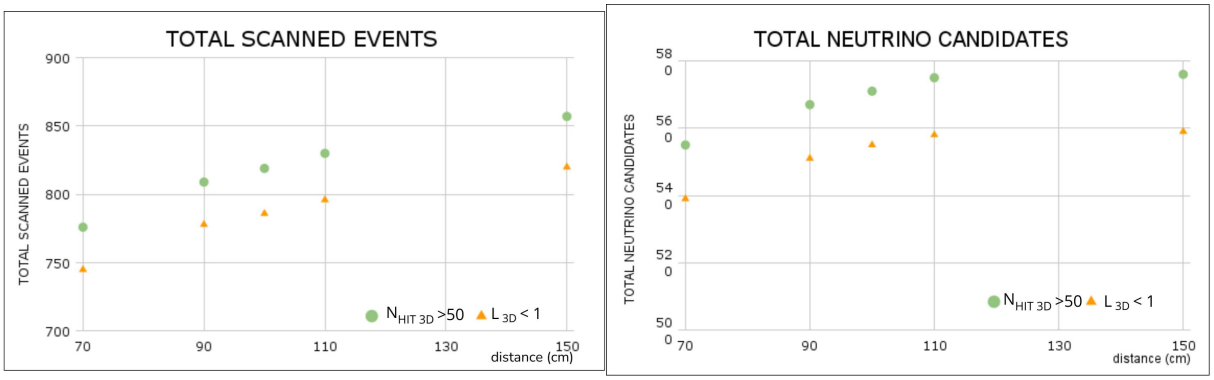

Figure 5.13: Number of total scanned events (left) and total number of neutrino candidates identified (right). These results are shown as a function of the maximum distance ΔBar applied for the light-charge association and for the two different conditions for the 3D quality of the track.

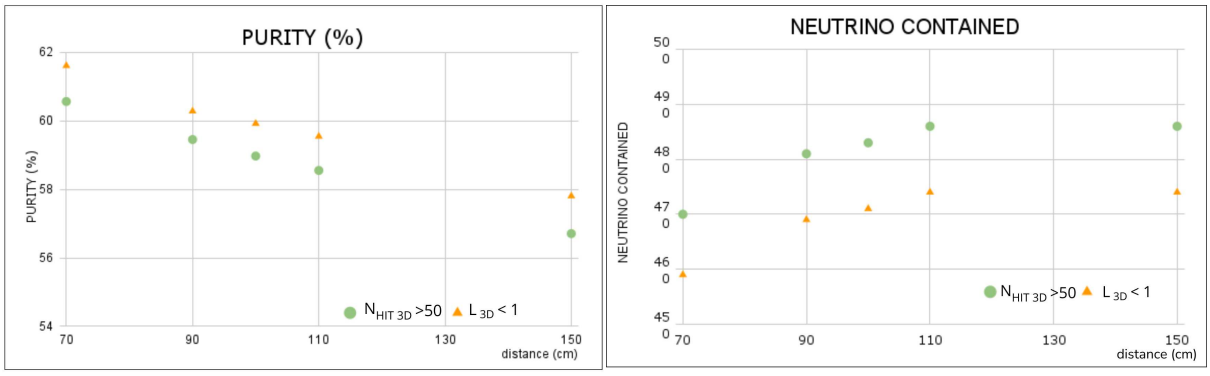

Figure 5.14: Purity (left) and number of neutrino fully contained recognized in the scanning (right) in both run 8460 and 9435. These results are shown as a function of the maximum distance ΔBar applied for the light-charge association and for the two different conditions for the 3D quality of the track.

[2]During the scanning phase, the track length is evaluated as the 3D distance between the start and end point of the track.

ΔBar (cm)	**Total scan events**	ν **contained**	**Total** ν **candidates**	**Cosmics**	**Other interactions**	**Purity (%)**
70	776	470	555	136	85	60.6
90	809	481	567	156	86	59.5
100	819	483	571	162	86	58.9
110	830	486	575	168	87	58.5
150	857	486	576	194	87	56.7

Table 5.5: Number of events selected by the filter and visually studied and their classification as a function of ΔBar with the request for the quality of the track to have at least 50 3D points in Collection.

ΔBar (cm)	**Total scan events**	ν **contained**	**Total** ν **candidates**	**Cosmics**	**Other interactions**	**Purity (%)**
70	745	459	539	124	82	61.6
90	778	469	551	144	83	60.3
100	786	471	555	148	83	59.9
110	796	474	558	154	84	59.5
150	820	474	559	177	84	57.8

Table 5.6: Number of events selected by the filter and visually studied and their classification as a function of ΔBar with the request for the quality of the track in Collection $L_\mu/N_{HIT3D} < 1$.

These results indicate ΔBar=110 cm as an optimal choice: beyond this value no additional contained neutrinos are identified while the number of cosmics still increase. This indicates that for distances between the light and charge barycenters larger than 110 cm the filter is in most cases wrongly associating out-of-time cosmic tracks to the in-time studied flash.
The purity results higher considering ΔBar in the 70-90 cm range, but the total number of observed neutrino candidates is reduced. In addition the comparison between ΔBar = 70 cm and ΔBar = 90 cm shows that the observed variation in the purity is relatively smaller with respect to the corresponding variation in the observed neutrinos. Finally, even if the purity is higher requiring L_{3D}<1 for the quality of the 3D reconstruction, the condition N_{HIT3D}>50 leads to a higher number of neutrino events found by the filter. For all these reasons the selection filter for the collected events has been setup using the following requests:

- presence of a light flash signal with a flash time between -0.68 and -0.54 μs, corresponding to the particle generating the trigger;
- identification of a track whose charge barycenter along the z longitudinal direction has a distance smaller than 110 cm from the light barycenter;
- the selected track should be longer than 50 cm;
- the selected track should be contained;
- the selected track should not be classified as clear cosmic by Pandora;
- the selected track should have at least 50 3D space points associated to the hits in Collection;
- in the event, there should be no CRT hit signals in coincidence with the trigger;

The impact of each selection criteria on all the studied datasets are summarized in table 5.7 for both off-beam and on-beam data and for the simulated neutrino interactions.

Selection criteria	8460 **BEAM OFF**	**BEAM ON**	9435 **BEAM OFF**	**BEAM ON**	**MC ν_μ CC-QE fully contained $L_\mu > 50$ cm**
All available events	2952	3788	10577	7372	7696
At least 1 track and 1 flash	2662	3437	9816	6904	7672
Light - charge association	2660	3417	9809	6884	7609
$L_{track} > 50cm$	2648	3343	9741	6746	7291
Containment	1093	1466	3836	2992	7143
No "clear cosmic"	403	648	1335	1295	7135
Good 3D track reconst.	241	504	846	988	7018
No CRT hit intime	32	286	116	544	6979

Table 5.7: Impact of the selection criteria when applied to our data sets. For the light charge association, the maximum accepted distance between the barycenters is 110 cm, while for the track 3D quality condition N_{HIT3D}>50 is applied. In order to have a more direct comparison, in each run the same POT/livetime statistics has been considered for the on-beam and for the off-beam data. For the MC events, only the ν_μ CC contained within 5cm con L_μ di 50 cm have been considered.

The selection criteria with the most significant impact on the real data are the containment within 5 cm and the "clear cosmic" tag: both cuts remove about 60 % of the events. These cuts are essentially removing the events where a cosmic particle has produced the trigger. Another requirement that has a substantial impact on the number of events is the CRT veto, providing a strong reduction of the residual cosmic events that survive the previous cuts. This is also confirmed by the comparison between BEAM ON and BEAM OFF real events: while the reduction for the ON beam events is about a factor 2, for the OFF beam events, where only cosmics are present, the reduction is about a factor 7. The impact on Monte Carlo events is instead minimal because the previous requirements already select contained neutrinos with a 50 cm long muon. It is interesting to notice that a 4% reduction is introduced by the request of a track longer than 50 cm in the studied MC ν_μ CC-QE. Considering that these are events with a muon track longer than 50 cm, this decrease is due to some inefficiency in the track reconstruction, as for example when the track is split into pieces that are not merged together.
Table 5.8 shows the classification provided by the visual scanning of the events selected in the studied on-beam events in real data.

	RUN 8460	**RUN 9435**
Cosmics	58	110
Neutrino contained	183	303
Neutrino not contained	24	58
Other interactions	18	69
Candidates nue	3	4
Total scan	286	544

Table 5.8: Number of events after the scan procedure for the on-beam data of both run 8460 and 9435.

Some examples of the neutrino events recognized in the studied sample are shown in figures from 5.15 to 5.21. In total the visual study identified 486 ν_μ CC contained candidates with muon length L_μ distribution as shown in figure 5.22.

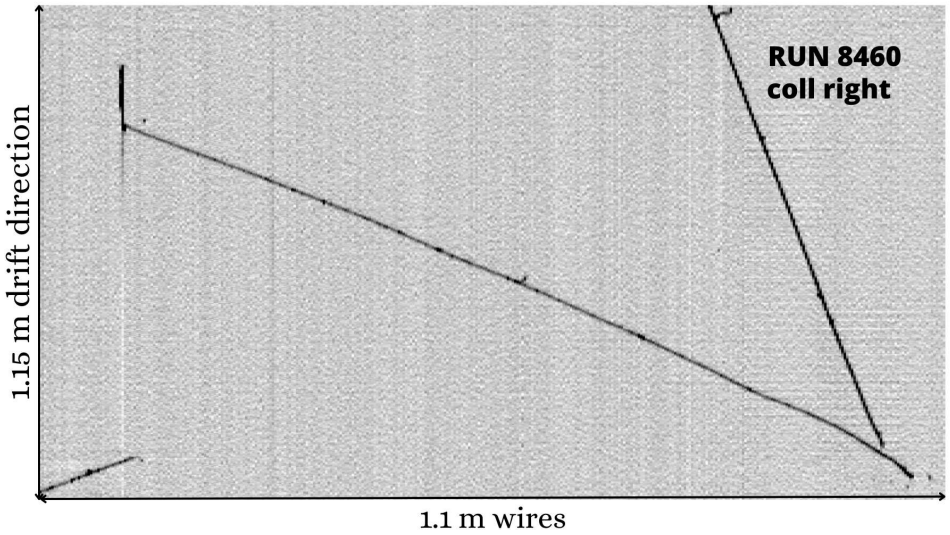

Figure 5.15: Event from run 8460, event number 1082, collection view. In the figure is evident the presence of a muon track and a shorter track, a proton, at the primary vertex.

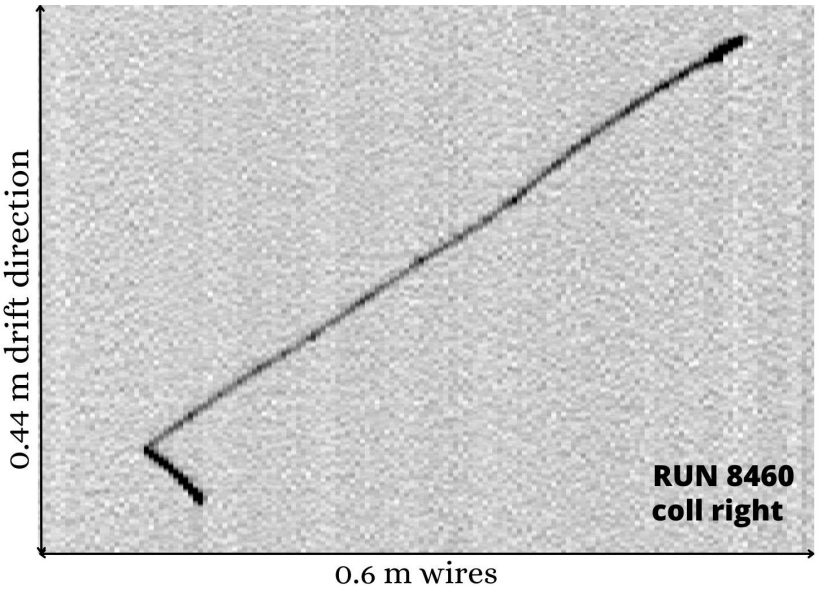

Figure 5.16: Event from run 8460, event number 3309, collection view. This is an example of a muon neutrino CC QE event. At the primary vertex two tracks are present: the proton (3D length 6.9 cm) and the muon (3D length 57 cm). It is also visible that the ionization at the end of the muon track is higher as expected: the signal associated at the track is in fact darker at the end of the track.

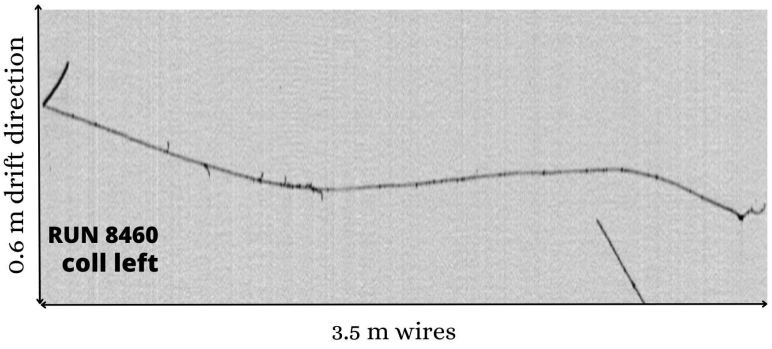

Figure 5.17: Event from run 8460, event number 4040, collection view. The muon length, measured as the distance between the start and the end point, is about 3.4 m

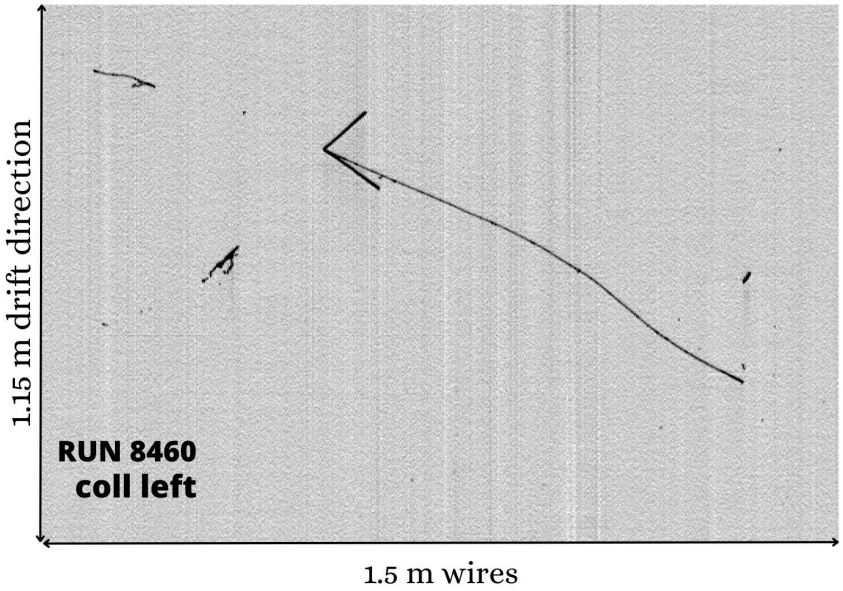

Figure 5.18: Event from run 8460, event number 1052, collection view. In this event, there are three tracks connected to the same vertex, two protons and a long muon track with L_μ=1.17 m. Two electromagnetic showers are also visible and they are both pointing to the vertex indicating the possible decay of a neutral pion.

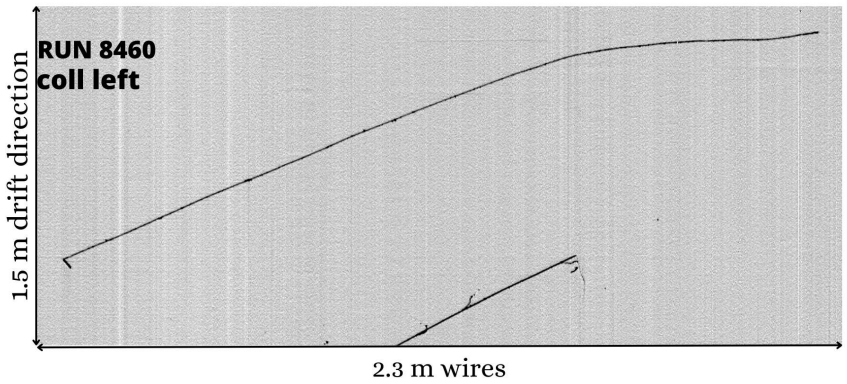

Figure 5.19: Event from run 8460, event number 2372, collection view. This event is characterized by a very long muon track (3.9 m) with a small proton at the vertex (L=5.3 cm). This is an example of a muon neutrino CC QE event.

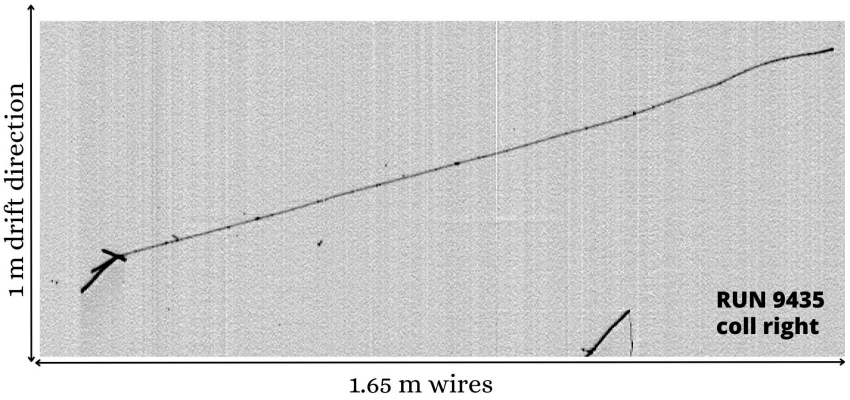

Figure 5.20: Muon neutrino fully contained interaction with 4 proton tracks at the primary vertex (Event 11259 from run 9435). The length of the muon is 1.6 m while the lengths of the proton tracks are 30, 7.3, 5.7 and 3.1 cm.

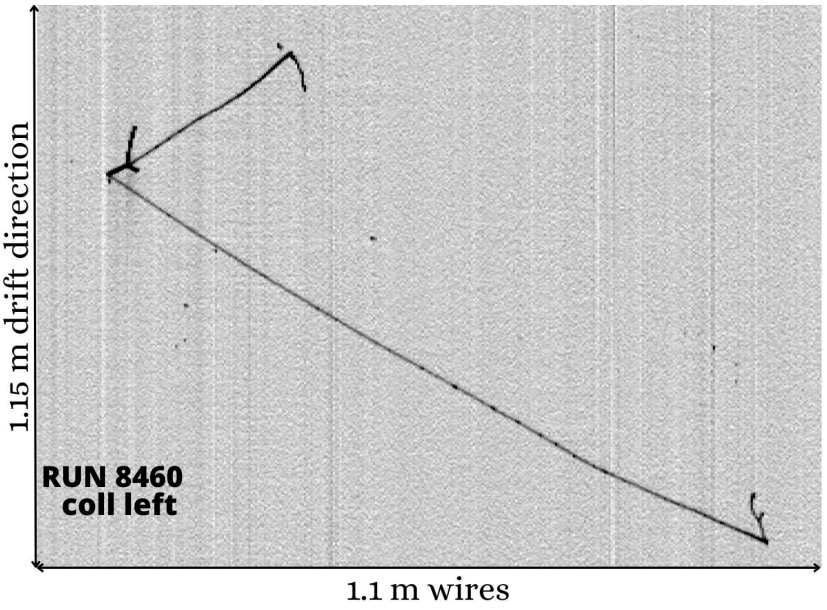

Figure 5.21: Selected muon neutrino CC fully contained (Event 11294 from run 8460). The muon track is 1.15 m long and the Michel electron produced by the muon decay is clearly visible at the end of the track.

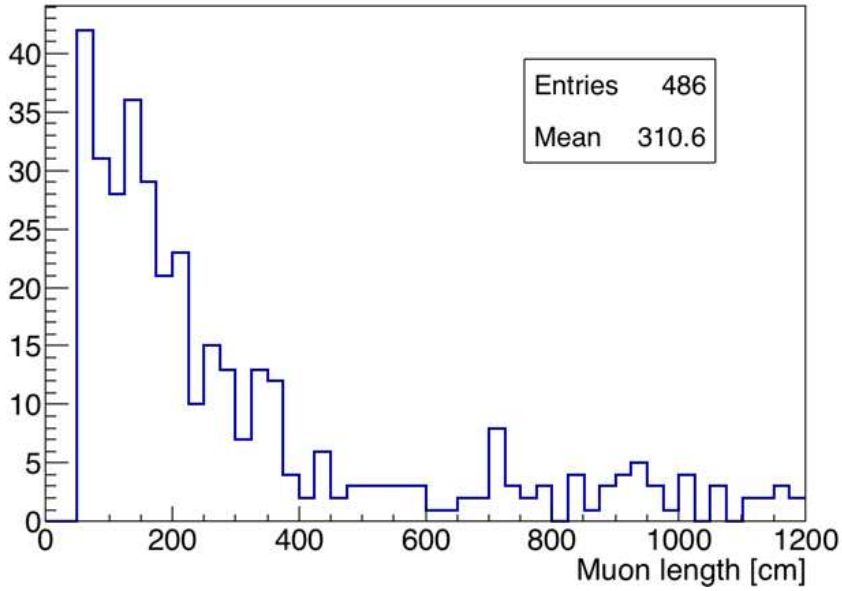

Figure 5.22: Distribution of the muon length of the 486 events found with the scanning procedure. L_μ is defined as the 3D distance between the start and the end point of the track.

5.4 Discussion on the selection results

The filter defined in the previous section has been applied to all the available event samples and the consistency of the obtained results, including a comparison between real data and Monte Carlo simulations will be presented in this section.

The number of cosmic events found by the scanning group in the on-beam data, 58 from run 8460 and 110 for run 9435, can be first of all compared with the number of events selected in the off-beam sample (32 from run 8460 and 61 from run 9435) (tab. 5.4). In fact, even if the scanning on the off-beam events has not been performed, all the events selected in the off-beam sample are associated to cosmics.

RUN	off-beam	on-beam
8460	32	58
9435	61	110

Table 5.9: Number of cosmics events in off-beam and on-beam data after the scanning procedure.

The number of cosmics identified during the scanning in the on-beam events is larger compared to expectations from the off-beam data due to the presence of additional contributions in the on-beam events with respect to the off-beam data. It is important to remember that the selected cosmics can be related to the particle generating the trigger but also to cosmics randomly crossing the detector during the drift time (not distinguished in this study). This last contribution is essentially proportional to the number of events observed. In the on-beam events, in addition to the events whose trigger is generated by cosmics, there are also the interactions related to the neutrino beam and also in these events some out-of-time cosmics can be selected by the filter. For example, in an event with no contained neutrino, a badly reconstructed cosmic track out of time can be selected, increasing the number of events seen in the on-beam data. Another example is

related to the dirt events: in these events a neutrino interaction outside the active volume can inject particles inside the active volume, inducing a trigger. In some cases these particles can be selected by the filter (and from the scanning, this event can be classified as "other interaction") or, as for the neutrino interactions, also in these events an out-of-time cosmics can be selected, enlarging the number of cosmics seen in the on-beam sample. Furthermore, even the dirt events themselves are sometimes characterized by incoming tracks that can be incorrectly labelled as cosmic muons during scanning. An example is a muon that enters the detector because the vertex is outside the active volume, as shown in figure 4.30. Finally, it is also possible that the filter selects by mistake a passing out-of-time cosmic event recorded in an event with a not contained neutrino interaction that is properly removed.
The filter has been applied to all the simulated MC events to see the impact of this selection on different neutrino event topologies; in particular, the following categories, defined using the available MC truth information, have been considered[3]:

1. ν_μ CC QE contained with $L_\mu > 50$ cm
2. other ν_μ CC interactions contained and with $L_\mu > 50$ cm
3. ν_μ CC contained with $L_\mu < 50$ cm
4. NC contained events with a primary proton/pion longer than 50 cm
5. other NC contained
6. ν_μ interactions not contained
7. ν_e interactions

Event topology	**Pre filter**	**Post filter**	**Efficiency (%)**
1	7696	6979	90.7
2	7968	7178	90.1
3	4054	1062	26.2
4	1256	1129	89.9
5	15062	1246	8.27
6	30681	2746	8.95
7	432	220	50.9

Table 5.10: Comparison of the number of events obtained before and after applying the filter with $\Delta Bar = 110$ cm and the requirement of at least 50 3D points along the track. The efficiency of the filter is the ratio between post/pre application of the filter. The classification 1 to 7 of the event topology is reported in detail in this paragraph.

Table 5.10 presents the results obtained by applying the chosen filter to all these categories.
As expected all the categories of contained neutrino events with a primary track longer than 50 cm (categories 1-2-4) pass the filter with an high-efficiency, about 90% levels. Instead the neutrino events that do not meet the selection criteria (categories 3-5-6) are largely rejected by the filter. For example, the not contained neutrino interactions (category 6) are selected in $\sim 12\%$ of cases mostly because an exiting long track is split into segments and is reconstructed

[3] In all these categories the containment is defined within 5 cm, as previously discussed.

as contained. A track merging algorithm more sophisticated than the one described in Chapter 4 could improve the identification of uncontained tracks.
The higher efficiency for the ν_μ CC contained con $L_\mu < 50$ cm (category 3) can be instead related to the possible presence of pion or proton tracks at the primary vertex that results longer than 50 cm: on the sub-sample of these events (that are 594), a 90% efficiency is found, similar to the other categories where a long track is present.
In category 5 (NC interactions with no primary particle track longer than 50 cm), the presence of a track associated with a particle produced in a secondary interaction vertex can explain the selection of these events.
The final step is to verify the consistency between the observed neutrino events in the on-beam real data and the Monte Carlo (MC) simulations of neutrino interactions. The first element needed for this analysis is related to the impact of the visual study of the events. During the scanning phase, the possible neutrino candidates are studied and classified on the basis of the signals seen in the event display, with no reconstruction information. In order to evaluate the effect of the visual study a sample of MC event has been scanned with the same procedure as the real data, estimating how many events for each category would be classified as fully contained neutrino with a muon longer than 50 cm. For the ν_μ CC contained with a long muon (category 1 and 2) the scanning procedure was not applied assuming the scanning to be fully efficient for this simple topology. Similarly category 6 has not been further studied assuming that not-contained muon neutrino interactions should be easily recognized in the scanning phase. No comparison will be performed for this category since this event topology is not the focus of this analysis. Finally the ν_e interactions (category 7) has not been studied in detail for the moment. The electron neutrinos are the golden sample to study the $\nu_\mu \rightarrow \nu_e$ oscillation but the ν_e intrinsic contamination in the beam is about 0.6 % of the muon neutrino interactions resulting in an expected number of events in the considered runs too small to extract any conclusion.
For the ν_μ CC contained with a short muon (category 3) and for the contained NC events (categories 4 and 5) a dedicated scanning campaign has been setup. For these event topologies, we know from the truth MC information that there are no muon tracks produced at the primary vertex with L_μ>50cm but there can be other particles (pions or protons) with associated long tracks that can be misidentified as muon during the scanning. Scanners do not have any a priori information about the simulated events, so the treatment is exactly the same as real data, selecting the events they judge to be a "good candidate" fully contained muon neutrino CC interaction with a muon track longer than 50 cm. Table 5.11 summarizes the outcome of this visual study of MC neutrinos: the "After filter" column shows the number of events selected by the filter and visually studied, while the "Scanning" column shows the number of events that are selected in the scanning as "good candidates"[4]. The scanning efficiency is determined by the ratio between the events selected by the scanning as good candidates and the events selected by the filter and visually studied. This efficiency will be used to evaluate for each category the expected number of events observed in real data.

[4] All the events used for the analysis of this thesis have been visually studied in collaboration with the ICARUS Scanning Working group

Event topology	After filter	Scanning	Scan Efficiency
3	252	103	40.9
4	198	108	54.5
5	105	13	12.4

Table 5.11: Number of events that pass the filter stage and the scanning stage. The visual scanning is performed only for the event topology 3 (ν_μ CC contained L_μ<50cm), 4 (NC contained events with primary proton/pion > 50 cm), and 5 (other NC contained interactions).

In figure 5.23 and 5.24 there are two examples of MC events that have been selected by the filter and then visually studied. Both events are not ν_μ with L_μ>50cm but a clear long track, associated to a pion, is visible. In the event 5.23 the pion doesn't make any visible hadronic interaction and decays: for this reason in the scanning it is misidentified as a muon track and the event is considered a ν_μ CC contained; in the second event during the scanning the hadronic interaction of the pion has been recognized and the event has been classified as "other interaction".

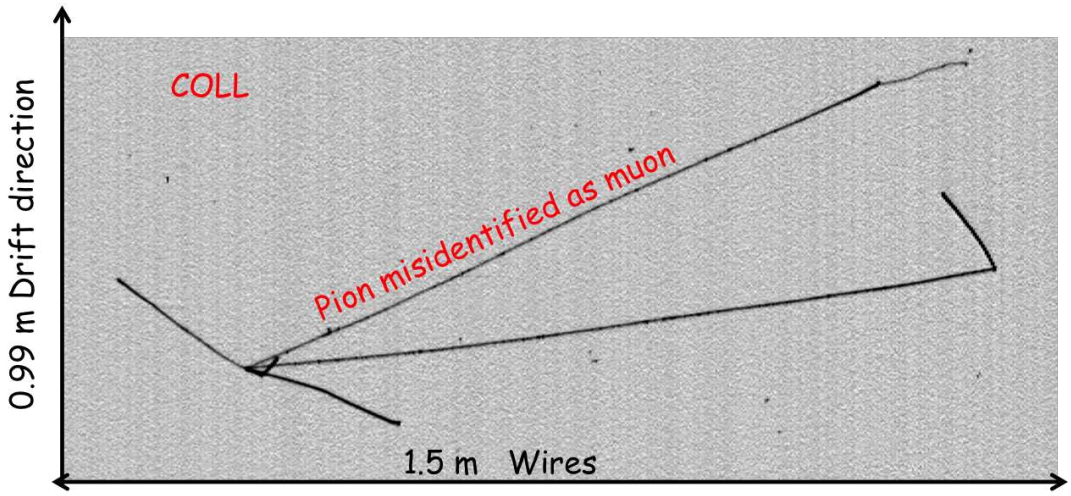

Figure 5.23: Example of a simulated muon neutrino CC interaction fully contained but with a muon shorter than 50 cm event. This event has been selected by the filter and it has been visually studied. In this event, a pion is generated at the primary vertex and it produces a track with a length of about 1.4 m. This track results to be similar to a muon track and for this reason in the scanning this event is classified as a muon neutrino CC contained and with a muon longer than 50 cm.

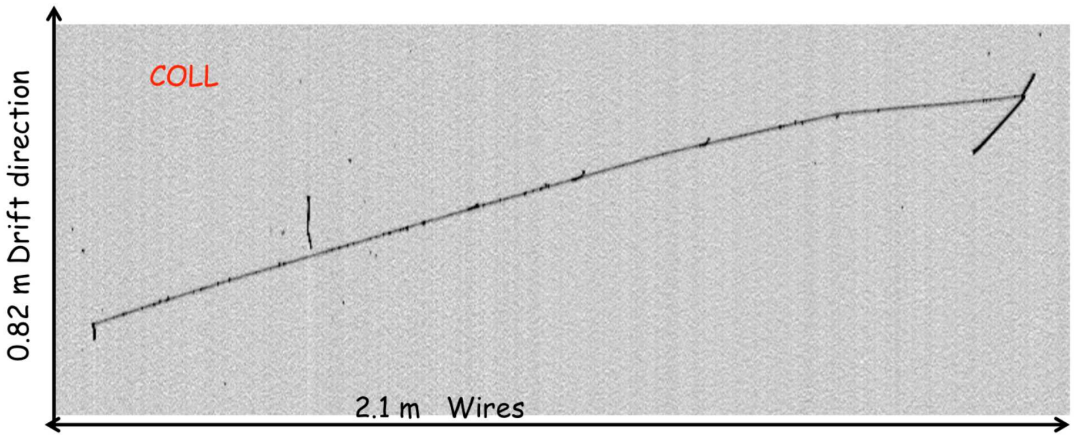

Figure 5.24: Example of simulated Neutral Current event fully contained and with a primary pion longer than 50 cm selected by the filter. In this event, a long track is clearly visible and for this reason the event is selected. Differently from the previous example, in this case the pion produces a hadronic interaction: at the scanning level it is possible to recognize that this is a pion and to discard this event including it in the scanning category "other interactions"

To perform a quantitative comparison between the observed number of neutrinos in the studied runs and the expectations from MC, the amount of protons on target (POT) directly associated with the number of interactions in the detector is required. The number of neutrino events that are present in the MC simulation ($\#\text{evt}_{MC}$) should be scaled with the ratio between the POT of data and MC samples[5] to predict the expected number of events $\#exp_{data}$ in the studied runs:

$$\#exp_{data} = \#evt_{MC} \cdot \frac{pot_{RUN}}{pot_{MC}} \tag{5.1}$$

where pot_{RUN} and pot_{MC} are the POT collected in the data and simulated in MC.
In table 5.12 the expected number of events $\#exp_{data}$ in the studied runs are summarized. In the "Pre-filter" column, for each category, the number of expected event $\#exp_{data}$ is indicated before the application of any filter/scanning procedure. In the column "post filter+scan" the number of events expected at the end of full procedure based on the filter and on the visual study is reported: this number is obtained multiplying the number of expected events in the "Pre-filter" column for the filter efficiency (see table 5.10) and for the scanning efficiency (see table 5.11).

[5] In table 3.2 there are details on the two acquisition RUN used for the analysis

Event topology	RUN 8460		RUN 9435	
	Pre filter	post filter + scan	Pre filter	post filter + scan
1	75.7	68.7	137.67	124.9
2	78.4	70.6	142.53	128.4
3	39.9	4.3	72.52	7.8
4	12.4	6.1	22.47	11.0
5	148.2	1.5	269.43	2.8
Total sum	354.6	151.2	644.62	274.9

Table 5.12: Number of events expected based on the POT number on data for both run. "Pre filter" is the expected number of event before the application of any filter/scanning procedure while "after filter+scan" represents the expected number of events selected by the filter and classified as good contained neutrino candidates by the scanning. The proton on target statistics for RUN 8460 is 5.64x10^{17} POT and for RUN 9435 is 1.03x10^{18} POT

To finalize this study, in table 5.13 is reported the comparison between the MC predictions and the events observed in real data and classified as ν_μ CC contained with a long muon (flagged as "found events"). In this table the "MC prediction" and "Found events" refer to the sum of the events associated to RUN 8460 and RUN 9435 and the "MC prediction" is obtained by summing the expected number of events for categories 1→5 including scanning and filter efficiency.

MC prediction	Found events	Ratio (%)
151.2+274.9=426.1	183+303=486	114

Table 5.13: Direct comparison of the events expected as $\nu\mu$CC contained. "MC prediction" is the predicted number of neutrino based on the Monte Carlo events, while found events are the number of events identified during the visual scanning in data.

The "Ratio" reported in table 5.13 is obtained dividing the number of observed events in real data ("found events") and the number of expected events extracted from the analysis on MC neutrinos ("MC prediction"). The obtained result shows an excess of about 14% of events in real data. This difference can be explained by considering three different elements:

1. Monte Carlo simulation: there can be some small differences between simulated Monte Carlo events and real data. These differences lead to some possible differences in the efficiency of the scanning and of the filter. However, taking into account of the relatively simple requests that are applied in the filter, this contribution should be relatively small;

2. Dirt events: as previously mentioned, there could be interactions of neutrinos with the primary vertex outside the active volume ("dirt events") that might inject particles, for example neutrons, in the active volume. These could generate an interaction vertex that could be misidentified as a ν_μ charged current event in the scanning. Currently, this type of event has not been studied, so an accurate estimation of these cases is not yet available. For this reason the MC expectations are slightly under-estimated.

3. Systematic error from the MC simulation: the simulation of the neutrino interactions is based on the available information related to the BNB flux and composition and to the neutrino cross sections provided to the Genie program. These are both affected by an ∼10% uncertainties ([22]). These relatively large uncertainties will be strongly reduced in the SBN experiment thanks

to the direct comparison between the neutrino events collected in the near and the far detector. In this analysis, a minimum 10 % systematic error associated to the cross-section and to the flux will be considered.
This last systematic error contribution will be considered in the evaluation of the expected number of events the most important. In fact, the statistical error is smaller and can be considered negligible because a large sample of MC events has been used. The expected number of events is 426 ± 43 (syst.) to be compared with the observed events in real data 486 ± 22 (stat.) showing an agreement between the two measurements.

Chapter 6

Conclusion and future prospects

The main purpose of this thesis is the preparation of a pre-selection filter for the identification of neutrino interactions in ICARUS LAr-TPC. The prepared filter is meant in particular as a support for the visual study of the events providing the identification of a sample enriched with neutrino events. The selected events can be then visually studied in detail and most of all they will be used as a benchmark for the validation of the high-level reconstruction/selection tools used for the oscillation analysis in the ICARUS experiment. For this reason, the developed procedure is based on simple requirements, to ensure a large efficiency on the neutrino events and at the same time a strong rejection of the background from cosmics.
The proposed filter is primarily based on the identification of the particle generating the trigger in the detector. For this purpose, the light signals recorded on the PMTs and generating the trigger are used to identify a Region of Interest (ROI) where the tracks recorded by the TPC and associated with the interaction that generates the event trigger are located. This TPC-PMT association is based on the comparison of the barycenters along the longitudinal beam direction of the light signals recorded by the PMTs and the charge signals recorded in the TPC associated to the tracks. A TPC track can be preserved in the analysis only if the difference between its barycenter and the studied light barycenter is sufficiently small. The detailed study of this TPC-PMT association in Chapter 4 has shown that using a ROI of ± 1 m around the light barycenter provides a good identification of the neutrino events exceeding 98% of efficiency.
The focus of this thesis is on the selection of fully contained neutrino interactions with a muon track longer than 50 cm and in particular on the selection of the quasi-elastic interactions, which are the subject of ICARUS initial analysis for the verification of the claim of Neutrino-4. For this reason, I studied in detail the properties of the tracks to establish proper containment criteria. A track can be considered fully contained only if its start and end points are at a distance larger than 5 cm from the active volume boundaries. In addition, only tracks longer than 50 cm are considered to match the requirement on the muon length from the neutrino vertex.
Since the detector is shielded only by 2.85 m of concrete overburden, one of the most significant background is associated to cosmic rays which can be minimized by using two additional information to the 5 cm containment. First of all the Pandora pattern recognition tool used in the TPC reconstruction provides an identification of the tracks that are clearly associated to a cosmic muon ("clear-cosmic" tag). Furthermore, the signals from the Cosmic Ray Tagging system (CRT) surrounding the detector can help to recognize events with a cosmic particle generating

the trigger or with a not fully contained neutrino interactions by the presence of a CRT signal in coincidence with the trigger. The combination of the CRT hits information, the containment and the no "clear-cosmic" requirements resulted in a powerful tool to drastically reduce the tracks associated to cosmic rays, as verified directly on the collected events.
Finally, I applied the prepared filter on simulated neutrino events and on two specific data runs recently collected in the T600 detector. The filter efficiency on the fully contained muon neutrino interactions with a muon track longer than 50 cm results $\simeq$ 90%. The selected events in the studied runs have been also visually examined to recognize the genuine neutrino interactions selected by the filter from the residual background. The obtained purity for the filtered sample results approximately 60% determined by the data themself. This indicates that about 2 out of every 3 selected events are a good neutrino candidate. For example in the studied run 9435, starting from a sample of 7372 events, only 544 events have been selected by the filter and visually studied (factor 13.5 of reduction) and among them, 303 events are muon neutrino CC interactions fully contained. In addition, it was subsequently verified that accounting for the beam and cross-section related systematics, for the selection and the scanning efficiency there is a rough agreement between the number of events expected from the Monte Carlo simulation and the events observed in the data (see Table 5.13).
The developed procedure can be now applied to a larger sample of events in order to provide an enriched sample of neutrinos. These interactions will be used to evaluate the performance of the high-level selection/reconstruction tools that will be used for the ICARUS analysis. The selected and visually studied neutrinos can be used for example to check the capability of the Pandora pattern recognition tool to identify the vertex position, to recognize the particles produced at the primary vertex and the completeness of the event.
In conclusion, this study has provided a pre-selection filter that, together with the visual study of the events, will help in the validation of the higher-level reconstruction and analysis based on Pandora, which will be used for oscillation analysis. Another potential application of this selection procedure is related to the events collected using the Min-Bias trigger: for a small subset of beam spills, the events are recorded without any requirement on the light collected by the PMTs (as opposed to the PMT Majority runs used in this thesis). This sample results very helpful, for example, to study the performance of the main Majority trigger used in the experiment. Given the high efficiency of the filter and the relatively high purity, it could be applied to these types of events to select neutrino candidates that can be used to verify if they satisfy the trigger condition used in the data taking.
This filter can be also used for studies related to dirt events, that were not included in this thesis. The application of this filter will allow to recognize particular topologies that can originate potential background for the oscillation studies.
Finally thanks to this selection procedure, a few electron neutrino candidates have been also identified in the visual scanning and are now under study. The electron neutrinos are the golden sample in view of the analysis of the $\nu_\mu \rightarrow \nu_e$ oscillation. The electron neutrino candidates identified using this pre-selection can be used to tune automatically the high-level selection based on Pandora and to validate the capability to reconstruct the electron showers and their associated energy.

Bibliography

[1] Raymond Davis, Jr., Don S. Harmer, and Kenneth C. Hoffman Phys. Rev. Lett. 20, 1205

[2] Gribov, V. and Pontecorvo, B. (1969) Physics Letters, B28, 493

[3] X. Qian, P. Vogel (2015) "Neutrino Mass Hierarchy" arXiv:1505.01891

[4] A. Bellerive et Al. (2016) "The Sudbury Neutrino Observatory" arXiv:1602.02469

[5] The super kamiokande collab. (1998) "Evidence for oscillation of atmospheric neutrinos" arXiv:hep-ex/9807003

[6] Yoshitaka Itow for Hyper-Kamiokande Collaboration "Construction status and prospects of the Hyper-Kamiokande project" PoS(ICRC2021)1192

[7] Tsuyoshi Nakaya and Robert K. Plunkett, "Neutrino oscillations with the MINOS, MINOS+, T2K, and NOvA experiments", (2016) New J. Phys. 18 015009

[8] P. Adamson et Al. (2008) Measurement of Neutrino Oscillations with the MINOS Detectors in the NuMI Beam, arXiv:0806.2237

[9] The DUNE collab. "Long-baseline neutrino oscillation physics potential of the DUNE experiment" (2021) arXiv:2006.16043v2 [hep-ex]

[10] Daya Bay Collab. (2023) "Precision Measurement of Reactor Antineutrino Oscillation at Kilometer-Scale Baselines by Daya Bay" Phys. Rev. Lett. 130, 161802

[11] Angel Abusleme et al, "Sub-percent precision measurement of neutrino oscillation parameters with JUNO" (2022) Chinese Phys. C 46 123001

[12] A. Aguilar et al. [LSND Coll.], "Evidence for Neutrino Oscillations from the Observation of Electron Anti-neutrinos in a Muon Anti-Neutrino Beam", (2001) Phys. Rev. D 64, 112007

[13] B. Armbruster et al. [KARMEN Coll.], "Upper limits for neutrino oscillations muon-antineutrino to electron-antineutrino from muon decay at rest" (2002), Phys. Rev. D 65, 112001

[14] The MiniBooNe collab. "Significant excess of electronlike events in the MiniBooNE short-baseline neutrino experiment" (2018) Phys. Rev. Lett. 121, 221801

[15] Luis Alvarez-Ruso, Eduardo Saul-Sala (2021) "Neutrino Interactions with Matter and the MiniBooNE anomaly" hep-ph/2111.02504

[16] AIP Conference Proceedings 1666, 110002 (2015); doi: 10.1063/1.4915574

[17] G. Mention, M. Fechner, Th. Lasserre (2011) "The Reactor Antineutrino Anomaly", hep-ex/1101.2755

[18] A. Letourneau et Al.(2023) "Origin of the Reactor Antineutrino Anomalies in Light of a New Summation Model with Parametrized β^- Transitions" Phys. Rev. Lett. 130, 021801

[19] V. V. Barinov et al., (2022) "Search for electron-neutrino transitions to sterile states in the BEST experiment", Phys. Rev. C 105, 065502

[20] Serebrov, A.P., Samoilov, R.M., Chaikovskii, M.E. et al. "Result of the Neutrino-4 Experiment and the Cosmological Constraints on the Sterile Neutrino" (Brief Review) (2022) Jetp Lett. 116, 669–682

[21] S.J. Brice, et Al. "A New Method for Measuring Coherent Elastic Neutrino Nucleus Scattering at an Off-Axis High-Energy Neutrino Beam Target" hep-ex

[22] The ICARUS, The LAr1-ND and The MicroBooNE collaborations, (2015) "A Proposal for a Three Detector Short-Baseline Neutrino Oscillation Program in the Fermilab Booster Neutrino Beam", arXiv:1503.01520v1

[23] C. Rubbia "The liquid Argon time projection chamber: a new concept for neutrino detection", (1977) CERN-EP-INT-77-08

[24] A. Ereditatoa and A. Rubbiab "The liquid Argon TPC: a powerful detector for future neutrino experiments and proton decay searches" (2005) arXiv:hep-ph/0509022

[25] The MicroBooNE collaboration, "First constraints on light sterile neutrino oscillations from combined appearance and disappearance searches with the MicroBooNE detector" (2022), arXiv:2210.10216

[26] Abratenko, P., Aduszkiewicz, A., Akbar, F. et al. "ICARUS at the Fermilab Short-Baseline Neutrino program: initial operation", (2023) Eur. Phys. J. C 83, 467

[27] Christian Farnese and the ICARUS Collaboration "Short-Baseline neutrino oscillation searches with the ICARUS detector", (2021) J. Phys.: Conf. Ser. 2156 012141

[28] B. Ali-Mohammadzadeh et al "Design and implementation of the new scintillation light detection system of ICARUS T600", (2020) JINST 15 T10007

[29] C. Andreopoulos et al. http://www.genie-mc.org/

[30] Corsika website

[31] S. Agostinelli et al., "Geant4 - a simulation toolkit. Nuclear Instruments and Methods in Physics Research Volume 506, Issue 3, 2003, Pages 250-303,

[32] The MicroBooNE collab. "The Pandora multi-algorithm approach to automated pattern recognition of cosmic-ray muon and neutrino events in the MicroBooNE detector" (2018) Eur. Phys. J. C

[33] Robert D. Cousins, Kathryn E. Hymes, Jordan Tucker, "Frequentist evaluation of intervals estimated for a binomial parameter and for the ratio of Poisson means", (2009) https://doi.org/10.1016/j.nima.2009.10.156

[34] M. Antonello et al. "Study of space charge in the ICARUS T600 detector" (2020) JINST 15 P07001

[35] S. Palomares-Ruiz, S. Pascoli, T. Schwetz, (2005), "Explaining LSND by a decaying sterile neutrino", hep-ph/0505216